OAK RIDGE NATIONAL LABORATORY LIBRARIES
3 4456 0555971 2

CENTRAL RESEARCH LIBRARY

ORNL-TM-4914
Vol. I

Cy 94

Quarterly Progress Report on Reactor Safety Programs Sponsored by the NRC Division of Reactor Safety Research for January–March 1975

I. Light-Water-Reactor Safety

OAK RIDGE NATIONAL LABORATORY
CENTRAL RESEARCH LIBRARY
DOCUMENT COLLECTION
LIBRARY LOAN COPY
DO NOT TRANSFER TO ANOTHER PERSON
If you wish someone else to see this document, send in name with document and the library will arrange a loan.
UCN-7969
(3 3-67)

OAK RIDGE NATIONAL LABORATORY
OPERATED BY UNION CARBIDE CORPORATION • FOR THE U.S. ATOMIC ENERGY COMMISSION

Printed in the United States of America. Available from
National Technical Information Service
U.S. Department of Commerce
5285 Port Royal Road, Springfield, Virginia 22161
Price: Printed Copy $5.45; Microfiche $2.25

This report was prepared as an account of work sponsored by the United States Government. Neither the United States nor the Energy Research and Development Administration, nor any of their employees, nor any of their contractors, subcontractors, or their employees, makes any warranty, express or implied, or assumes any legal liability or responsibility for the accuracy, completeness or usefulness of any information, apparatus, product or process disclosed, or represents that its use would not infringe privately owned rights.

ORNL-TM-4914
Vol. I
UC-78, -78a, -78c

Contract No. W-7405-eng-26

QUARTERLY PROGRESS REPORT ON REACTOR SAFETY PROGRAMS SPONSORED BY THE NRC DIVISION OF REACTOR SAFETY RESEARCH FOR JANUARY–MARCH 1975

I. LIGHT-WATER-REACTOR SAFETY

JULY 1975

NOTICE This document contains information of a preliminary nature and was prepared primarily for internal use at the Oak Ridge National Laboratory. It is subject to revision or correction and therefore does not represent a final report.

OAK RIDGE NATIONAL LABORATORY
Oak Ridge, Tennessee 37830
operated by
UNION CARBIDE CORPORATION
for the
U.S. ENERGY RESEARCH AND DEVELOPMENT ADMINISTRATION

OAK RIDGE NATIONAL LABORATORY LIBRARIES
3 4456 0555971 2

CONTENTS

Page

FOREWORD v

SUMMARY vii

1. BLOWDOWN HEAT TRANSFER PROGRAM 1

1.1 Fuel Rod Simulation 1

1.1.1 Heater Rod Life 1
1.1.2 Thermocouple Drift 3
1.1.3 Thermocouple Shadow Effect 6
1.1.4 Heater Procurement for the THTF 6

1.2 Experimental Plans and Evaluations 8

1.2.1 RELAP4 Calculations of THTF Isothermal Blowdowns 8
1.2.2 Data Processing Codes 19
1.2.3 Data Analysis Codes 19

1.3 Multirod Transient and BDHT Experiments 20

1.3.1 THTF Instrumentation 20
1.3.2 Test Bundle Assembly 26

1.4 Two-Phase Flow Instrumentation Studies 32

1.4.1 Densitometer Operation 32

References 50

2. NUCLEAR SAFETY INFORMATION CENTER 51

2.1 Routine Services 52

2.2 Special Activities 52

2.3 ORNL-NSIC Reports 53

2.4 System Developments 53

2.5 Nuclear Safety Journal 54

3. FISSION PRODUCT BETA AND GAMMA ENERGY RELEASE 55

3.1 Introduction 55

3.2 Experimental Progress 55

Reference 56

4. ZIRCONIUM METAL—WATER OXIDATION KINETICS 57

4.1 Thermometry 57

4.2 Diffusion of Oxygen in β-Zircaloy 58

4.3 Reaction Rate Studies 59

4.3.1 Apparatus Development 60
4.3.2 Preliminary Isothermal Oxidation Results 64

4.3.3 Temperature Measurements during Oxidation 64
4.3.4 "Perturbation" Errors in Temperature Measurements 70
4.3.5 Computer-Simulated Oxidation Experiments 75

References 77

5. MULTIROD BURST TESTS 78

5.1 Introduction 78

5.2 Program Plans 79

5.2.1 Planning and Analysis 79
5.2.2 Posttest Examination of Fuel Pin Simulators 80
5.2.3 Temperature Profiles in No. 1 (4 × 4) Bundle 82

5.3 Design, Development, and Procurement 88

5.3.1 Zircaloy Tubing Procurement 88
5.3.2 Grids 88
5.3.3 Component Development 89
5.3.4 Heater Development and Procurement 90
5.3.5 Instrumentation and Data Acquisition 95
5.3.6 Design 101

5.4 Fabrication and Construction 102

References 104

6. FISSION PRODUCT RELEASE FROM LWR FUEL 105

7. CREEPDOWN AND COLLAPSE OF ZIRCALOY FUEL CLADDING 107

Reference 108

FOREWORD

This is the fourth in a series of quarterly progress reports on programs conducted at Oak Ridge National Laboratory (ORNL) under the sponsorship of the NRC Division of Reactor Safety Research. Although this report is issued quarterly, some activities may be carried over to the next quarter in order to be able to report meaningful progress. However, the report will maintain the order of presentation. Because of the diversity of reader interest and the desire to keep the documents to a practical size, the report is presented in four volumes.

Volume I, Light-Water-Reactor Safety Programs, includes activities on fuel rod behavior, blowdown heat transfer, the Nuclear Safety Information Center, and fission product transport and energy release.

Voluem II, Heavy-Section-Steel Technology Program, covers work performed by ORNL as well as by subcontractors at other installations. The closing period for this volume will always be one month earlier than the specified period to allow sufficient time for subcontractors to prepare contributions and obtain the proper clearance from their respective companies.

Volume III, Liquid-Metal-Cooled Fast Breeder Reactor Safety programs, includes work at ORNL on aspects relating to the safe operations of the liquid-metal-cooled fast breeder reactor.

Volume IV, High-Temperature Gas-Cooled Reactor Program, covers progress on work pertinent to high-temperature gas-cooled reactors.

Copies of the report are available from the Technical Information Center, Energy Research and Development Administration, Oak Ridge, Tennessee.

SUMMARY

1. BLOWDOWN HEAT TRANSFER PROGRAM

Testing of the production heater rod now installed in the FCTF continued at a reduced rate. This rod has now survived for a total operating time of 60.7 hr, 25.5 of which were at full power; during this period there was a total of ten blowdowns and one steady-state CHF measurement. There are still no indications of leaks from the Viton O-ring seals at the top of the heater rod. For the last five blowdowns, sheath and interior thermocouples gave substantially the same readings prior to blowdown when the rod was at full power and loop flow and pressure were the same. Prior to this, these thermocouples had indicated progressively higher temperatures after heatup to the same operating conditions subsequent to each blowdown. Testing will be continued to determine whether the thermocouple drift problem can be minimized by some preconditioning procedure.

Preliminary analysis of the results from calibration tests of the first production heater rod in the single-rod loop indicates that the observed increase in sheath thermocouple temperature can be accounted for by a gap coefficient of 2000 to 5000 Btu $hr^{-1} \cdot ft^{-2}$ $(°F)^{-1}$. These are in the range expected for contact resistance of two stainless steel surfaces swaged together under conditions similar to those used in fabricating the present heater rods. These calculations suggest that the leveling off of sheath thermocouple temperatures, described above, is no more than what should be expected with the present design of dual-sheath heater rods.

Prediction of isothermal blowdown performance of the Thermal-Hydraulic Test Facility continued. As expected, placing a 1/4-in.-diam orifice in the line connecting the pressurizer with the main loop resulted in an almost immediate drop of pressure to saturation at the instant of blowdown. In comparison, calculations indicated that, without the orifice, 1 to 2 sec would be required for the pressure to decrease to saturation. Other calculations indicate that variations in break area and break distribution appear to afford a wide choice of pressure and flow transients.

The first isothermal blowdown was conducted successfully on February 21, 1975. Initial pressure was 1300 psi, loop temperature was 450°F, and the orifice was 1/4 nominal (based on RELAP predictions). All systems appeared to perform successfully. The pressure suppression system contained the loop discharge; the pump was apparently undamaged by the blowdown event as was true for the drag disks and turbine meters. Pressure transducers were also undamaged by the event. The flow reversed at the instant of blowdown and for the first 20 sec was consistent with the RELAP predictions for this test.

A series of two-phase, air-water flow tests were conducted using a THTF spool piece with a drag disk, a turbine meter, and a gamma densitometer. Two different dispersers were used, one having a $\Delta P \sim 30\%$ greater than the spool piece with no disperser and the other having a $\Delta P \sim 330\%$ greater than the spool piece alone. With the low-pressure-drop disperser, accuracy of mass flow measurement appeared to be dependent on flow regime in a consistent fashion. With the high-pressure-drop disperser, it appeared that mass flow rates could be measured to within ±20% over a range of superficial air velocities from 2 to 130 fps and water flow rates from 130 to 300 $lb_m\ sec^{-1}\ ft^{-2}$

2. NUCLEAR SAFETY INFORMATION CENTER

The Nuclear Safety Information Center continues to collect, store, evaluate, and disseminate information to the nuclear community at a high level. During the past quarter, this included the addition of 3374 new safety documents to the computerized file as well as the preparation of three ACRS bibliographies and response to 338 inquiries. Most notable among the Center's many other activities was the completion of *Nuclear Safety* drafts for 16(3), while *Nuclear Safety* 15(6), 16(1), and 16(2) were published. *Nuclear Safety* was awarded first place in the Technical Publications Category by the East Tennessee Chapter of the Society for Technical Communication.

3. FISSION PRODUCT BETA AND GAMMA ENERGY RELEASE

This program completed the evaluation of the overall method proposed to measure fission product decay heat by spectroscopic techniques for in-pile irradiations. During the quarter the electrical and electronic hardware, which are required to control and monitor movements of the position, were completed and installed. Software programming was completed, so that the computer controls the experiment from the time the rabbit is sent to the reactor until the subsequent counting time has expired. *In situ* calibration of the gamma-ray detector was initiated.

4. ZIRCONIUM METAL—WATER OXIDATION KINETICS

The calibration of our Pt—Rh vs Pt thermocouples was completed, and our newly acquired optical pyrometer was submitted for calibration. Both tracer and chemical diffusivity measurements for oxygen in β-Zircaloy were made in the range 1000 to 1400°C (1832–2552°F). The two types of diffusion coefficients were identical within experimental error, and the chemical diffusivity was independent of oxygen concentration in the range 0.1 to 0.6 wt %. Preliminary reaction rate data were obtained at 1000°C (1832°F) in the MiniZWOK apparatus, and extensive tests and modifications were made on this device to identify potential sources of error in our temperature measurements and to improve the accuracy of such measurements. Various heat flow models were analyzed to provide maximum possible values for so-called "perturbation" errors in our thermocouple temperature measurements. The computer code SIMTRAN-I was developed and is being tested.

5. MULTIROD BURST TESTS

A program plan, describing in detail the objectives, scope, and technical approach to be used in this research, was completed and submitted to RSR for review and concurrence. Plans and accomplishments to date were presented to the RSR Fuel Cladding Research Review meeting in February; these meetings provide for informal exchange of results and ideas of mutual interest to the various programs. New test schedules,

consistent with delays encountered with heater development and procurement, were formulated.

Methods for posttest examination of the test geometries were investigated; for the single-rod assemblies, the "Scotch tape method" will be used to obtain circumferential measurements of the deformed cladding. Examination of the bundles will be more tedious, since the tape method is not applicable. Both a Quantimet-720 Image Analyzing Computer and an electronic planimeter probably will be used to automate measurement of the multirod arrays. Both of these techniques require casting the array in epoxy, sectioning at discrete axial positions, and polishing to provide a suitable cross-sectional profile for detailed measurement.

Detailed plans were formulated for experimental determination of the temperature distribution in the first 4 x 4 test bundle. For these experiments, each of the fuel pin simulators will be provided with four inside surface thermocouples; several of the simulators will be instrumented with outside surface thermocouples. The measurements will provide temperature profiles of interior, corner, and midwall exterior rod positions. The data will be used to model the temperature distribution in subsequent burst test arrays.

Procurement of Zircaloy tubing for use in all the RSR-sponsored fuel cladding studies is approximately on schedule. Prototype reactor grids, being made available to the test program by one of the reactor vendors, will be on hand in May. Some delays were encountered in procurement of special thermocouples for evaluation and for use in the initial tests.

Tests of lower seal gland concepts for the fuel pin simulators, while encouraging, have not yet resolved all the problems; testing of improved concepts is in progress. Progress was made in development and testing of other components and equipment, including a special fixture for positioning and welding thermocouples inside the cladding.

Tests and evaluation of development heaters supplied by three manufacturers indicated that significant improvement in fabrication techniques is needed to produce acceptable heaters. Based on these tests, the heater was redesigned to improve performance and to circumvent fabrication difficulties; procurement of improved heaters was initiated. A

decision was made to apply a protective plasma spray coating on the heaters after they are delivered to Oak Ridge; procedures and evaluation of candidate refractory metal and oxide coatings were initiated. Availability of suitable heaters continues to be the critical path item that determines the start of the test program.

Progress was made on design of the multirod test facility; construction modifications to the existing dc power supply will commence next quarter. A versatile single-rod test stand was designed and fabricated. This bench-type apparatus will be used to develop components and test procedures and to conduct burst tests on instrumented fuel pin simulators.

6. FISSION PRODUCT RELEASE FROM LWR FUEL

The work plan has been revised to reflect comments which resulted from NRC's review of the preliminary draft, and the revised plan has been transmitted to ONRR-NRC. Cleanup of a contaminated hot cell has been completed; installation of our experimental apparatus in this cell is currently in progress. Specifications for the preparation of experimental assemblies from irradiated LWR fuel rods have been developed, and cost estimates for sample preparation are being collected.

7. CREEPDOWN AND COLLAPSE OF ZIRCALOY FUEL CLADDING

Progress has continued on both the theoretical and the experimental aspects of cladding collapse behavior. A review of prior work on collapse, in general, and on anisotropic mechanical behavior, specifically, has been completed. Equipment design has been completed, and procurement and installation are proceeding rapidly. All safety reviews for the use of high-pressure equipment have been completed and approvals obtained.

1. BLOWDOWN HEAT TRANSFER PROGRAM

Reactor Division

D. G. Thomas

1.1 FUEL ROD SIMULATION

J. D. White, R. F. Bennett, D. L. Clark

1.1.1 Heater Rod Life

Testing of indirect electrically heated fuel pin simulators in the Forced Convection Test Facility is continuing. The 0.422-in.-diam heater rod W150/74 has operated for a total of 60.7 hr in the facility. This heater is a sample from the heater lot purchased for the first bundle of the THTF. The heater has survived 8 blowdowns and 23 1/2 hr of operation at full power (144 kW) and maximum loop temperature (550°F) as shown in Table 1.1. The comparison between operating histories of the six heaters tested (shown in Table 1.1) points out that this heater (W150-74) has survived considerably more hours at full power than the others – except preprototype W150-2 which was retired before failure.

O-rings

The upper pressure seals of the FCTF and THTF facilities are provided by rubber O-ring seals. These O-rings are compressed between heater bearing surfaces and grooves machined into the seal plates of the loops. This design allows heaters to grow and contract axially (thermal expansion) through the O-rings during the experiments. The two Viton O-rings used in the testing of heater W150-74 have performed without failure during its operating history.

Nickel electrode

A nickel plate with machined tapered holes is to provide a lower electrical contact with the tapered bottoms of the heaters in the THTF. This type of arrangement has been utilized with a nickel electrode in

Table 1.1. Operational history of Watlow indirect heater assemblies

	Type					
	Preprototype			Prototype		Production
	Heater No.			Heater No.		Heater No.
	150-1	150-3	150-2	150-5	150-1	150-74
	Number of blowdowns					
Total power at blowdown, kW						
75	1		3	1		
100	2	1	4		1	1
140 to 150	5	2	4	9	3	7
Total	8	3	11	10	4	8
Total hours with power on	44	35	31	43	42	60.65
Total hours at full power	6	1	0.5	8.5	10	23.50
On-off cycles	34	22	11	18	12	15
Fate	Fail[a]	Fail[b]	Retire	O-ring failure	O-ring failure	Operating

[a]Split in sheath, sheath damaged by centering screw.

[b]Split in sheath.

the FCTF for the testing of the two prototypical heaters and the testing of W150-74. The nickel electrode contains a tapered hole machined to the same specifications as those in the nickel plate of the THTF. No assembly, disassembly, or operational difficulties with this design have arisen during the testing program. After a heater is removed from the electrode, the inside of the tapered hole is polished before the next heater is installed.

1.1.2 Thermocouple Drift

Considerable discrepancies in the outputs of the thermocouples of the heater W150-74 were reported in the last quarterly report. The thermocouple outputs generally increased from one experiment to the next throughout the 16 hr of full-power operation described in the report.

After the third blowdown (16.5 hr at full power), a steady-state critical heat flux experiment was performed. Heater power was 155 kW during the experiment until CHF conditions were induced by decreasing test-section inlet subcooling. When the thermocouple outputs rose abruptly, indicating onset of CHF, the heater power was decreased to nearly zero. Some of the skin temperatures reached 2000°F during the experiment. These temperatures fell quickly to 700°F within 20 sec of onset of CHF.

Five blowdown experiments followed the critical heat flux test. The outputs of the thermocouples varied considerably between the first two of these blowdowns as shown in Figs. 1.1 and 1.2. Then most of the thermocouple responses seemed to stabilize with respect to run-to-run variation. Sheath thermocouples C1 and C2 exhibited the most severe changes in output. For example, thermocouple C1 was reading about 845°F ±2°F before the third 144-kW blowdown. After that blowdown and the following CHF run, thermocouple C1 was reading 788 ± 2°F before the next blowdown. This thermocouple then read 821, 821, and 805°F during steady-state conditions in later blowdown experiments.

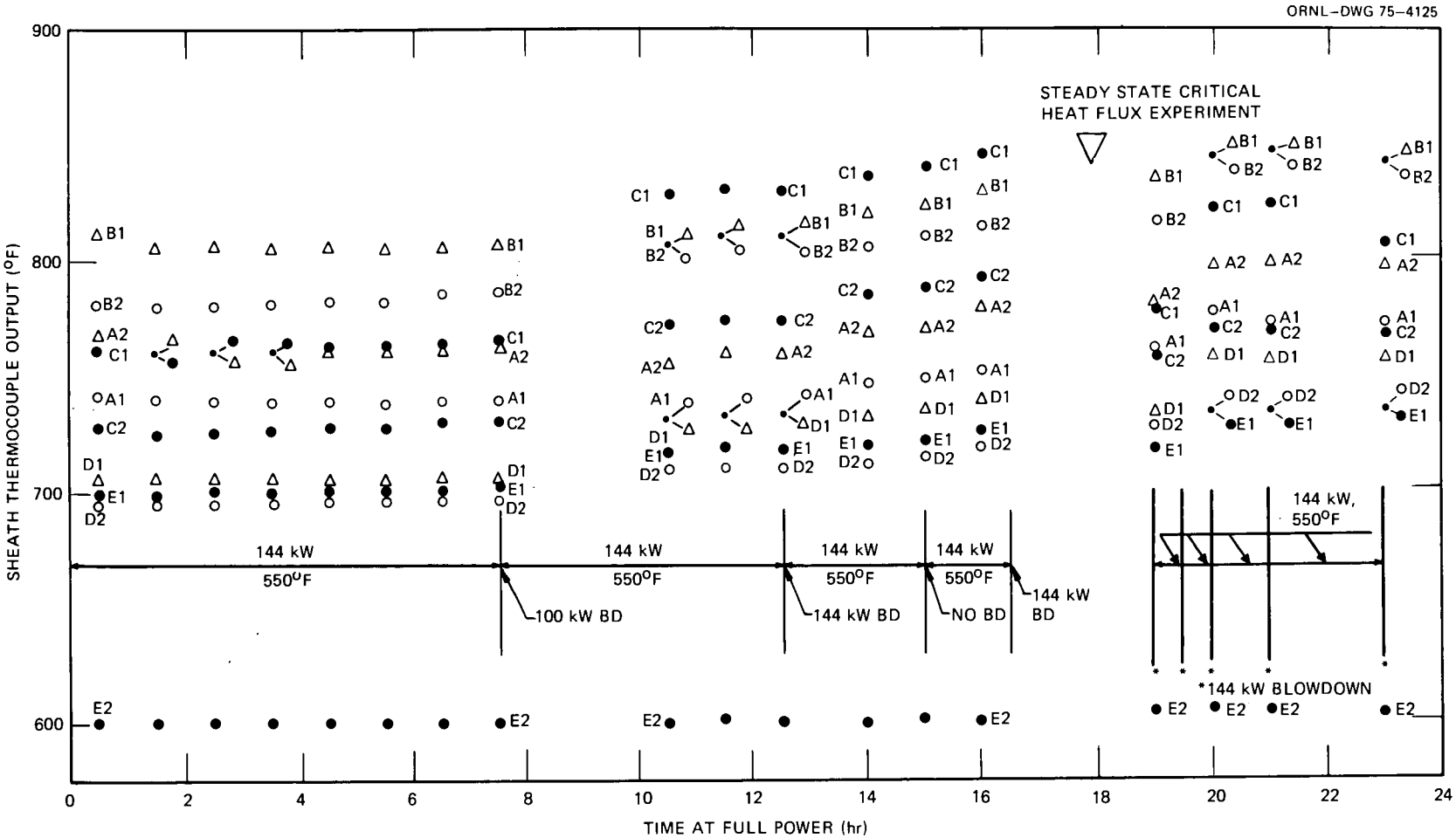

Fig. 1.1. Heater W150-74 sheath thermocouple output as a function of time at full power and blowdown number.

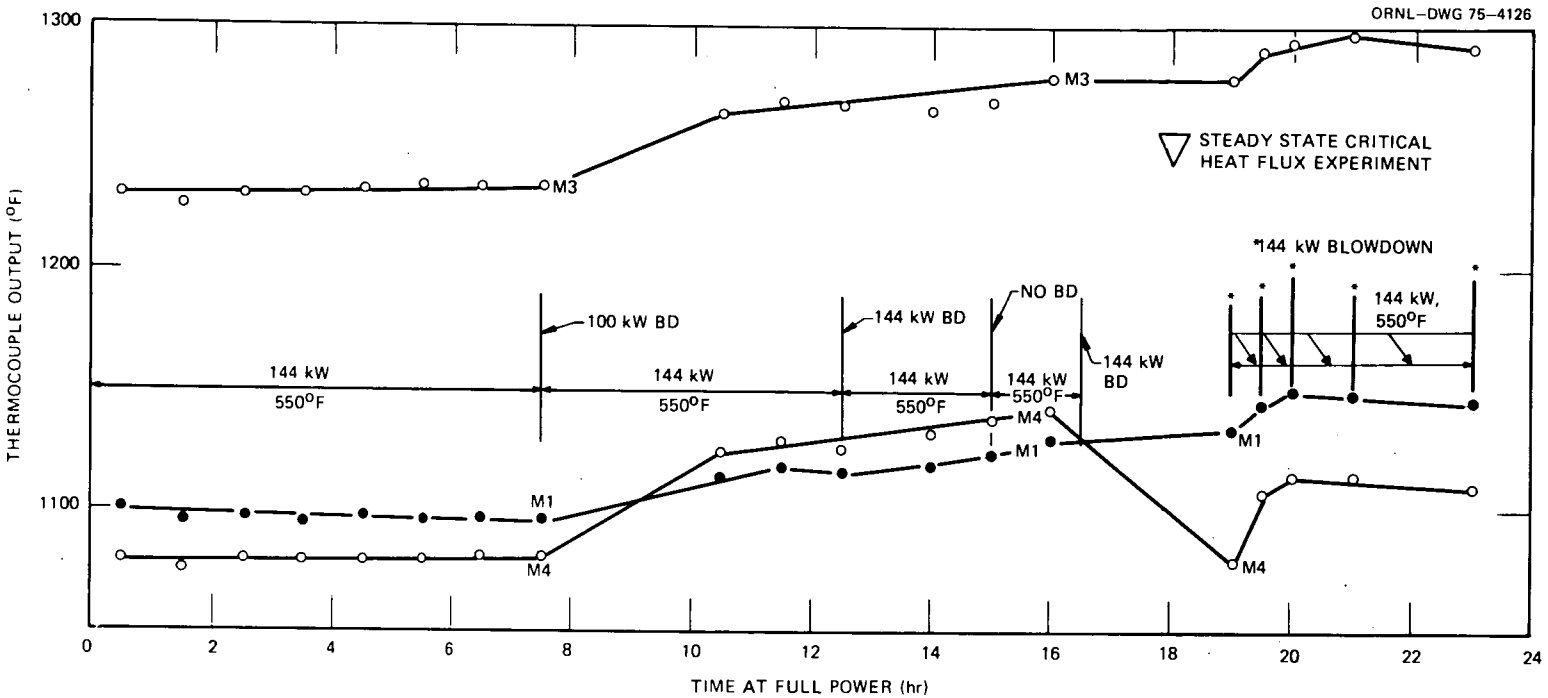

Fig. 1.2. Interior thermocouple output of production heater W150-74 at 144 kW.

1.1.3 Thermocouple Shadow Effect

Rod temperature measurements with sheath thermocouples will be used to infer surface heat fluxes and heat transfer coefficients. Thus it is necessary to determine the relationship between measured sheath temperatures and possible rod fouling.

The thermocouple measurement reflects the temperature field surrounding it, which may be strongly distorted by localized contact resistance.[1] These contact resistances take two forms: contact resistances in and around the thermocouple itself, and contact resistance between the inner and outer rod sheaths. Together these resistances may be responsible for measured sheath temperatures higher than would be expected to occur if the thermocouple measured a point temperature at the center of a uniform rod sheath.

The thermocouple measurement at steady state may be modeled as in Fig. 1.3. Both schemes presented should adequately predict thermocouple temperature, or infer an average surface temperature, assuming thermocouple behavior is not a function of surface flux or temperature (though thermal conductivity dependence on temperature may be incorporated). Changes in thermocouple behavior may be interpreted as changes in thermocouple equivalent position or inferred gap coefficient.

Thermocouple equivalent positions in Watlow rod 150-74 have been estimated by the procedure outlined in the April-June quarterly,[2] and the results are presented in Table 1.2. Variation of the thermal conductivity of stainless steel with temperature has been included in the calculations.

This rod has exhibited marked changes in the thermocouple measurement with increased operation time; hence the results presented to not describe stable rod characteristics. The equivalent thermocouple positions appear unrealistic; however, the inferred gap coefficients are reasonable.[3]

1.1.4 Heater Procurement for the THTF

The balance of the heaters for bundle No. 1 have been received and have passed all inspections at ORNL, including infrared scanning tests and

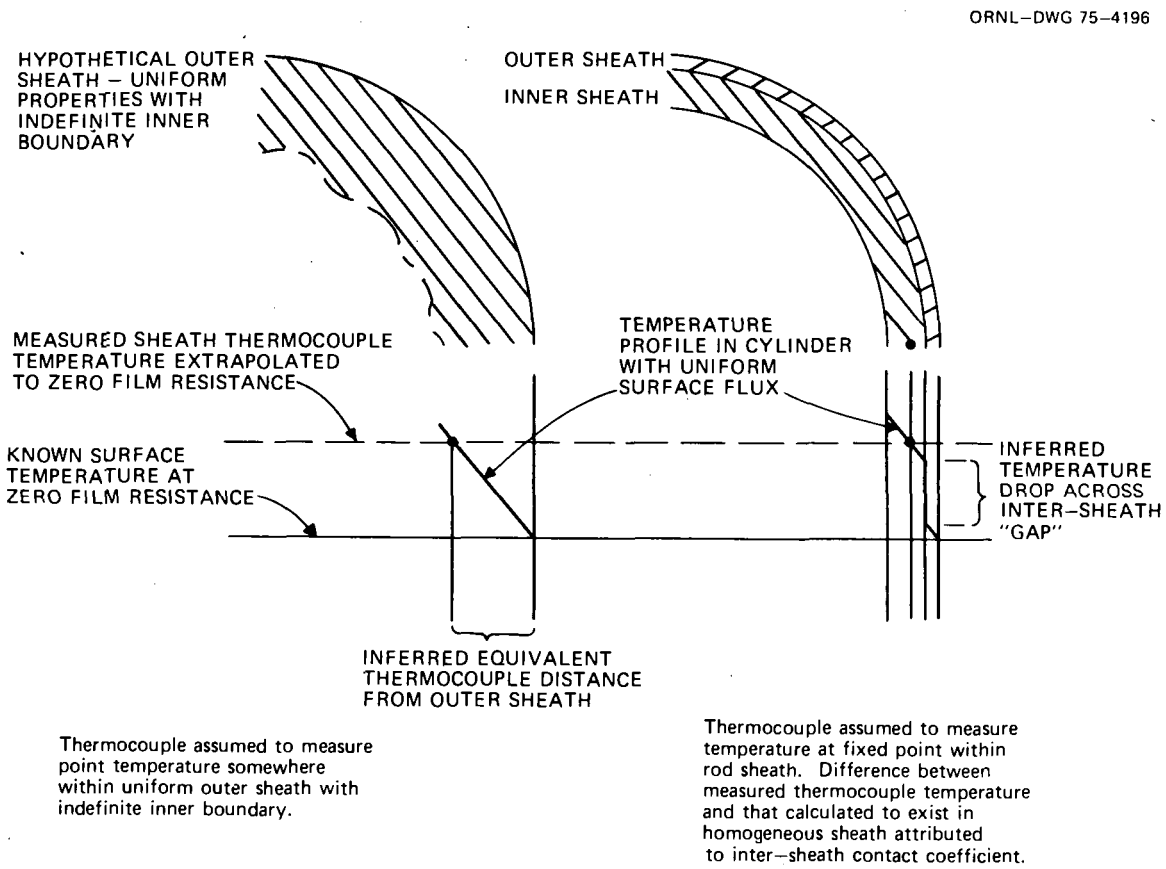

Fig. 1.3. Methods of modeling steady state performance of sheath thermocouples.

Table 1.2. Observed external thermocouple equivalent position and gap coefficient[a] – Watlow rod 150-74

Thermocouple	Equivalent distance from outer wall (mils)	Inferred gap heat transfer coefficient[a] Btu hr^{-1} ft^{-2} $(°F)^{-1}$
A1	67.8	2040
A2	58.2	2610
B1	58.7	2580
B2	58.0	2630
C1	56.6	2740
C2	46.1	3920
D1	49.4	3460
D2	41.2	4860
E1	69.2	1970

[a]Thermocouple assumed to measure undisturbed sheath temperature at a radius of 0.192 in. (19 mils from outer surface). Gap is assumed to exist between inner and outer sheaths at a radius of 0.201 in. (10 mils from outer surface).

thermal search for locating thermocouples. These heaters are available for use as replacement heaters as needed.

Except for the method of installing thermocouples in the heater sheath (and possibly the utilization of a single sheath rather than a dual-sheath design), bundle No. 2 heaters will be geometrically similar to the heaters for bundle No. 1. The tubular heating element material (three sizes) and the boron nitride powder (UCAR type TS-945) are on hand. The 0.020-in.-OD sheathed type K thermocouples are on order from Kaman Sciences Corporation. Procurement of the heater sheath material and the heaters themselves await the finalization of the thermocouple installation technique.

Negotiations are underway for procurement of heaters of alternate designs, including a heater essentially identical to the heaters RAMA is fabricating for the Aerojet Nuclear Corporation Semiscale program. Also to be procured are prototype heaters using alternate heater element designs. This activity has also been delayed pending revision or finalization of the thermocouple installation technique. The possibility of this revised installation technique, allowing for a larger diameter thermocouple (0.025 to 0.030-in.-OD) is also under consideration.

1.2 EXPERIMENTAL PLANS AND EVALUATIONS

R. F. Bennett and N. E. Clapp*

1.2.1 RELAP4 Calculations of THTF Isothermal Blowdowns

In preparation for the THTF isothermal blowdown tests, several blowdown configurations have been modeled with RELAP4. Pressurizer line resistance, total break area, and break area distribution have been varied. A base set of loop conditions has been chosen that should be used during the isothermal tests.

Calculation parameters are summarized in Table 1.3, and loop steady-state conditions are given in Fig. 1.4.

---

*Instrumentation and Controls Division.

Table 1.3. THTF isothermal blowdown conditions

Steady state

Loop temperature	550°F
Pressures	
Test section	2250 psia
Pressurizer	2198 psia
Flows	
Loop	423 gpm (44.11 lb/sec)
Main heat exchangers	80 gpm/heat exchanger
Total pump	700 gpm at 1940 ft (631 psi)
Loop flow resistances	
No orifices in circulating portions of loop	

Valve	ΔP	Flow area
FCV-1	152 psi	0.0079 ft^2
HCB-2	478	0.0106
FCV-18	98	0.0135
HCV-32	40	0.0092
TCV-52, 54, 56	30	0.0146 total

Blowdown parameters

Total break area	Fraction inlet break	Pressurizer isolated from loop during blowdown	Pump during blowdown
0.0135	1.0	Yes	Off
0.0135	1.0	No	Off
0.0034	1.0	Yes	Off
0.0250	1.0	Yes	Off
0.0135	0.5	Yes	Off
0.0135	0.3	Yes	Off

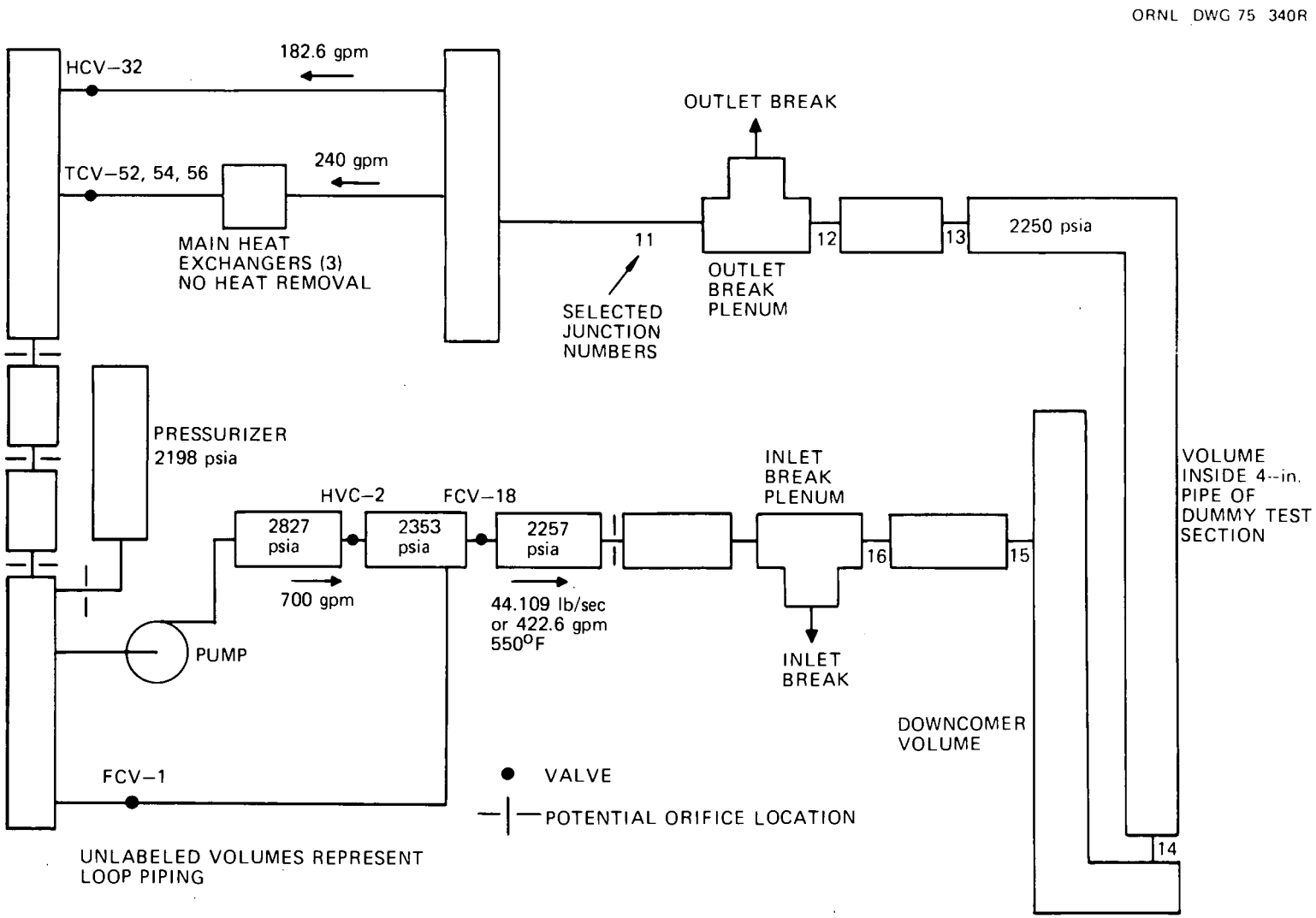

Fig. 1.4. RELAP4 model of THTF for isothermal tests.

Influence of pressurizer line resistance

For isothermal operation with 500°F, 2250 psia circulating fluid, saturation pressure is ~1100 psia, well below the pressurizer condition. If the pressurizer is effectively isolated from the loop during blowdown, pressures will drop to saturation almost immediately at blowdown. If the pressurizer is allowed free communication with the loop, the initial pressure transient will be rapid but not abrupt (except for short-term wave effects). In this instance, the pressurizer is a source of higher enthalpy fluid, elevating the local saturation pressure in the vicinity of the pressurizer outlet. During the first several seconds, the loop pressure decay is primarily controlled by fluid expansion in the pressurizer. As pressure approaches loop saturation conditions, fluid mixed with the pressurizer flow will flash first, followed by the unmixed loop water.

The pressurizer influence on blowdown is determined by the ratio of pressurizer line resistance to break resistance, i.e., the ratio of pressurizer line orifice area to total break area. During a rapid blowdown, a given orifice may effectively isolate the pressurizer from the loop, while during a slow blowdown the same orifice may allow the pressurizer to control the pressure decay.

Figure 1.5 demonstrates the influence of pressurizer line resistance on a given blowdown configuration. With the pressurizer isolated by an orifice, pressure drops abruptly to saturation; with no orifice in the line, the pressure requires ~2 sec to reach saturation conditions near the pressurizer outlet.

The slower pressure transient obtained with no restriction in the pressurizer line delays fluid flashing near the test section, resulting in a fairly constant density over ~4 sec followed by a rapid drop as local saturation occurs (see Fig. 1.6). With a high resistance in the pressurizer line, density begins to drop immediately upon blowdown, controlled primarily by the fluid expansion allowed by the break flow.

Pressurizer influence on test section flows is strong (compare Figs. 1.7 and 1.8). With the pressurizer isolated, flow at the test section outlet hovers about zero for the first 5 sec, while fluid in the test section, downcomer, and inlet piping flashes and flows to the inlet break.

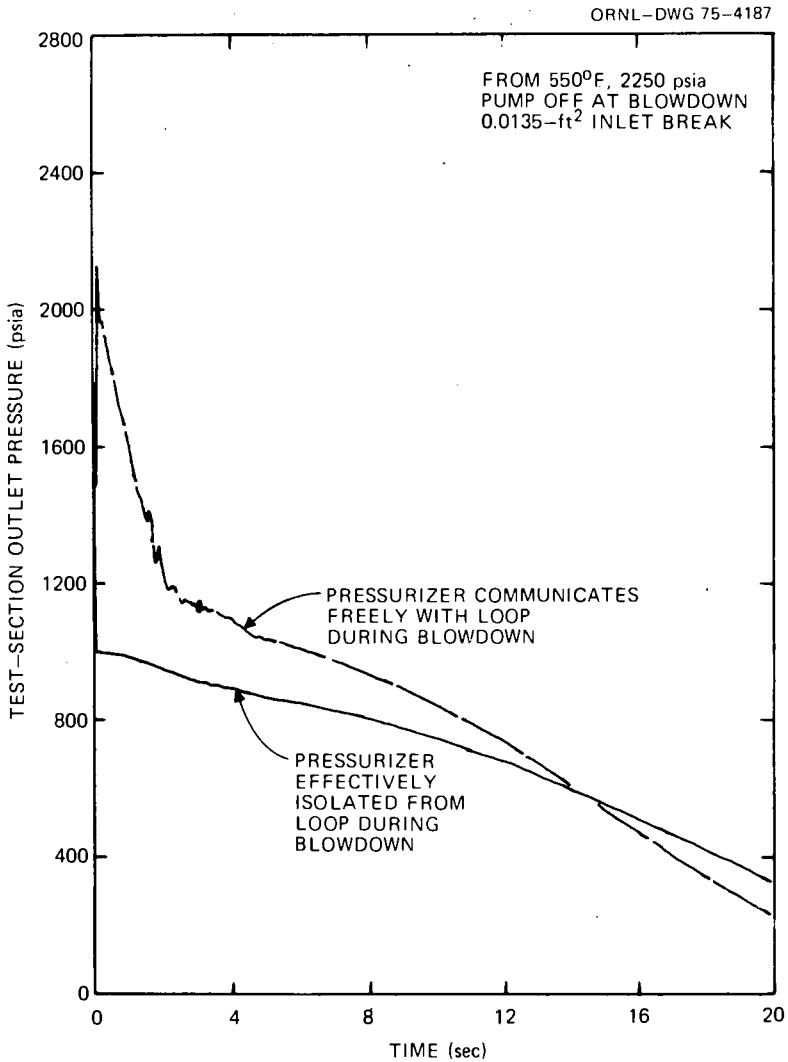

Fig. 1.5. Effect of limiting cases of pressurizer line resistance on calculated THTF isothermal blowdown pressure transient.

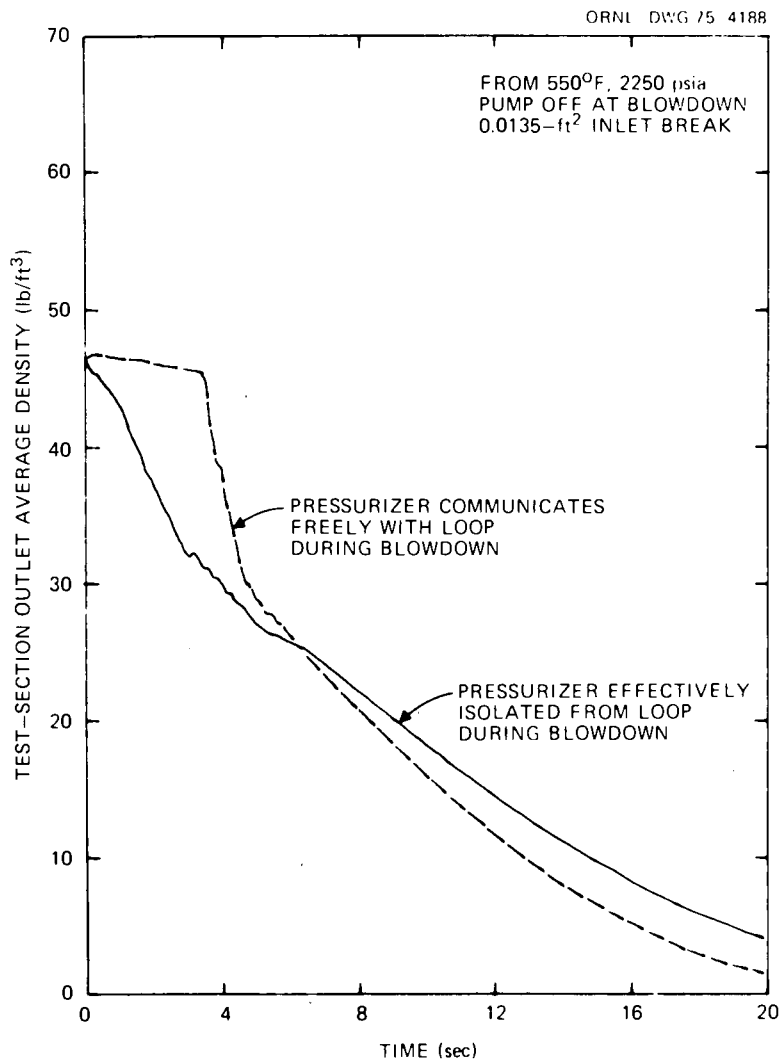

Fig. 1.6. Effect of limiting cases of pressurizer line resistance on calculated fluid densities during a THTF isothermal blowdown.

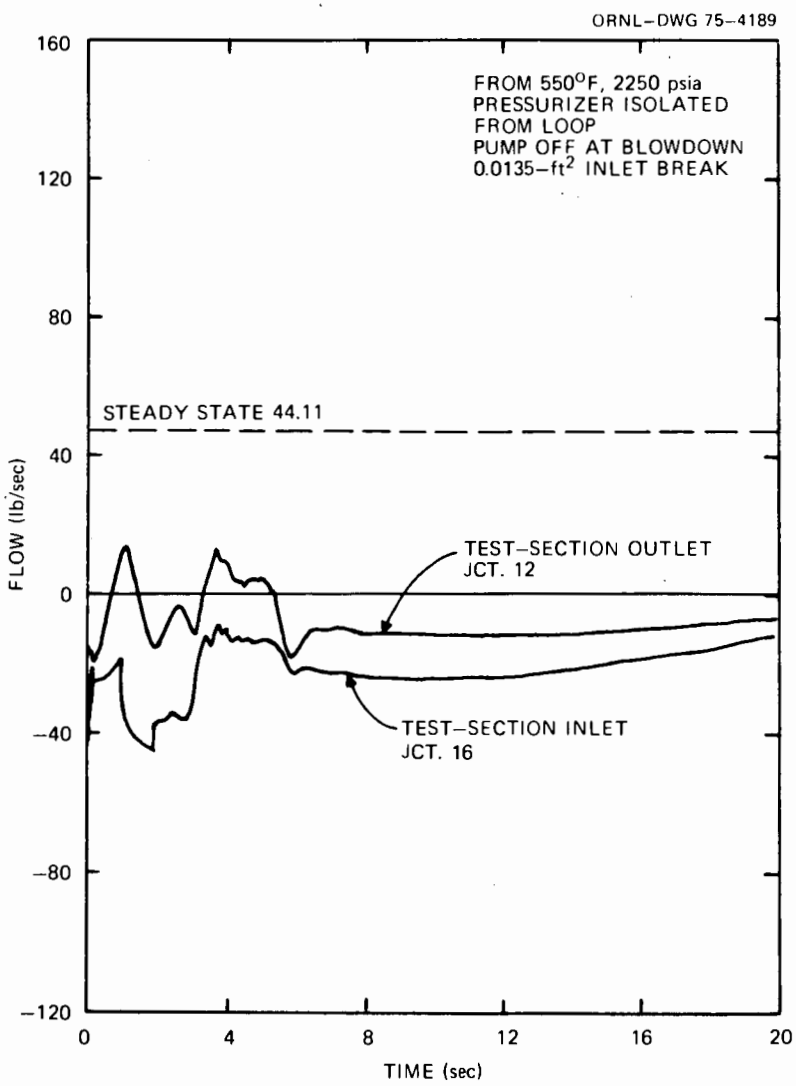

Fig. 1.7. Calculated flows about THTF dummy test section during an isothermal blowdown. Pressurizer effectively isolated from loop.

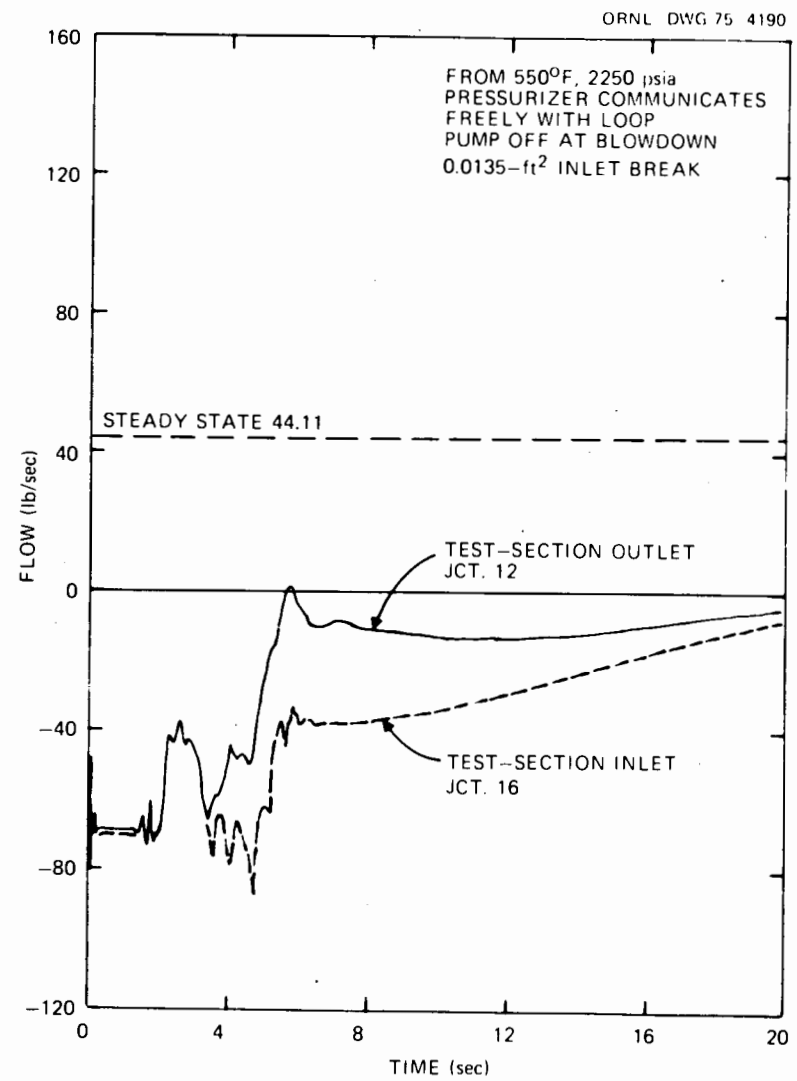

Fig. 1.8. Calculated flows about THTF dummy test section during an isothermal blowdown. Pressurizer communicates freely with loop.

With no resistance in the pressurizer line, the relatively cold loop fluid does not flash for ~4 sec, and flow from the pressurizer and nearby piping, through the outlet line and test section to the inlet break, dominates the test section flows.

The calculated pressure trace is a function of the loop modeling near the pressurizer outlet. In the calculation, pressurizer water mixes intimately with the water in piping volume 5 (see Fig. 1.4); in reality, it will proceed as a wave and flash throughout the early decompression. Thus, one would expect the experimental pressure trace to exhibit a more gradual transition toward the flashing of loop fluid than the calculation predicts. With the pressurizer isolated, however, the calculation and experiment should agree well.

For the above reason, the remaining comparisons are with the pressurizer effectively isolated from the loop. In practice, this would be accomplished with a small bore orifice in the pressurizer line, sized to accommodate the gradual fluid expansion during heatup. This presents no undue hazards during isothermal operation. During powered operation, short-term imbalances between the heat exchangers and the rod bundle from rapid power transients (inadvertent or otherwise) may require momentary large flows to or from the pressurizer to assure stable loop pressure. If the pressurizer is to be isolated during blowdown, its response during powered startup may be inadequate to assure safe loop operation. Hence, with the present loop design, the pressurizer should be allowed to communicate freely with the loop during powered runs.

Break area

Blowdowns with three different break areas were calculated. In all cases, the break was at the test section inlet and the pressurizer was effectively isolated from the loop during blowdown.

Figure 1.9 compares pressure transients. The middle break area (0.0135 ft^2) is expected to yield a pressure transient in powered THTF blowdowns similar to that calculated for a PWR. The largest break area (0.025 ft^2) induces a rapid blowdown; loop pressure is less than 50 psi in 20 sec. With the smallest break area (0.0034 ft^2), pressure remains almost constant during the calculated transient.

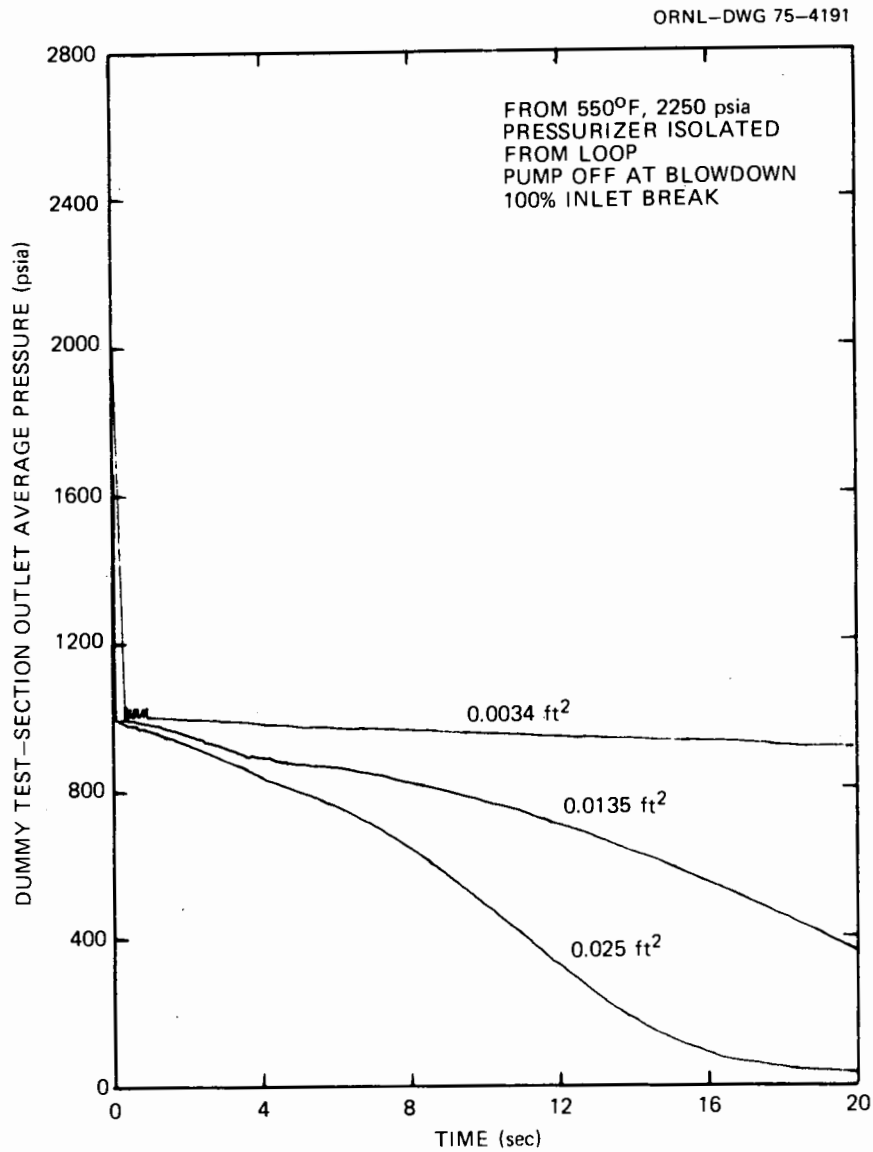

Fig. 1.9. Effect of break area on calculated THTF pressure transient during isothermal blowdown.

The influence of break area on test section flows is instructive (see Figs. 1.10 and 1.11). Pump flow is more than adequate to supply break flow in the 0.0034-ft^2 run, and flow remains positive during blowdown. The larger breaks exhibit immediate flow reversals, and test section flows generally remain negative throughout blowdown. The largest break area shows the greatest negative flows during the first 12 sec, but flows rapidly approach zero beyond this point as loop fluid is depleted.

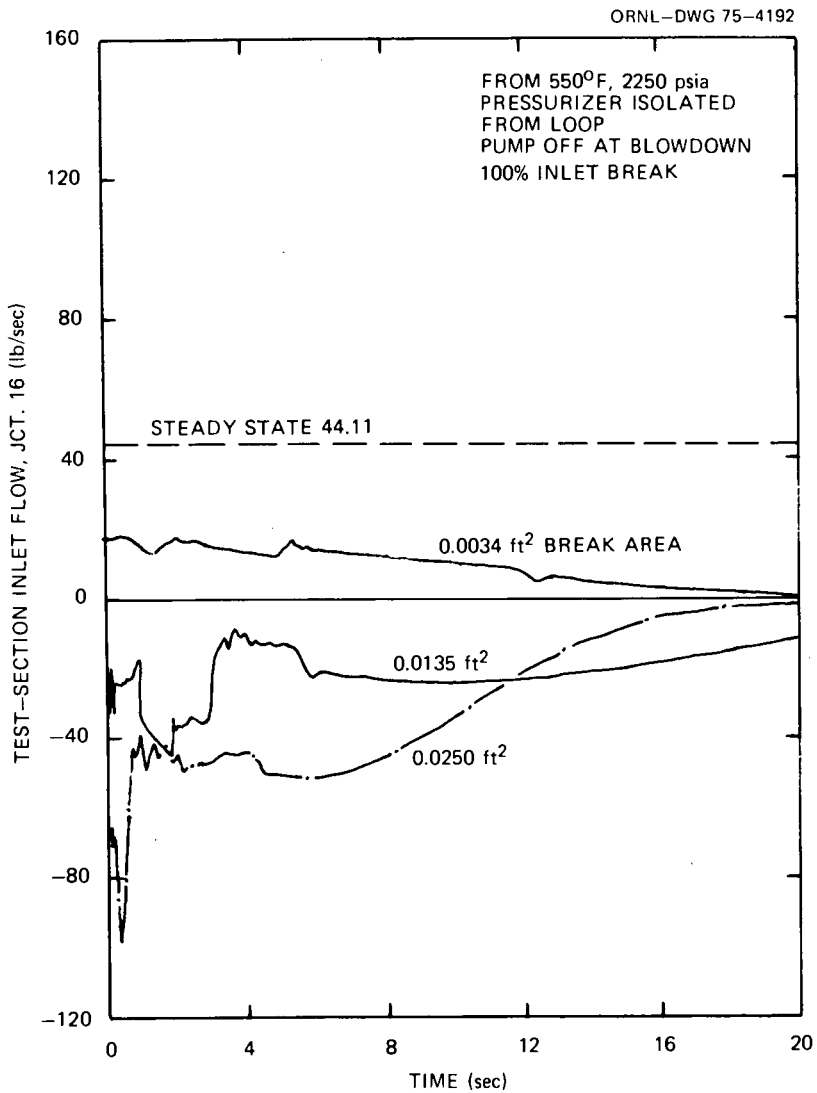

Fig. 1.10. Effect of break area on calculated dummy test section inlet flow in THTF isothermal blowdowns (100% inlet break).

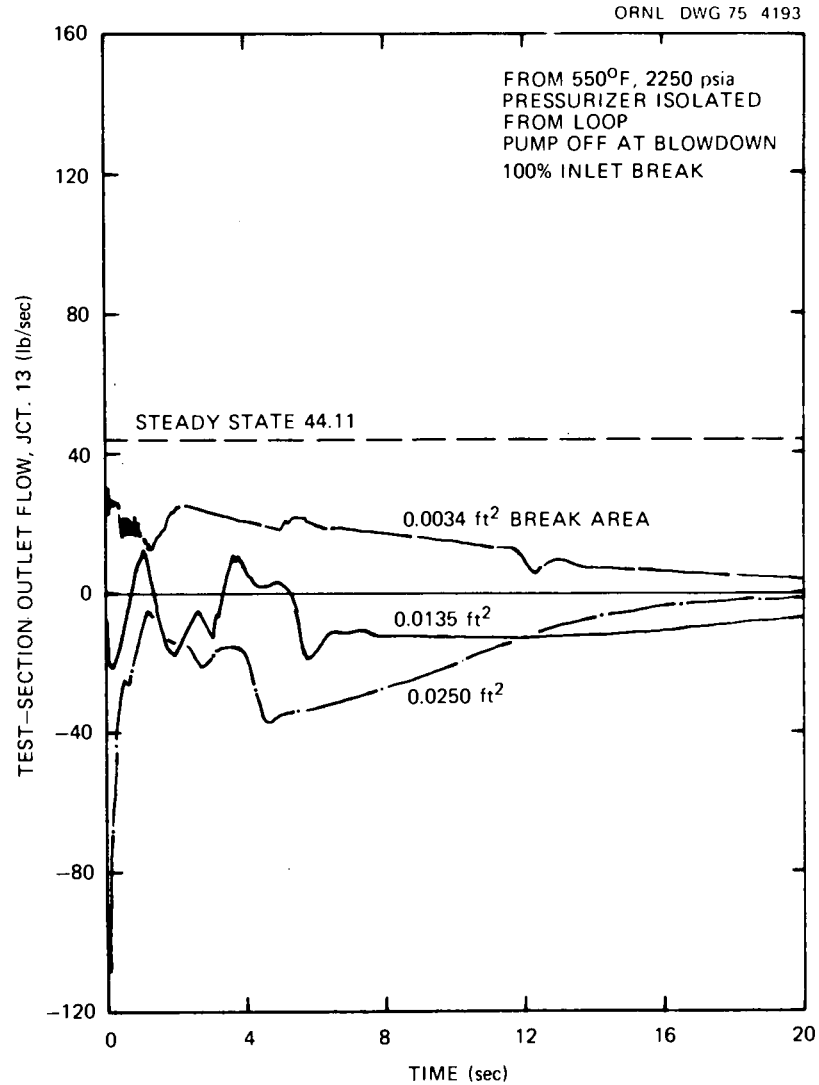

Fig. 1.11. Effect of break area on calculated dummy test section outlet flow in THTF isothermal blowdowns (100% inlet break).

Note that in all cases flows at the test section outlet are relatively positive and flows at the inlet are relatively negative, due to flashing of fluid in the test section and downcomer volumes.

Break area distribution

To a first approximation, total break area determines the pressure transient, and break area distribution determines the test section flow transient (see Figs. 1.12 and 1.13). Increasing outlet break area promotes positive flow through the test section during blowdown and delays flow reversal.

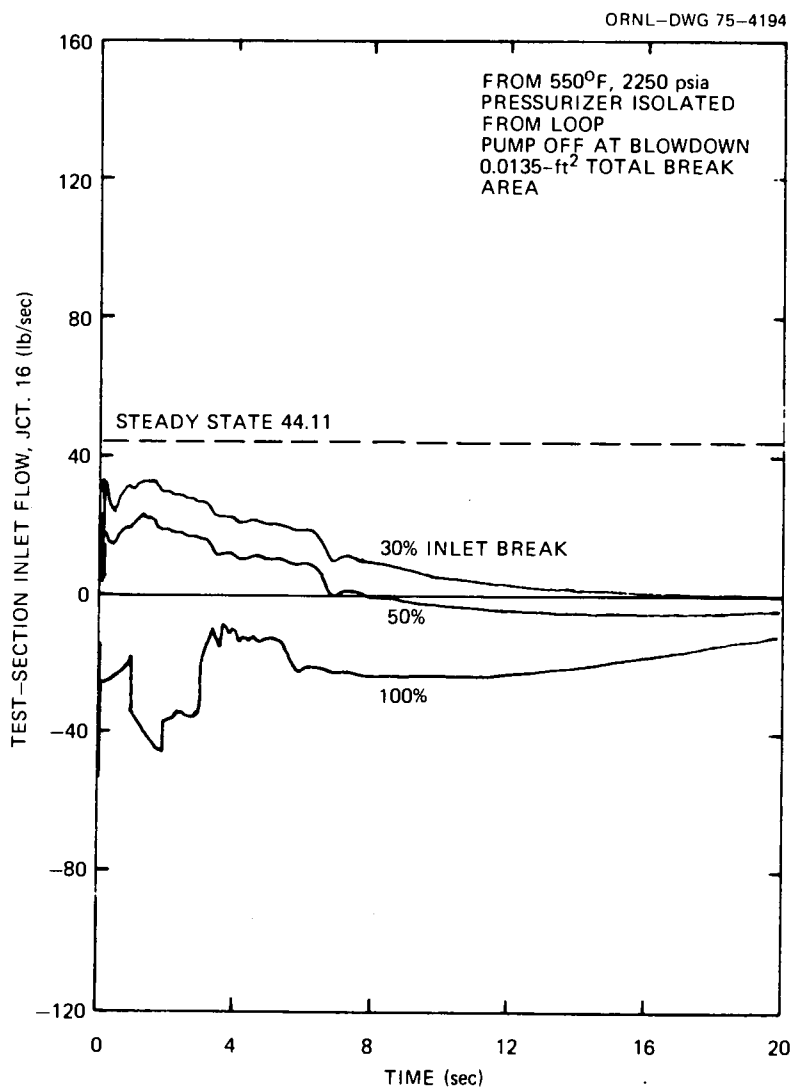

Fig. 1.12. Variation of test section inlet flow with break area distribution in a calculated THTF isothermal blowdown.

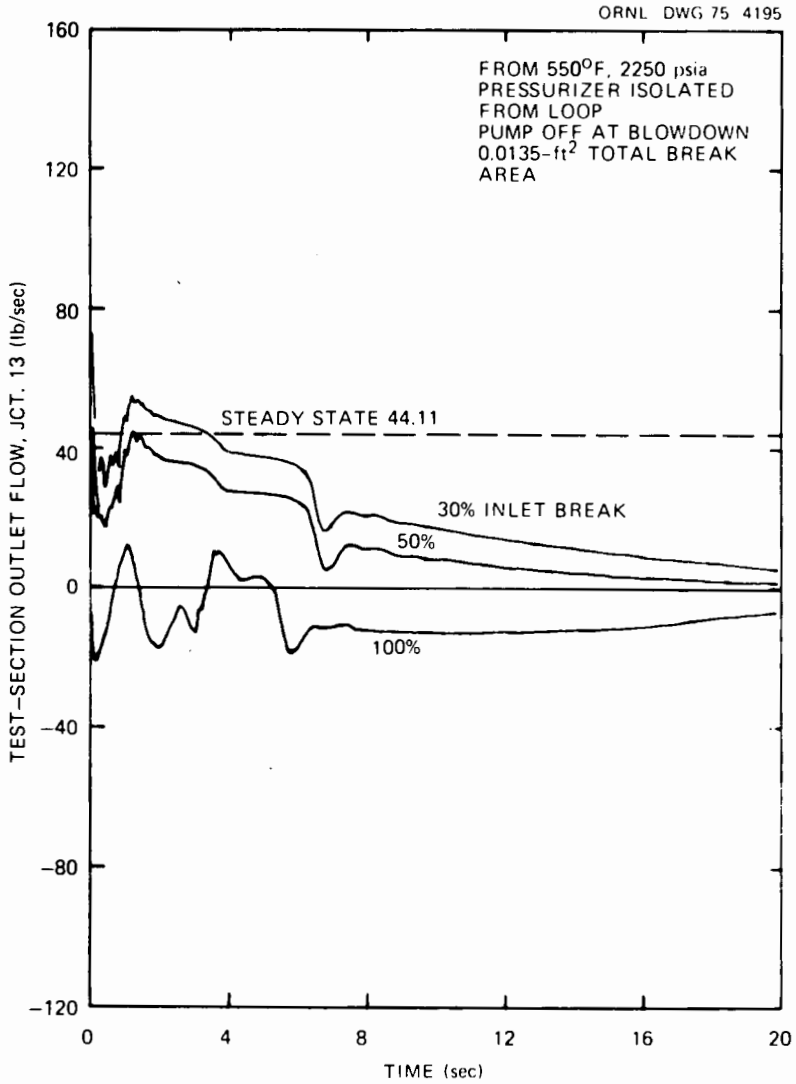

Fig. 1.13. Variation of test section outlet flow with break area distribution in a calculated THTF isothermal blowdown.

Summary

Resistance in the pressurizer line has been shown to be a major factor in determining transient flows and pressures. The pressurizer will probably communicate freely with the loop in powered runs to assure safe steady-state operation; hence, the flow resistance in this line will not be varied to adjust powered blowdown transients, at least initially. Variations in total break area and break distribution appear to afford a wide variety of flow and pressure transients.

All calculated flows must be examined qualitatively, as they are subject to model structure as well as uncertainties in the RELAP program. Weaknesses in the model are apparent. For example, the dummy test section and downcomer have been modeled in homogeneous flows, an obviously poor assumption at low flow rates. The incorporation of phase separation in this region is approximate at best, and a guess may offer no greater accuracy in flow prediction over the homogeneous model during the 20 sec calculated.

1.2.2 Data Processing Codes

Two codes have been written and debugged for processing the seven-track binary data tape written by the PDP-8E computer. The first code is used to convert the seven-track binary data tape to a nine-track IBM tape that contains appropriate millivolt values for the recorded data. The second code converts the millivolt values obtained by the first code into the appropriate engineering unit values and writes this information on either a nine-track IBM tape or an IBM disk file.

1.2.3 Data Analysis Codes

Three codes have been written and debugged for use in the analysis of the data generated by THTF. The first code is a plotting routine that reads the engineering unit data and produces the desired number of plots with up to four variables with respect to time on each plot using the Cathode-Ray Tube (CRT) plotter available at the computing center. The second code, used for steady-state data, calculates and outputs the average value and the standard deviation for each signal monitored by the data system. The third code is used to determine the time to CHF using heater rod sheath thermocouple data obtained during a blowdown test.

1.3 MULTIROD TRANSIENT AND BDHT EXPERIMENTS

B. G. Eads,* R. E. Helms, A. M. Smith

1.3.1 THTF Instrumentation

B. G. Eads,* C. Brashear,* D. G. Davis,*
J. A. Hawk,* R. L. Moore,* W. Ragan*

Installation and verification of instrumentation required for loop shakedown and isothermal blowdown operations were completed and an isothermal blowdown was performed on February 21, 1975. The major areas where design and installation remain incomplete are:

1. bundle overtemperature protection system,
2. dc generator power programmer,
3. test section data sensors installation, and
4. generator and heater rod current and voltage signal system.

Installation of instrumentation required for powered bundle operation is continuing, with verification of this instrumentation being made as it is installed.

Blowdown rupture disk system

Installation is complete for that portion of the blowdown rupture disk system required for single-ended blowdown operation. All materials are on hand to complete the entire system to permit double-ended blowdowns.

Data acquisition systems

An on-site training course on the use and maintenance of the two 14-track tape recorders was conducted by a manufacturer's representative. These two recorders are now being calibrated and will be used for recording fast transient data in the next isothermal blowdown.

Approximately 100 data signals have been connected to the CCDAS (total capacity at present is 384 channels). A "rough" calibration of the CCDAS itself was performed previously. A precision calibration of this system

---

*Instrumentation and Controls Division.

is now underway and will be completed prior to the next isothermal blowdown. Also verification on each channel from sensor to CCDAS is nearing completion. The remaining 284 channels not yet connected are associated with powered bundle operation, and installation of much of this instrumentation is not complete.

The dc power system programmer

Two types of function-generation programmers are now under consideration – the programmable read-only memory (PROM) type system mentioned in last quarter's report and a commercially available "Digital Datatrak" system. Either of these systems will generate a predetermined time-dependent voltage, which will be the demand signal for the regulators for the four dc generators.

In the PROM system the desired function is stored in digital form in a read-only memory. On receipt of a "Start" signal, clock pulses will be input to the PROM at predetermined rates and the stored information will be transmitted in parallel digital form to a digital-to-analog converter. This signal is conditioned and amplified and is the input for the four regulator systems.

The "Digital Datatrak" system uses a punched paper tape for program information storage. Digital data on this tape are read into the system and used to control the setting of four digital potentiometers that provide the programmed signal to the regulators.

First isothermal blowdown

An isothermal blowdown test at approximately 1000 psig and 450°F was conducted on February 21, 1975. All postoperational checkouts of instrumentation conducted thus far indicate that all process instrumentation and controls performed satisfactorily and were not damaged by the blowdown transient. Testing of data instrumentation to determine any changes in calibration or damage is not complete. The two analog tape recorder systems were not operational for this test; therefore, no fast transient data were obtained. The CCDAS verification has not been completed; therefore only portions of its data signals were logged during this test.

The turbine meters and drag disks were functional, and their signals were recorded during the test. The gamma densitometers were not operational during the test; therefore, transient two-phase flow data may not be obtainable for this test.

The dc generator step response tests

Programming of the THTF heater rod bundle power during blowdown can be accomplished by several means. The simplest and fastest means (and the one that will be used on the first heated blowdown) is to trip the generator load breaker. This will produce a step change to zero power in a few milliseconds. Tripping the generator field breaker will produce an exponential voltage decay to zero voltage with a 4-sec time constant. Since power varies as the square of the voltage, the power will decay at a much faster rate than the voltage. Provisions are made in the control circuit for delay of the trip for preset times beyond start of blowdown.

Decays to power levels other than zero can be obtained by application of a programmed demand signal to the input of the existing regulator circuit, provided that the regulator response and stability are adequate. From analysis of the regulator system and prior observation of performance during Rod Burnout Test Facility operations, it was predicted that the regulator system should respond to a 90% downstep from full power in less than 2 sec and recover stably. To confirm these predictions, tests were performed using the setup shown in Fig. 1.14. For these tests, the generator was loaded with a 0.625-Ω, water-cooled resistor to produce a 400-A load current. To produce the step, a resistor was inserted between the existing demand potentiometer and the existing 200K demand input resistor. Shorting and unshorting this resistor has the same effect as making positive and negative steps in the demand voltage. A number of step changes were made from various initial generator voltages between 50 and 250 V and with step magnitudes varying from 1 to 75% of the initial voltages. Figure 1.15 shows typical small signal response to 1, 2.5, and 5% step changes at 250 V. Figure 1.16 shows a typical 75% step change from and to 250 V. In all cases, the large signal response was less than 1.5 sec and was proportional to the magnitude of the step. The small signal response was less than 0.75 sec in all cases. The shape of all large signal response curves

ORNL–DWG 75–4356

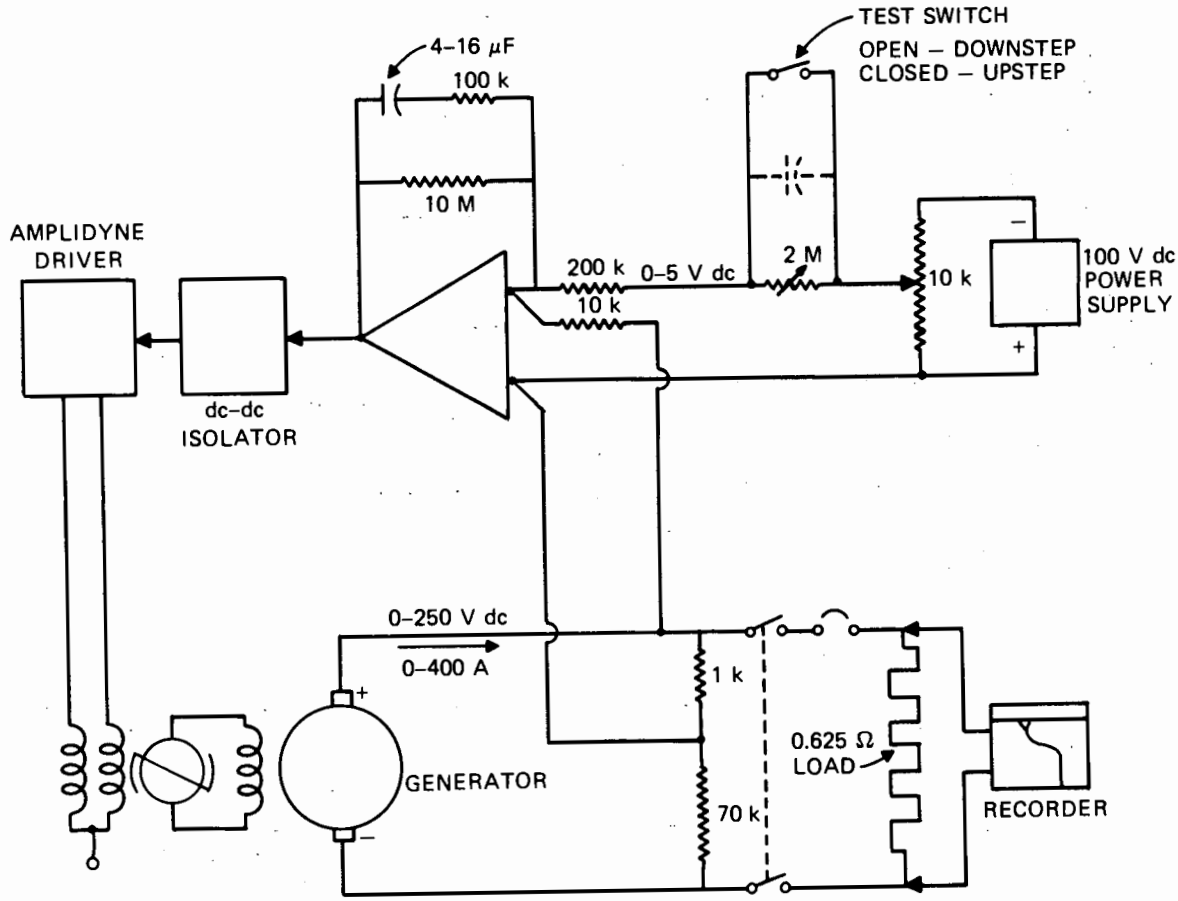

Fig. 1.14. Test setup for determining regulator step response of THTF dc generator.

was the same except for the length of the linear portion of the curve and the amount of overshoot. In these cases, the slope of the linear portion was always approximately 145 V/sec and the amount of overshoot was proportionate to the magnitude of the step change. These characteristics, which are not present in the small signal response curves, are the result of the amplifier output being quickly driven to its limits by the large step input voltage and remaining there until the system recovers. This causes a "field forcing" action via the amplidyne, which results in a voltage decay rate considerably faster than that corresponding to the 4-sec generator field time constant. The overshoot is the result of the integral (reset)

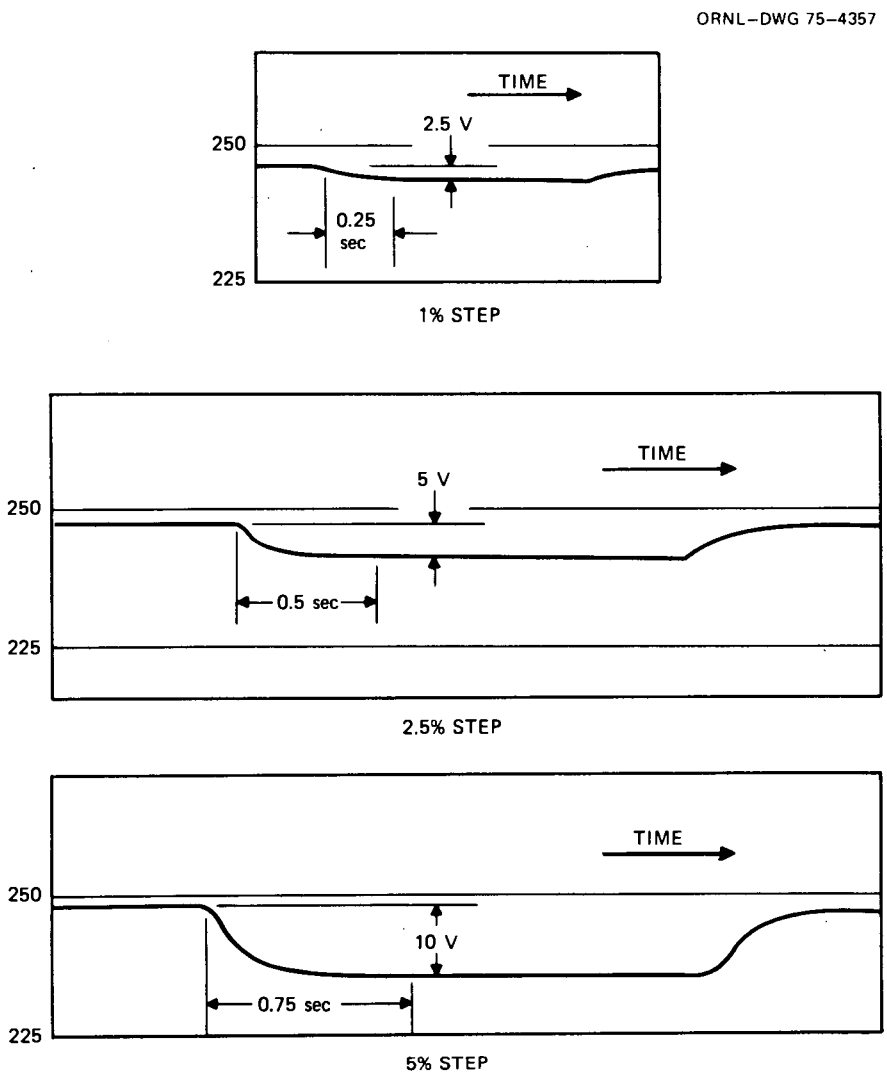

Fig. 1.15. Response of THTF dc generators to a step change in demand. Small signal – 1, 2.5, and 5% steps, 0.625 Ω load.

action of the amplifier, which produces a time integral shift in the effective demand set point during the period when the amplifier is overdriven. The overshoot recovery time corresponds to the reset rate of the closed loop regulator system.

Although the generators were not fully loaded during these tests, all portions of the regulator system external to the generator were fully exercised, and it is expected that further tests will show that the response and stability will not be appreciably affected by higher load currents.

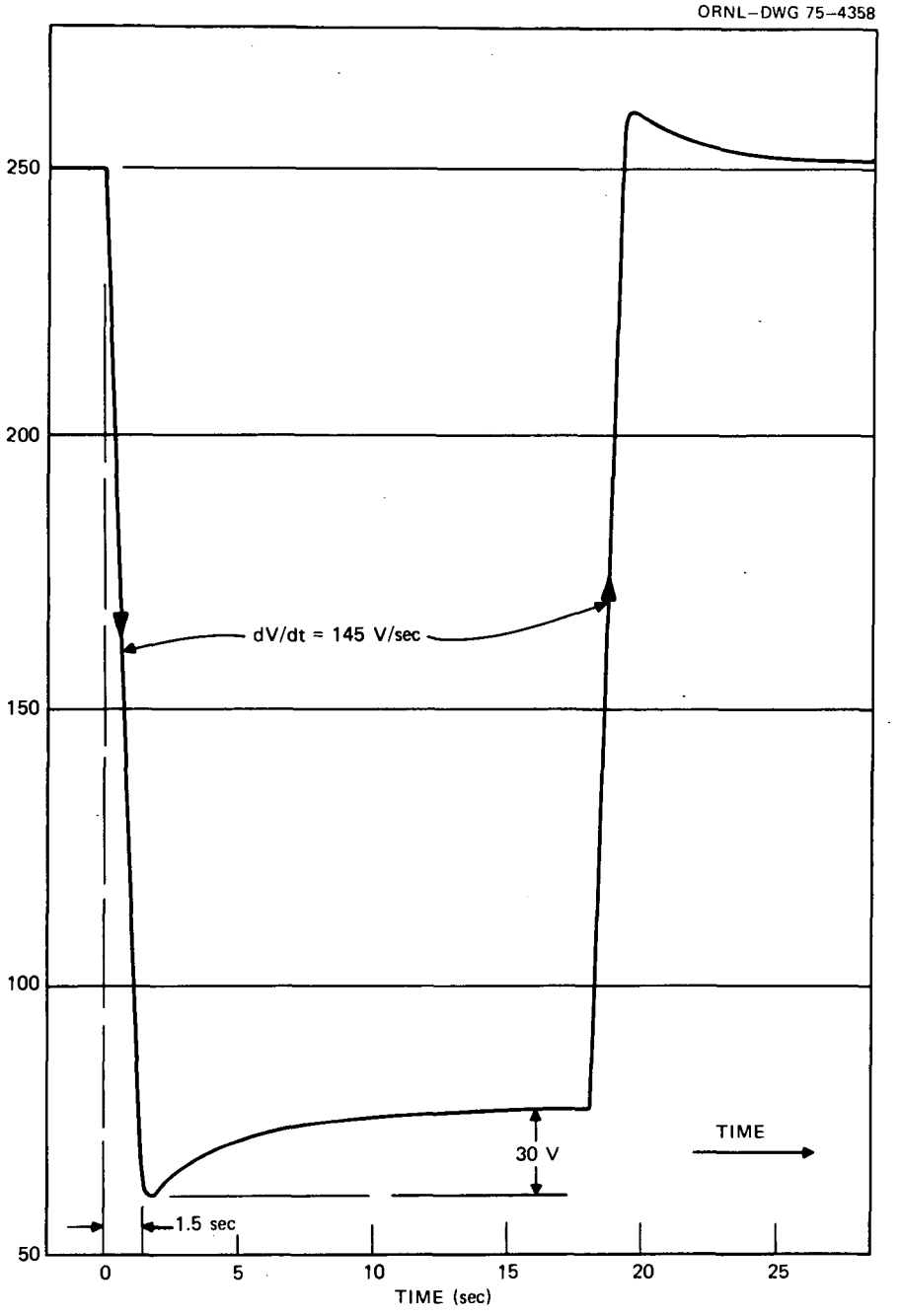

Fig. 1.16. Response of THTF dc generators to a step change in demand. Large signal – 75% step, 0.625 Ω load.

The test results indicate that the response of the existing regulator is fast enough to permit its use for decay heat programming. A circuit similar to that used for the step response tests will be used to obtain step setback action and to program step decays between two preset power levels during blowdown in those cases where the overshoot is tolerable. Simple exponential decays can be obtained by addition of a capacitor across the resistor to obtain the step action. More complex exponentials can be obtained by further addition of resistance capacitor networks in series with this resistor.

A function-generating type programmer will be used where decay characteristics other than simple step or exponential are required and/or where the overshoot is excessive. This programmer will replace the manually adjusted potentiometer presently used to develop the demand voltage.

1.3.2 Test Bundle Assembly

A. M. Smith

Assembly of the test bundle was completed, and the unit was placed in storage until it is required in the test facility.

The scratches which occurred along the length of the heaters installed during a trial assembly were reviewed and discussed with the manufacturer of the grids. Based on his recommendations, the dimension between the spacer tabs in each of the 13-grid plates was increased to reduce the built-in interference between the spacer tabs and the heater diameter. Using a special hardened steel tool, the vendor's representative increased the dimension between the tabs from 0.440 to 0.442 in. and reduced the diametrical interference to 0.002 in. This change in the spacer tab dimension did not eliminate the scratching but did reduce the depth to between 0.001 and 0.002 in. The scratches occurred as the heaters were drawn through each grid plate; therefore, as shown in Fig. 1.17, the scratches after the rods passed through the first grid plate were minor. Although every effort was made to keep the heaters absolutely straight as they were pulled through the grids, a closeup of a portion of the rods between the lower two grid plates showed several separate scratches along the heaters, indicating some rotation during axial travel. Figure 1.18

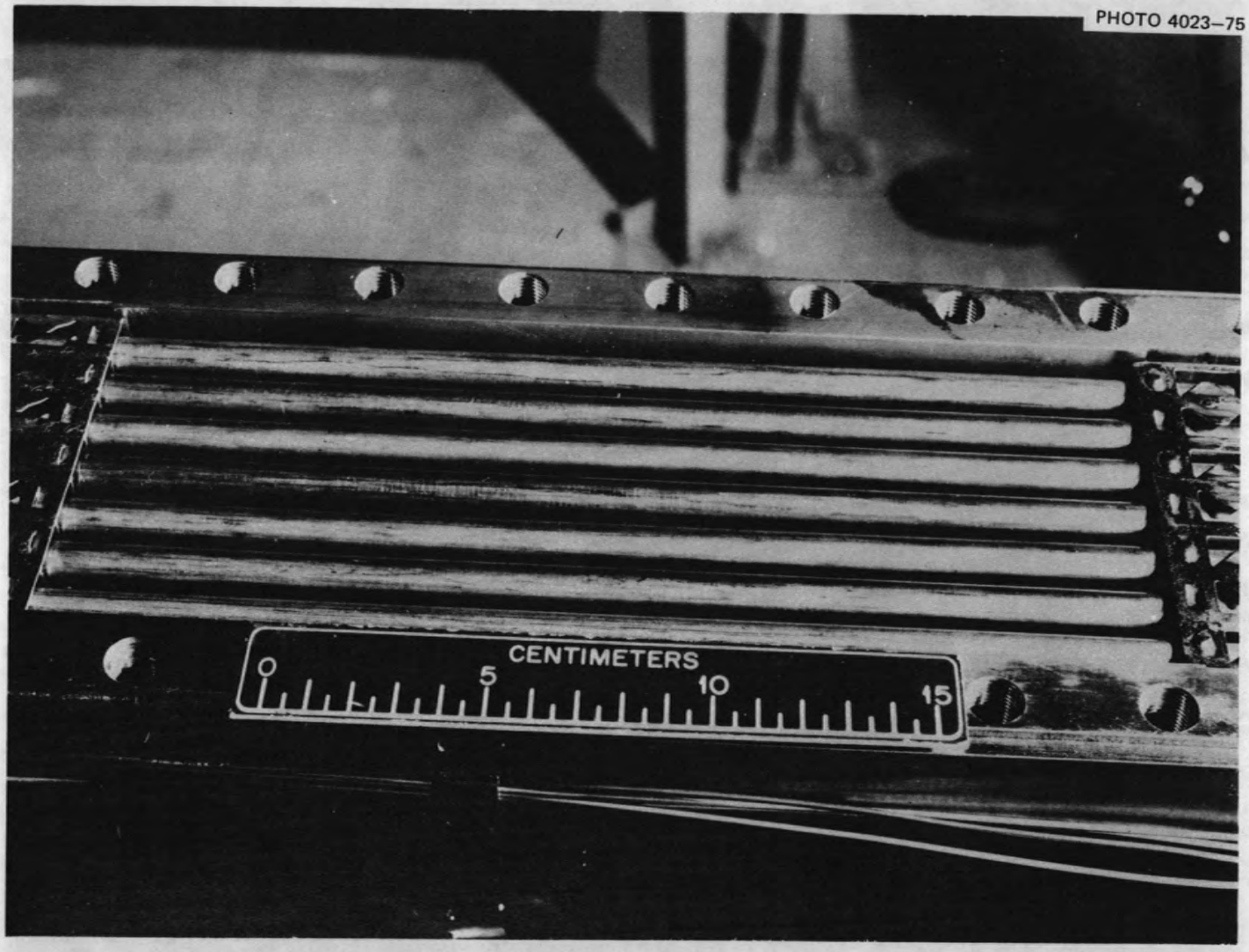

Fig. 1.17. Section of shroud box and test heaters located between the first and second grid spacers.

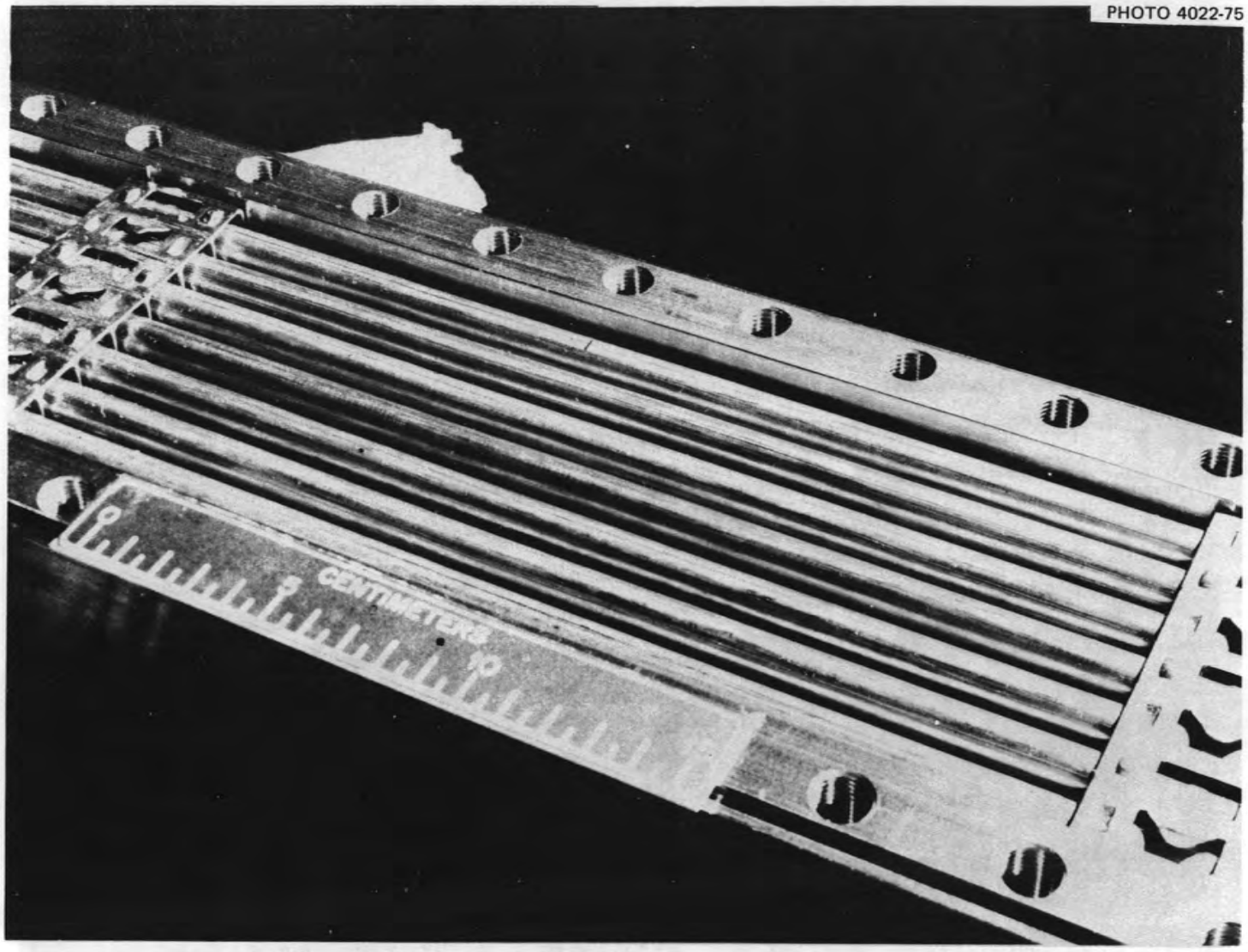

Fig. 1.18. Section of shroud box and test heaters located between the last two grid spacers.

shows an overall view of the heaters in the area between the two grid plates at the lower end of the bundle assembly. The resultant scratches are apparent.

During assembly of the test bundles, measurements were taken on the force necessary to pull the heaters through the grid plates. Heaters were inserted through the spool piece and the first two grid spacers by hand. A cable and pulling attachment connected to a hand winch was then connected to the bottom of the heater, and the heater was slowly pulled through the remaining grid spacers. During this operation, the heater sheath and grid spacers were lubricated with a mixture of distilled water and glycerine. The force necessary to pull the heaters was read from a spring scale attached to the winch. Figure 1.19 shows the shroud box, grid spacers, and winch attachment used to pull the heaters. Measurements varied from 20 lb force for movement through grid spacers one through four to a maximum of 140 lb as the heaters were moved through all 13 grid spacers. As the heaters were pulled further, the oversleeve on the heaters contacted the O-rings in the seal plates at the upper end of the spool piece and the readings noted increased to a maximum of 185 lb. During this assembly procedure, the seal plates, located on the top and bottom of the top flange, were separated from the flange to provide a means of checking for O-ring dislocations as the heaters were installed. Figure 1.20 shows the upper seal plate and flange arrangement with nine heaters installed.

After all heaters were installed in the assembly, the O-ring seal plates were moved along the heaters and bolted to the top flange. A water line was then connected to the upper flange, and the chamfer between the seal plates was pressurized to between 1000 and 1100 psig to check for seal leakage. Pressure decay tests showed the leak rate to be less than 2 standard cc/hr. Following this test, the top flange and heater rods were repositioned in the assembly, and the top flange was bolted to the flange on the spool piece. The assembly was then subjected to a second 1000-psig pressure decay test to check seal leakage across the O-rings. Again the leakage was of the order of 2 standard cc/hr.

The heater rods inside the shroud box and spool piece assembly were then cleaned using distilled water and alcohol to remove remaining traces of the glycerine used to lubricate the heaters during assembly. The

Y-12
PHOTO 158349

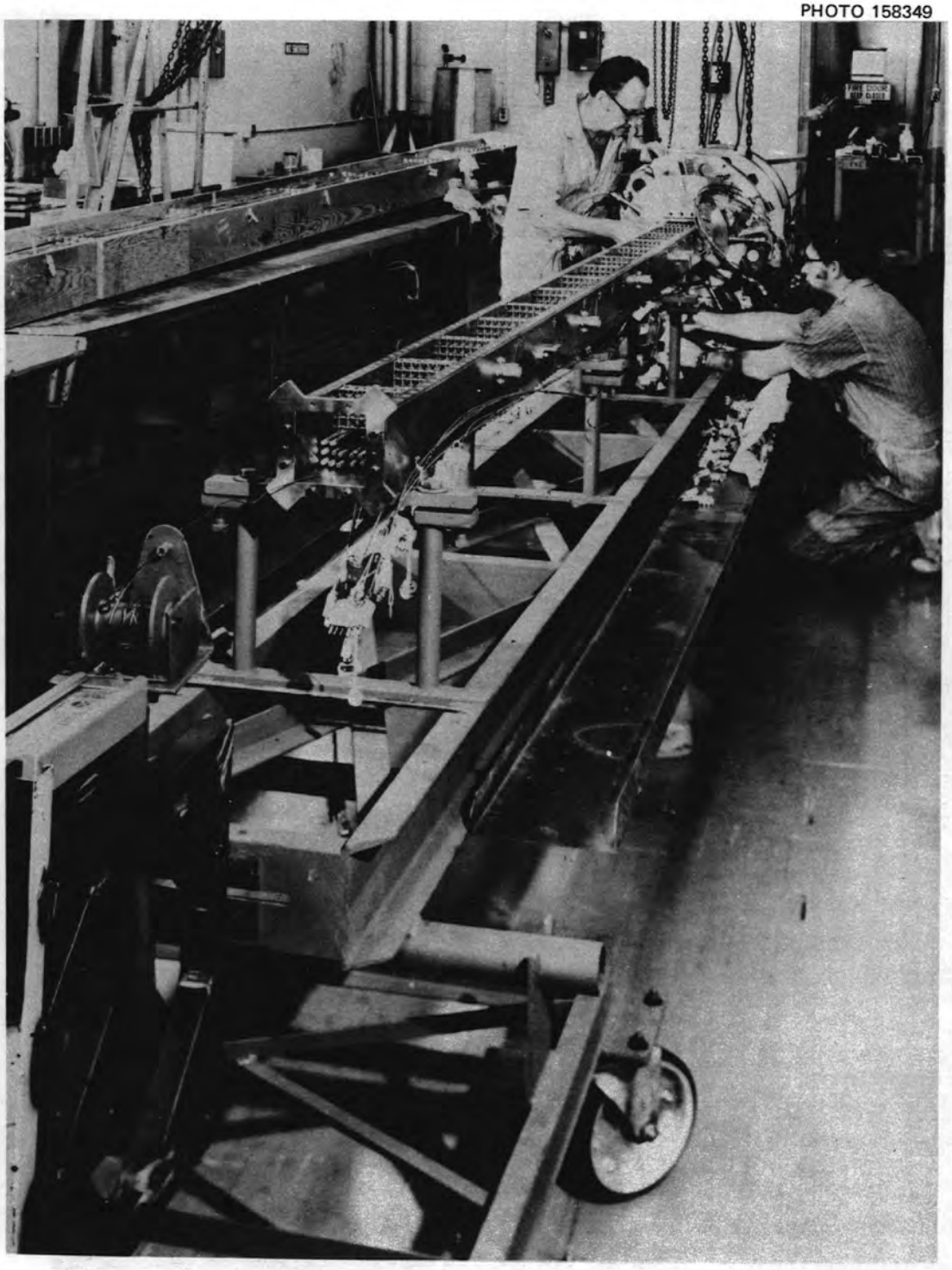

Fig. 1.19. Lower end of test bundle showing winch and scale arrangement used to measure force required to pull heaters during test bundle assembly.

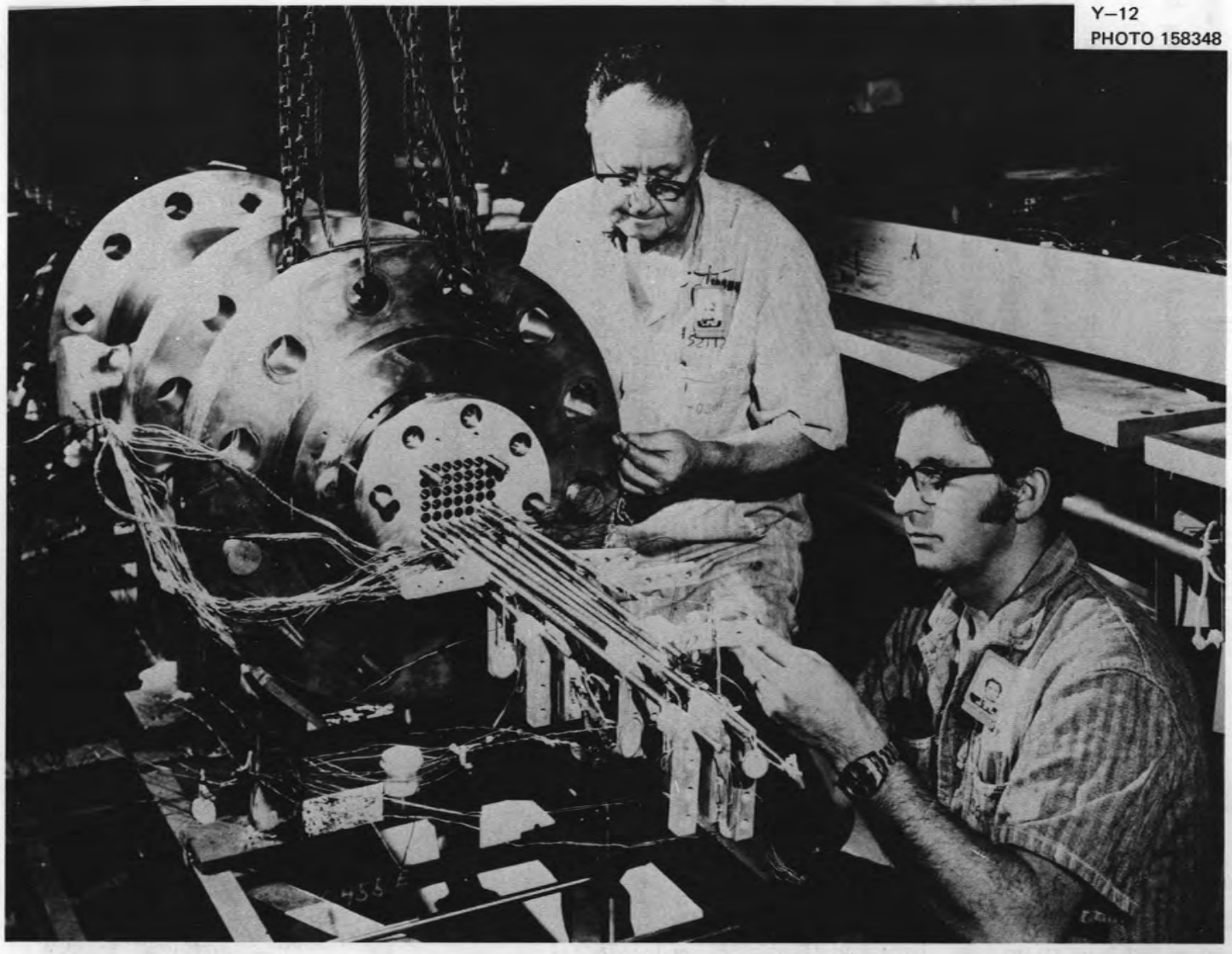

Fig. 1.20. Upper end of test section showing the top flange, top seal plate, and heaters during test bundle assembly.

shroud box cover was then installed as shown in Fig. 1.21. Spacers were also inserted between the heater rods extending beyond the end of the shroud box to help maintain the desired alignment and assist in the assembly into the electrical connector plate during the bundle insertion in the test facility.

At the upper end of the bundle assembly, the thermocouples in the individual heaters were separated into groups, the continuity rechecked, and several groups of thermocouples wrapped together to aid in the assembly. Figure 1.22 shows the thermocouples coming from the center of the heaters after they were checked and wrapped. Part of the thermocouples, located in the sheath of the heaters, are also shown inserted in the instrument duct bolted to the top flange assembly. A list of the usable thermocouples in each heater and the location in the test bundle is shown in Fig. 1.23. As can be seen, the majority of the unusable thermocouples are ones extending from the center of the heaters, which were found to be open when the heaters were received from the vendor.

Upon completion of the thermocouple check, the entire test bundle assembly was covered as shown in Fig. 1.24 and the unit put in storage until it is needed.

1.4 TWO-PHASE FLOW INSTRUMENTATION STUDIES

J. D. Sheppard

1.4.1 Densitometer Operation

One of the THTF gamma densitometers has been installed on the instrumented spool piece in the air-water calibration loop. The densitometer is a single beam instrument employing a 25-Ci ^{137}Cs source and is located at the center of the spool piece ~1 ft from both the turbine meter and drag disk.

Figure 1.25 shows some measurements of apparent density, ρ_a, as a function of superficial air velocity in the spool piece for two different water flow rates: 153 gpm (open circles) and 65 gpm (shaded circles). The two-phase flow was downward through the spool piece and a dispersing

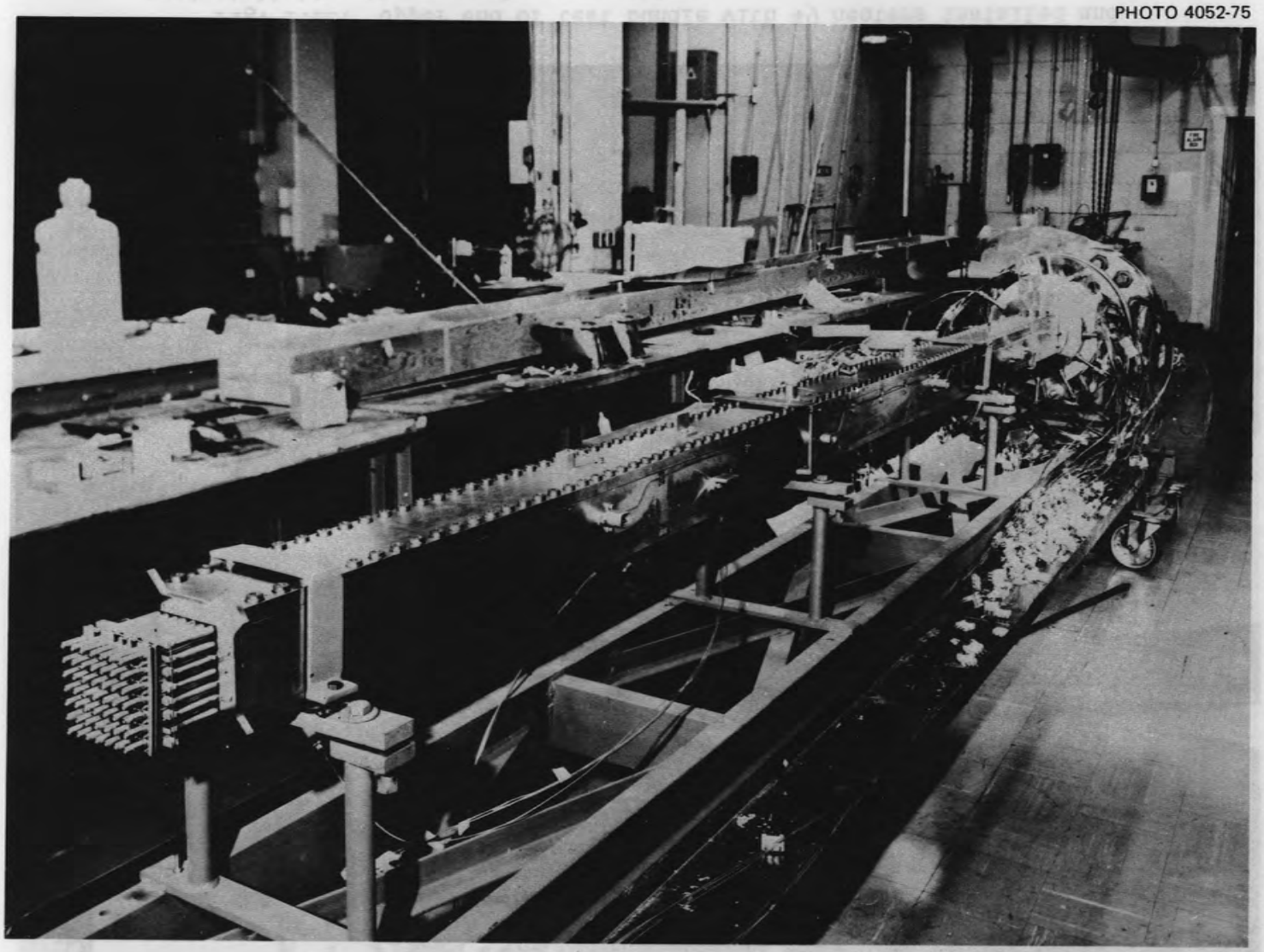

Fig. 1.21. Test bundle with heaters installed and shroud box cover installed.

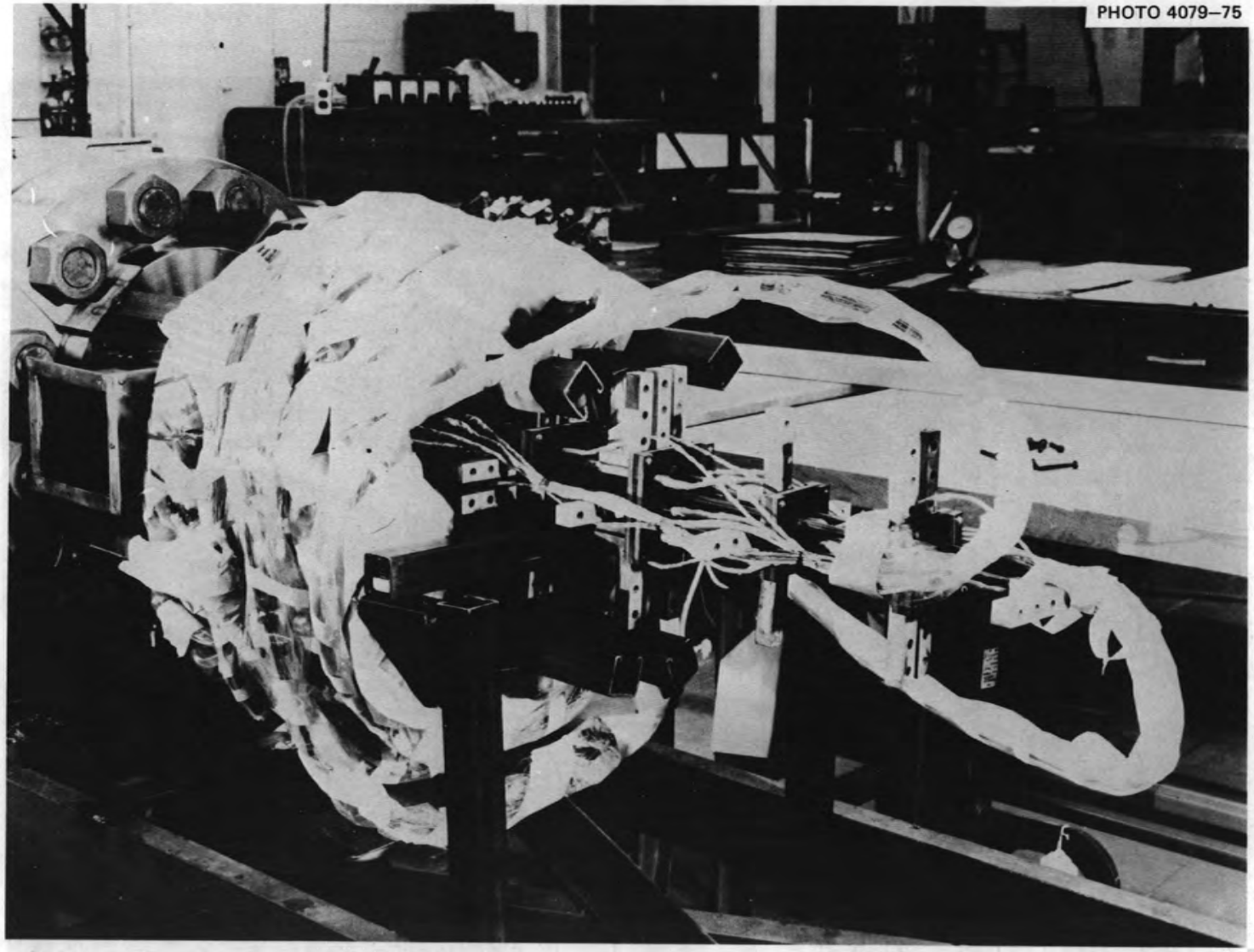

Fig. 1.22. Upper end of test bundle with 49 heaters installed and preinstallation thermocouple preparation.

ORNL-DWG 75-4534

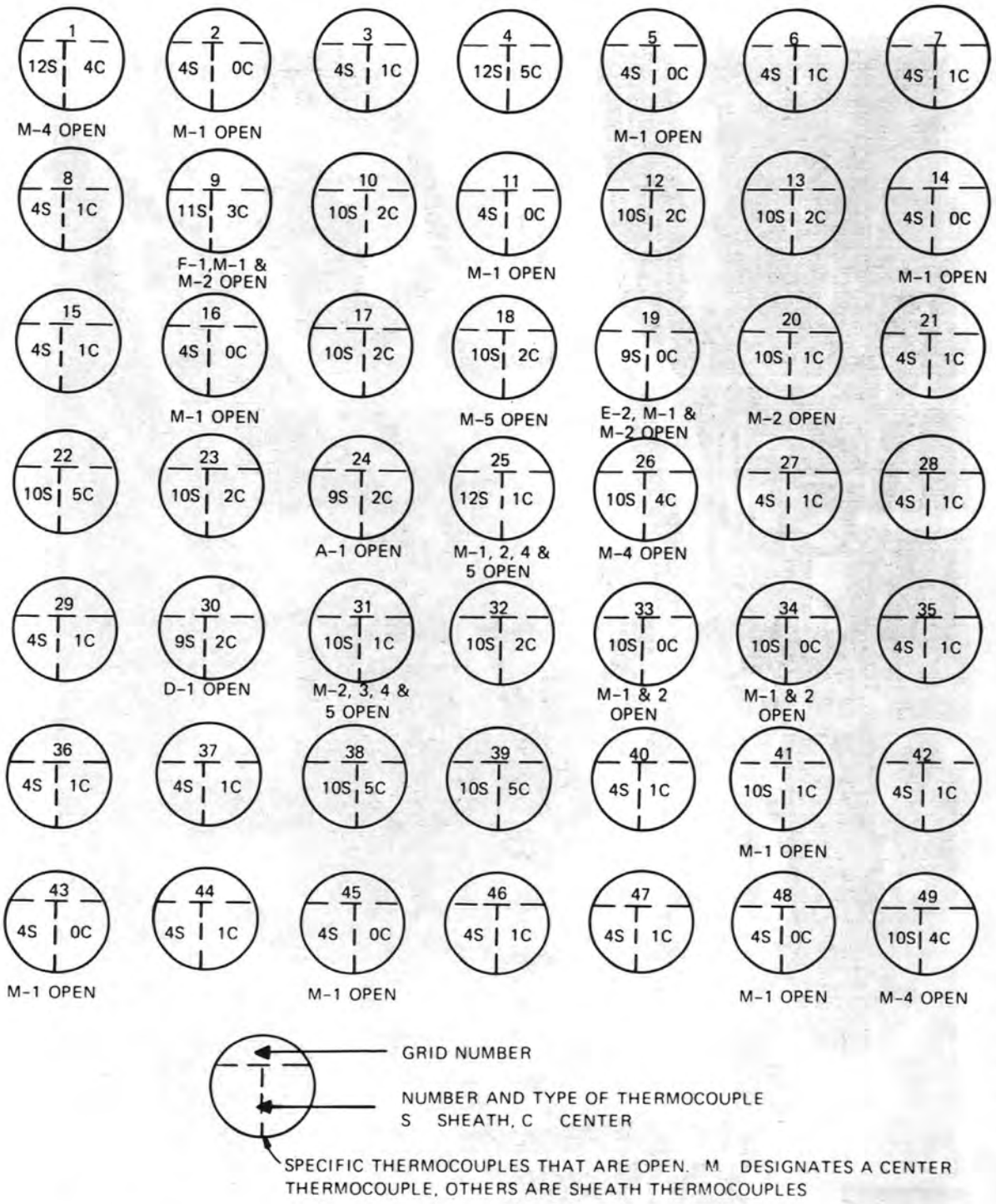

Fig. 1.23. Distribution of thermocouples in THTF test bundle No. 1.

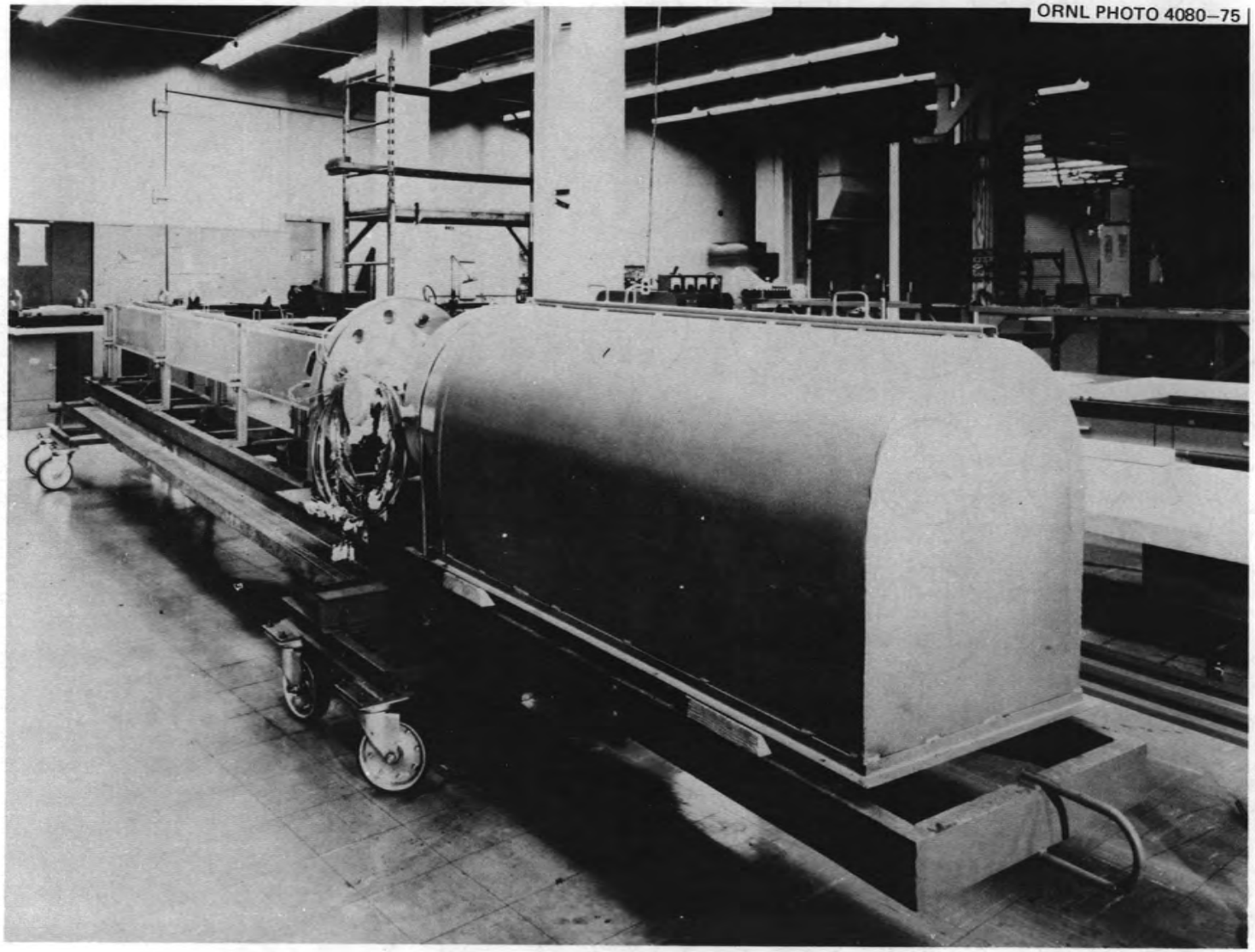

Fig. 1.24. Test bundle assembly with protective covers installed.

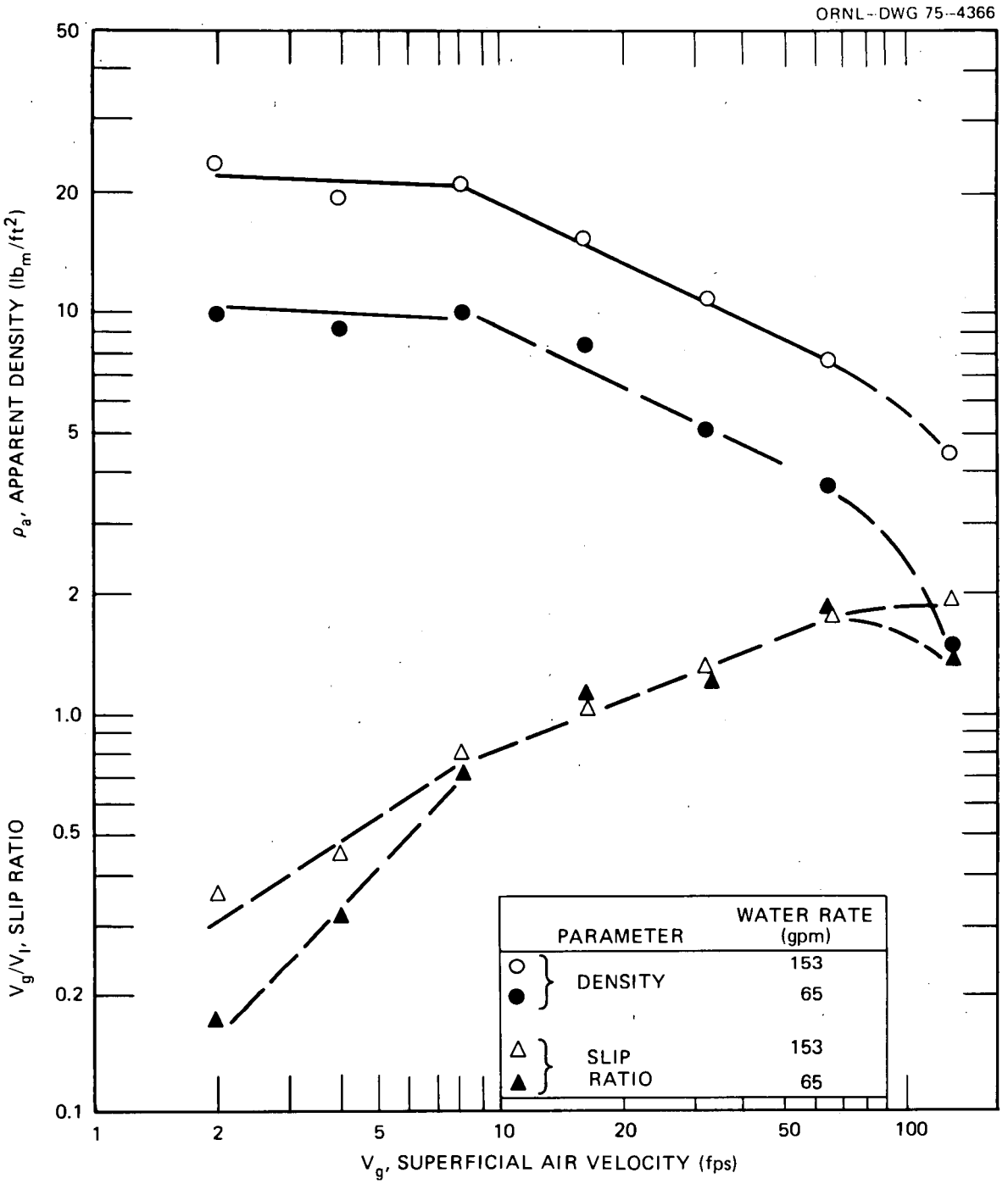

Fig. 1.25. Air-water density and slip ratio in instrumented spool piece as a function of air and water flow rates (vertical flow; 3.5-in.-ID pipe; single beam gamma densitometer).

screen (one 44-mesh, 5-mil-wire screen between two 8-mesh, 62-mil-wire screens) was located at the inlet flange of the spool piece; the drag disk was upstream of the densitometer and the turbine meter was downstream. The figure shows that when the water flow was constant, the apparent density was little affected by air flow rates from 2 to 8 fps (superficial velocity). However, for air velocities from 8 to 64 fps, the apparent density decreased with the square root of the air velocity, and the figure suggests that the density may decrease more rapidly at a higher velocity.

Assuming the flow of each phase is represented by a characteristic velocity (two-velocity model), the continuity relationship for each phase is

$$\alpha V_g = \alpha_h V_{gh} \tag{1}$$

and

$$(1 - \alpha) V_\ell = (1 - \alpha_h) V_{\ell h} \quad , \tag{2}$$

where α is the void fraction and subscripts g, ℓ, and h indicate gas, liquid, and homogeneous phases respectively. Of course, when assuming homogeneous flow V_{gh} and $V_{\ell h}$ are equal. Combining the continuity equations with the definition of apparent density,

$$\rho_a = \alpha \rho_g + (1 - \alpha) \rho_e \quad , \tag{3}$$

gives an expression for the slip ratio for the two-velocity model in terms of the apparent density and the homogeneous condition

$$\frac{V_g}{V_\ell} = \left(\frac{\rho_a - \rho_g}{\rho_f - \rho_a}\right)\left(\frac{\rho_f - \rho_h}{\rho_h - \rho_g}\right). \tag{4}$$

Figure 1.25 also shows calculated slip ratios based on Eq. (4); homogeneous densities were determined from the known input flow rates of air and water.

At the lower air flows, when density was not significantly affected by air velocity, the slip ratio was less than unity; this result suggests that the two-velocity model does not adequately represent the two-phase flow. However, it is notable that over the range of superficial air

velocities (8 to 64 fps), the slip ratio was greater than unity; and, at a given air velocity, the slip ratio was essentially the same for both water flow rates.

The flow regime map of Govier and Aziz[4] for vertical pipe flow, Fig. 1.26, shows that for the water flow rates of 65 and 153 gpm (2.2 and 5.1 fps superficial velocity) and superficial air velocities of 2 to 8 fps, flow is in the slug flow regime. As the air flow is increased at fixed water flow, froth and annular mist flows are approached. Due to the nature of slug flow, it is not surprising that a simple two-velocity model is not adequate to describe the slip ratio.

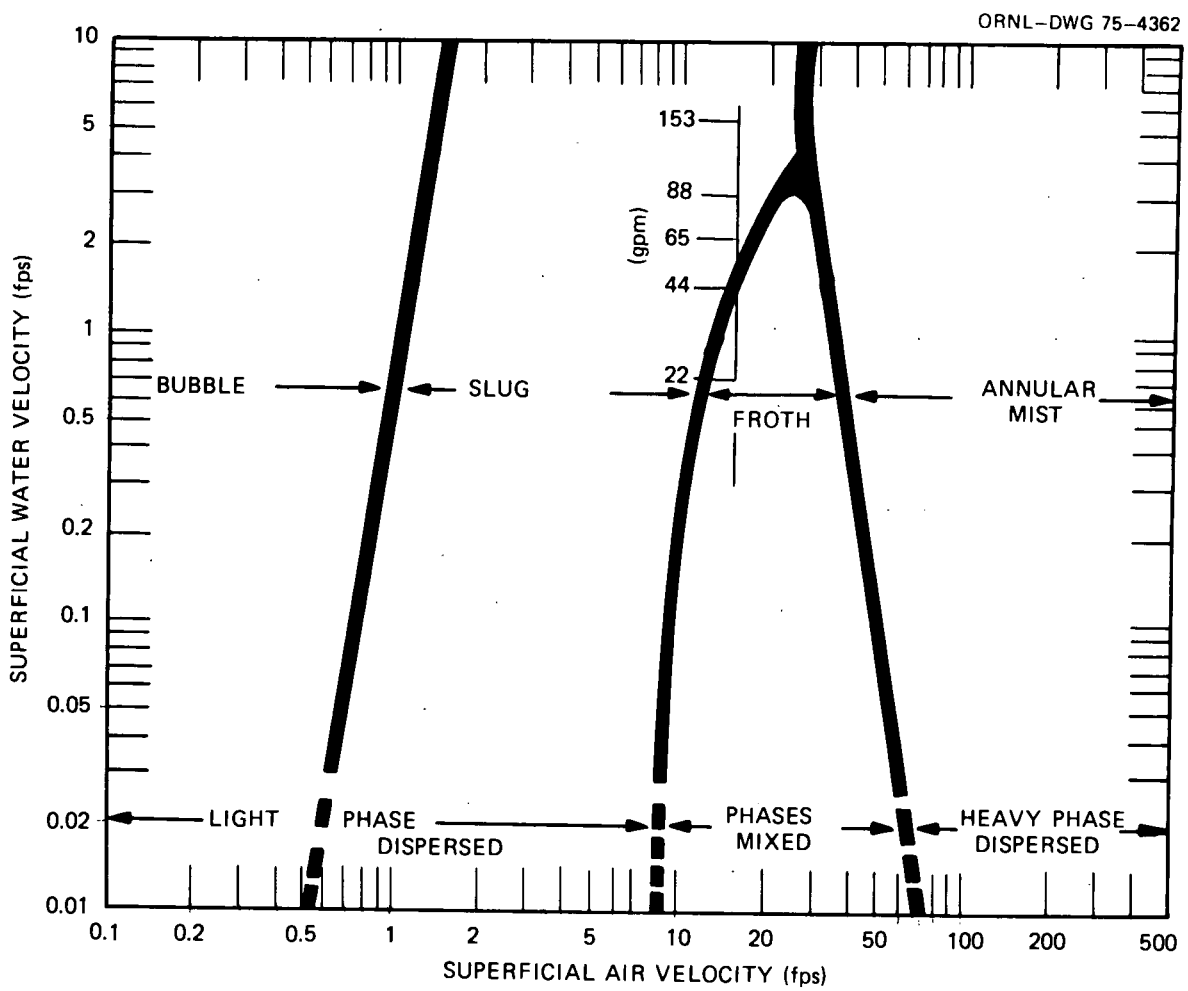

Fig. 1.26. Flow regime map of Govier and Aziz (1972) showing range of current experiments and application of Eq. (1) in text.

Flow regime effects

The flow regime map has also been useful in studying changes in the character of instrument signals. For example, Fig. 1.27 shows the recording of the turbine meter and drag disk signals at an air flow of 64 scfm (16 fps superficial velocity). The two phases were discharging downward through the spool piece, and a flow disperser (three 10-mesh 25-mil-wire screens) was located at the upstream flange of the spool piece. As the water flow was decreased from 153 to 88 gpm, the amplitude of the instrument signal fluctuation, particularly that of the turbine meter, increased significantly although the mean signal decreased. Further, a periodicity appeared in the turbine meter signal and persisted as the water flow was decreased to 44 gpm (1.5 fps). That the "beat phenomenon" was more distinct in the turbine meter reading probably reflects the fact that the turbine meter was farther downstream from the flow dispersing screen than was the drag disk.

It is notable that decreasing water flow rate to 22 gpm (0.73 fps) effectively decreased the fluctuation of the signal about the mean value and eliminated the strong beat phenomenon in the turbine meter reading. The beat phenomenon had a low frequency of 2 to 4 per minute. Inspection of Fig. 1.26 shows that as the water flow rate is decreased from 5.1 to 0.73 fps at an air velocity of 16 fps, a transition occurs from slug flow to froth flow. The beat phenomenon apparently results from the hydrodynamic instability associated with the transition region between slug and froth flow, which appears to be quite broad.[1] The flow regime map shows that the distinct change in instrument signal quality as the water flow was decreased from 44 to 22 gpm (1.5 to 0.73 fps) was the result of traversing through the transition region to fully froth flow.

Figure 1.28 shows turbine meter and drag disk signals as a function of water flow rate at a constant air flow rate of 256 scfm (64 fps superficial velocity). Inspection of Fig. 1.26 shows that this operation was in the annular-mist flow regime. As the water flow rate was decreased from 153 to 65 gpm, both instruments indicated decreasing flow rates and improvement in signal quality (i.e., reduced fluctuation around the mean signal). However, it is remarkable that when the water flow rate was

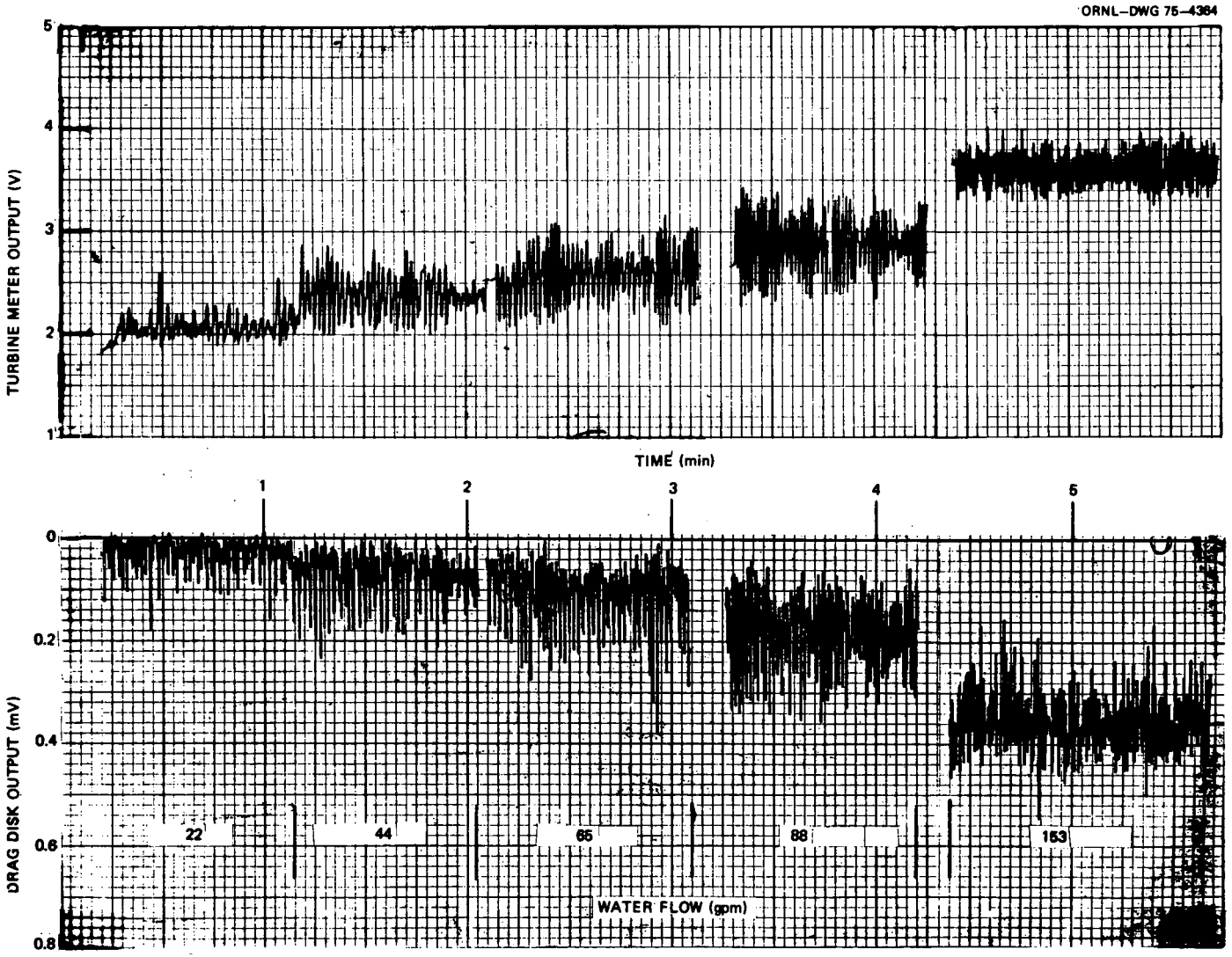

Fig. 1.27. Turbine meter and drag disk readings as functions of time and water flow rate at a superficial air velocity of 16 fps (downward flow through instrumented spool piece with three 10-mesh, 25-mil-wire flow disperser; turbine voltage attenuated by a factor of two).

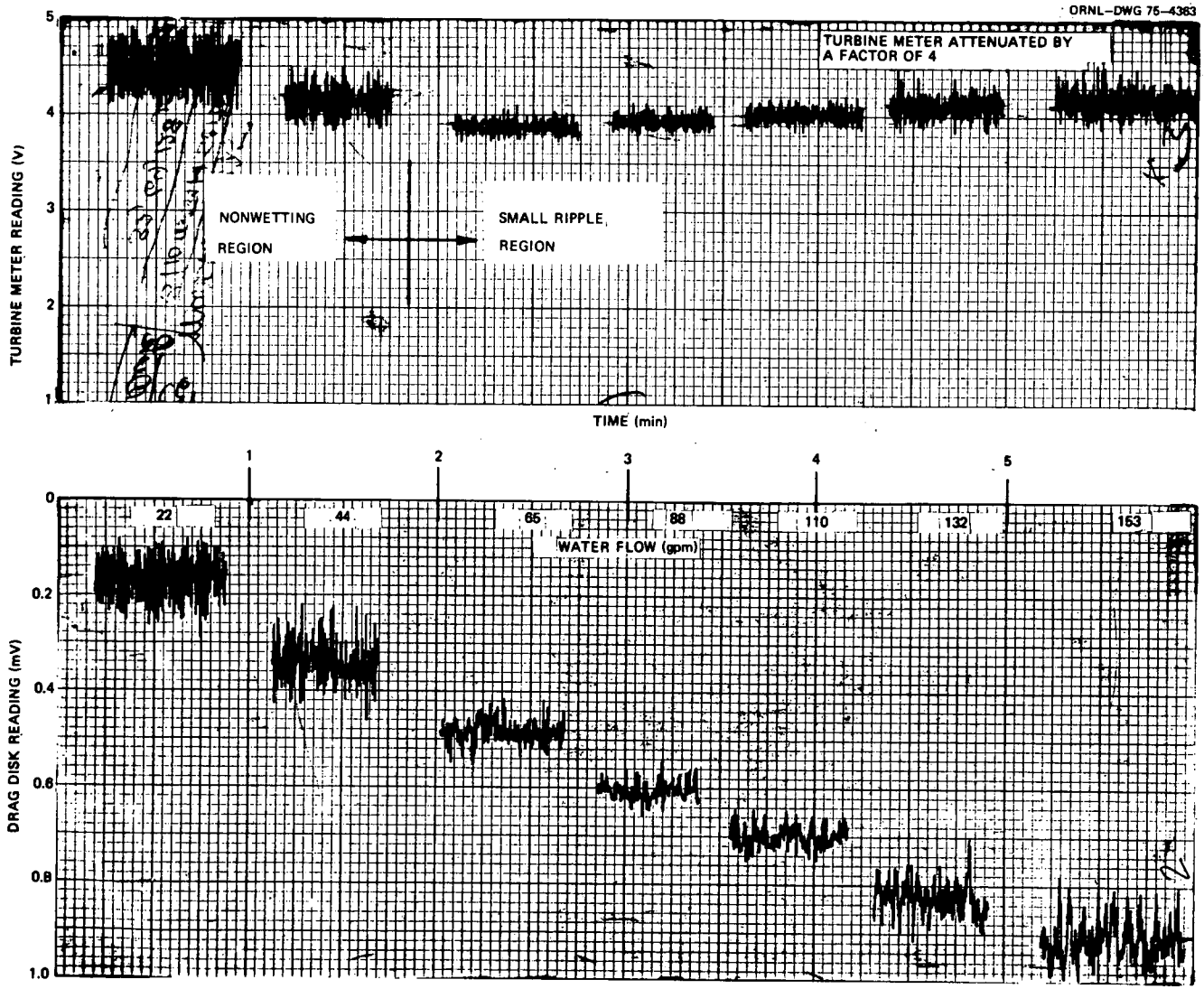

Fig. 1.28. Turbine meter and drag disk readings as functions of time and water flow rate at 64 fps superficial air velocity (three 10-mesh, 25-mil-wire screen disperser; downward flow; 3.5-in.-ID pipe).

decreased further to 44 gpm, signal fluctuations increased significantly for both instruments and the turbine meter showed an increase in flow rate. This trend continued as the water flow rate was decreased to 22 gpm.

The flow regime map of Govier and Aziz[4] does not show a phase transition over these ranges of flow rates. However, studies of Shearer and Nedderman[5] show that the flow rates at which transition was observed in the instrument signals correspond to minimum transport conditions for the adherence of a water film to the pipe wall. That is, at 64 fps air velocity, the annular film of water on the pipe wall thins as the water flow rate decreases until the water rate is too small to maintain the film. This high-gas-velocity, low-water-velocity region has been called the nonwetting region.[5] We are continuing to study mechanisms that may contribute to such extreme changes in signal quality as are observed in this transition from the wetting to the nonwetting region.

Flow dispersing screens

Installation of the gamma densitometer permits determination of two-phase flow rates in the same manner as at the THTF. That is, using any two of the three primary flow instruments, the mass flow rate can be calculated according to "one-velocity" models,

$$G = \rho_a V_T \quad , \tag{5}$$

$$G = \rho_a \left[\rho V_{DD}^2 / \rho_a \right] \quad , \tag{6}$$

or

$$G = \overline{\rho V_{DD}^2} / V_T \quad , \tag{7}$$

where ρ_a is the apparent density given by the densitometer, V_T is the characteristic velocity given by the turbine meter, and $\overline{\rho V_{DD}^2}$ is the momentum flux measured by the drag disk. Further, mass flow can be determined using all three instrument readings and a two-velocity slip model such as that proposed by Aya:[6]

$$G = \alpha \rho_g V_g + (1 - \alpha) \rho_\ell V_\ell \quad . \tag{8}$$

The void fraction α is given by density measurements [Eq. (3)], and the

two-phase velocities V_g and V_ℓ are determined by a model for the action of the two phases on the turbine and drag disk.[4] If the two-phase flow is well dispersed and the velocity characteristic of the turbine meter is the same as the velocity characteristic of the drag disk, one would expect the mass flow given by Eqs. (5) through (7) to be the same.

Figures 1.29 and 1.30 show the mass flow rate calculated using Eqs. (5) to (8) for two-phase flow operation over a range of superficial air velocities of 2 to 128 fps and at two water flow rates, 65 and 153 gpm. Each test included the use of a flow disperser at the inlet flange of the spool piece; for one test, Fig. 1.29, the flow disperser consisted of three stacked 10-mesh, 25-mil-wire screens; for the other test, Fig. 1.30, the flow disperser consisted of two 8-mesh, 62-mil-wire screens separated by a single 44-mesh, 5-mil-wire screen. The solid line through each set of data represents the actual mass flow rate metered into the system. Since the highest superficial air velocity of 128 fps contributes only about 9 $lb_m\ sec^{-1} ft^{-2}$ to the total mass flow rates for these tests (~140 and ~320 $lb_m\ sec^{-1} ft^{-2}$), there is little change in the actual mass flow over nearly two orders of magnitude change in air velocity.

Both figures show better agreement among the four models at higher water and air flows. When the flow disperser was three 10-mesh screens (Fig. 1.29), the range in mass flow rate determined by the three homogeneous models was as much as 80% of the actual flow rate at 65 gpm water and low air flow rate. At higher water flow (153 gpm), the scatter of data among models reduced to a range typically about 25% of the actual flow rate. It is notable that in each case Eq. (5) gave high results, Eq. (7) gave low results, and mass flows determined by Eq. (6) using the densitometer and drag disk were essentially the same as those of the two-velocity model, Eq. (8).

Inspection of the Fig. 1.30 shows that with the exception of data at water flows of 65 gpm and low air flow, the agreement among all calculational models was decidedly better for this test, which utilized the heavier screens (8-mesh, 62-mil-wire). At the high water flow rate, agreement was good, with essentially no difference among models over the entire range of air flows. The flow regime map, Fig. 1.26, shows that at air velocities less than 16 fps, operation was in the slug flow regime,

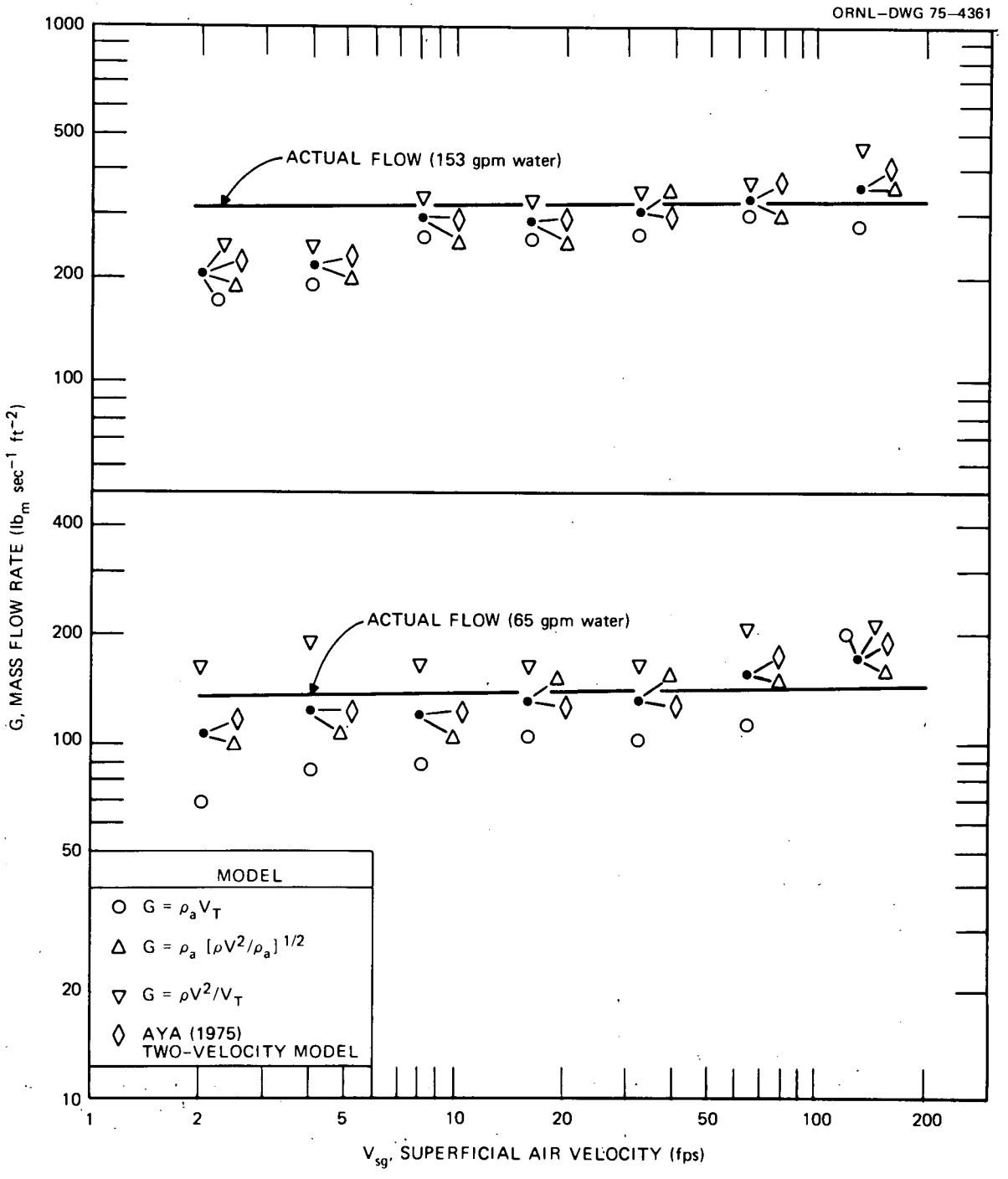

Fig. 1.29. Mass flow rate in instrumented spool piece, inlet disperser consisting of three 10-mesh, 25-mil-wire screens, as determined by homogeneous or two-velocity flow models (air-water; 3.5-in.-ID pipe).

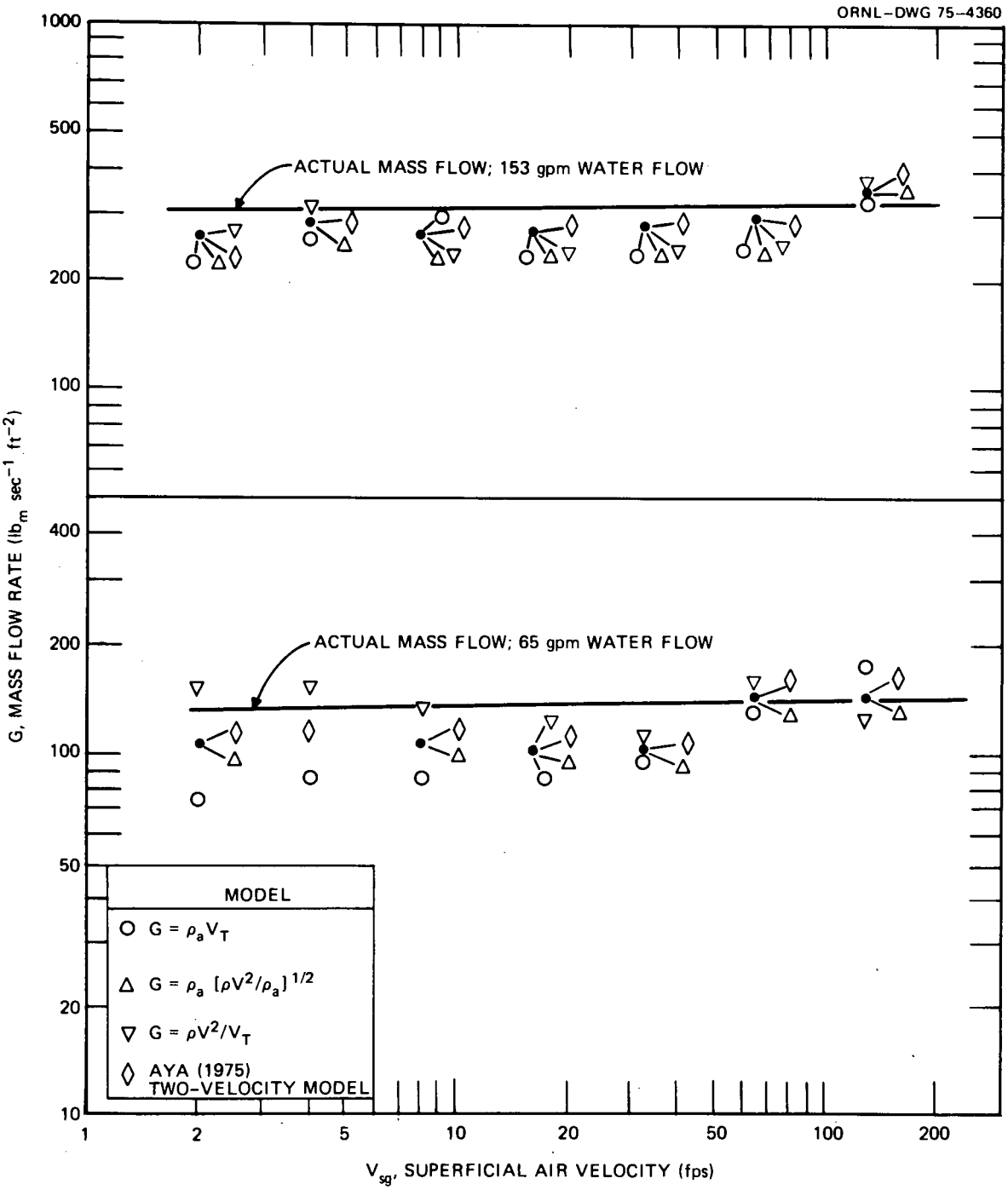

Fig. 1.30. Mass flow rate in the instrumented spool piece as determined by homogeneous and two-velocity flow models (inlet flow disperser was two 8-mesh, 62-mil wire screens separated by a single 44-mesh, 5-mil-wire screen; air-water).

clearly a challenge for any flow disperser. Generally, results were better in the slug flow regime when the disperser consisting of the heavier wire (two 8-mesh, 62-mil-wire screens) was used.

Further, since the deviation in results among models was generally characterized by Eq. (5) giving high results and Eq. (7) giving low results, we expect that the turbine meter was giving characteristic velocities that were lower than the homogeneous characteristic velocity. That is, since the turbine meter was farthest downstream from the flow disperser, ineffective dispersion at the spool piece inlet may be detected more readily in the turbine meter readings. If this is a valid assumption, Figs. 1.29 and 1.30 show that the two 8-mesh (62-mil-wire) screens separated by the single 44-mesh (5-mil-wire) screen dispersed flow more completely than did the three 10-mesh (25-mil-wire) screens.

One distinct difference in these two dispersers is their pressure drop characteristics. Figure 1.31 shows the pressure drop across the spool piece with no disperser and with each of the two dispersers discussed above. Superficial air velocity in the spool piece was 128 fps, and total mass flow ranged from 54 to 330 $lb_m\ sec^{-1} ft^{-2}$ (22 to 153 gpm water flow). Under these conditions, the pressure drop across the spool piece alone ranged from 4 to 10.6 psi; and, with the three 10-mesh screen disperser, the pressure drop ranged from 4.8 to 14.2 psi, 0.8 to 3.6 psi greater than that of the spool piece alone. However, pressure drop of the spool piece with the heavy wire/screen disperser ranged from 11.5 to 38 psi, 7.5 to 28 psi greater than that of the spool piece alone.

Studies of the decay of single-phase isotropic turbulence have shown that the magnitude of the fluctuating component of velocity, $(u')^2$, is a linear function of the drag coefficient of the grid.[7] Further, the magnitude of $(u')^2$ decreases linearly with distance downstream of the grid. Therefore, the induced velocity fluctuations will be stronger at a point downstream of the grid for grids with greater drag coefficients. Hinze[7] also reports that for a number of square-mesh grids of round bars the drag coefficient was a function of only the ratio of bar diameter, d, to mesh width, M,

$$C_D = \frac{(d/M)(2 - d/M)}{(1 - d/M)^4} \quad ; \tag{9}$$

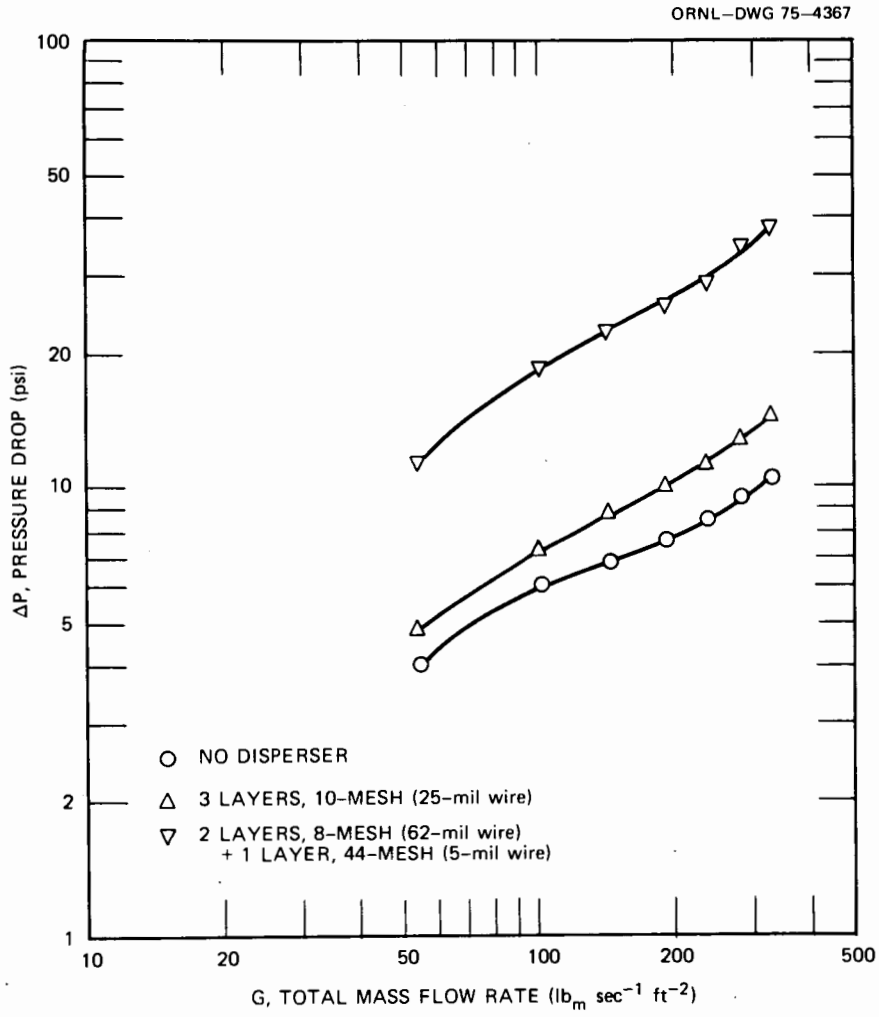

Fig. 1.31. Pressure drop across instrumented spool piece with different flow dispersers located at the inlet flange (air-water system; 128 fps superficial air velocity; 3.5-in.-ID pipe).

that is, two single screens with similar d/M ratios should have similar pressure drop characteristics and similar rates of decay of isotropic turbulence.

A high turbulence level should moderate the gross fluctuations in the two-phase flow by dispersing the liquid phase. So, based on the above discussions, it is expected that flow dispersers with greater drag coefficients would result in instrument signals with less fluctuation. Figure 1.32 shows the average fluctuations in the drag disk signal (in millivolts)

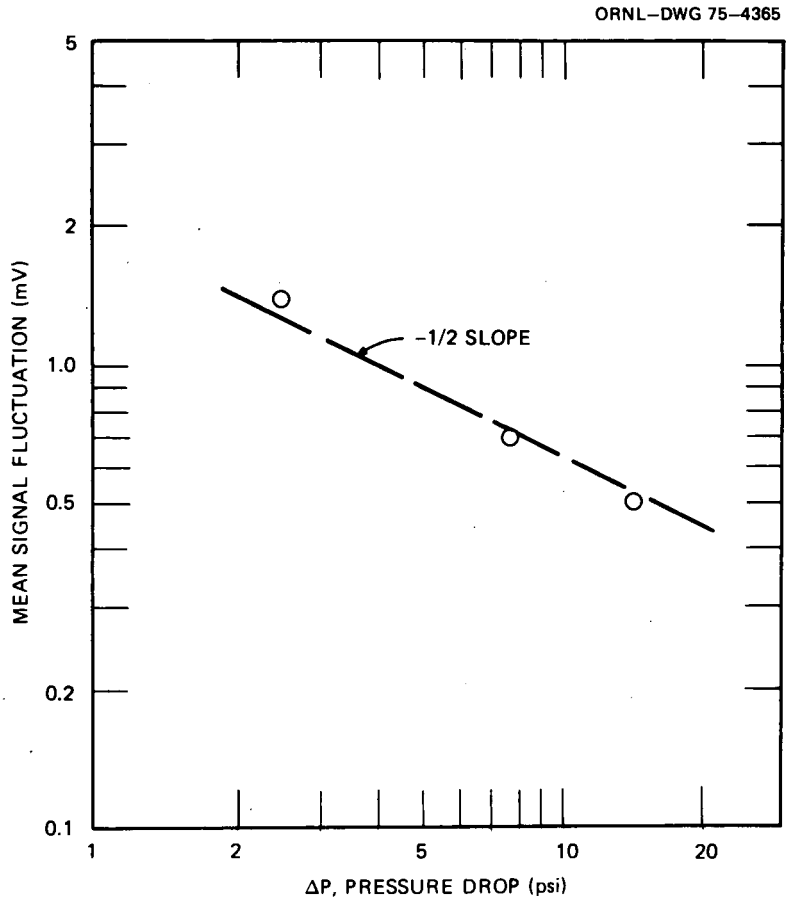

Fig. 1.32. Relationship between pressure drop across flow dispersers and mean fluctuations in the drag disk signal (drag disk located 6 in. downstream of dispersers; air-water system; 3.5-in.-ID pipe).

as a function of the pressure drop across three different dispersers. The fluctuation decreased with the half-power of the pressure drop, or according to the above discussion, the fluctuation in the drag disk signal decreased linearly with an increase in the rms component of turbulence $\sqrt{(u')^2}$. Further, these results are consistent with data shown in Figs. 1.29 and 1.30, which show that dispersion by the low-pressure-drop screen (see Fig. 1.29) was not sufficiently strong to effect accurate signals from the turbine meter far downstream from the disperser, whereas results from the higher pressure drop screens (see Fig. 1.30) indicate dispersion was sufficient so that both the drag disk and turbine saw similar flow distributions.

REFERENCES

1. Quarterly Progress Report on Reactor Safety Programs Sponsored by the Division of Reactor Safety Research for October–December 1974. I. Light-Water-Reactor Safety, ORNL-TM-4805, Vol. 1.

2. Quarterly Progress Report on Reactor Safety Programs Sponsored by the Division of Reactor Safety Research for April–June 1974. I. Light-Water-Reactor Safety, ORNL-TM-4655, Vol. 1, pp. 4–6.

3. W. M. Rohsenow and J. P. Harnett, Handbook of Heat Transfer, pp. 3.14–3.15, McGraw-Hill, New York, 1973.

4. G. W. Grovier and K. Aziz, The Flow of Complex Mixtures in Pipes, p. 337, Van Nostrand Reinhold, New York, 1972.

5. C. G. Shearer and R. M. Nedderman, "Pressure Gradient and Liquid Film Thickness in Co-Current Upwards Flow of Gas/Liquid Mixtures: Applications to Film-Cooler Design," Chem. Eng. Sci., 20, 671 (1965).

6. I. Aya, A Model to Calculate Mass Flow Rate and Other Quantities of Two-Phase Flow in a Pipe with a Densitometer, a Drag Disk, and a Turbine Meter, ORNL-TM-4759 (1975).

7. J. O. Hinze, Turbulence, p. 214, McGraw-Hill, New York, 1959.

2. NUCLEAR SAFETY INFORMATION CENTER

Reactor Division
Wm. B. Cottrell and J. R. Buchanan

In 1963, the Nuclear Safety Information Center (NSIC) was established by the USAEC as a focal point for the collection, analysis, and dissemination of information for the benefit of the nuclear community. It aids those concerned with analysis, design, and operation of nuclear facilities by providing, and/or identifying, relevant information on their nuclear safety problems.

The capabilities of the Center's technical staff are augmented by a computer file that contains 100-word abstracts of over 95,600 nuclear safety documents and is increasing at the rate of 12,000 documents per year. (This total does not include approximately 5000 documents, vintage 1962–1964, which were not added to the computer file when it was initiated in 1965.) Pertinent abstracts are readily retrievable from the computer to meet a number of requirements. These files are frequently queried for retrospective bibliographies to aid the staff in answering technical inquiries. The files are also extensively used during preparation of NSIC reports and review articles for the bimonthly journal, *Nuclear Safety*. A routine form of reference output from the storage files is a biweekly Selective Dissemination of Information (SDI) program that selects references according to individual user requirements. This computerized capability has recently been extended by the inclusion of the NSIC file on the ERDA RECON system where it may be accessed by the RECON network.

To date, NSIC services have been free to all users, but charges to non-ERDA and -NRC (or ERDA or NRC subcontract) users of NSIC are to be instituted in FY-75 as a result of a recently approved ERDA pricing policy for all of its information centers.

2.1 ROUTINE SERVICES

During the months of January, February, and March 1975, the staff of NSIC (a) entered 3374 documents, (b) responded to 338 inquiries, (c) received 12 visitors, (d) attended 36 meetings, (e) issued three bibliographies of safety documents for the ACRS staff, and (f) prepared data sheets on two new nuclear power stations. Our biweekly mailing of new references selected to match the recipient interest profile was limited to some 200 ERDA-NRC users (plus some trial usage) because of funding limitations. It is expected that the announced ERDA pricing policy will provide a mechanism for other potential users to receive this material. It should also be noted that the 3374 documents entered this quarter (about average) include only a selected fraction of the reactor licensing literature which we receive. While copies of all this literature are on hand, much of it is of limited value and is not being added to the computerized file.

2.2 SPECIAL ACTIVITIES

At the request of the Office of Nuclear Regulatory Research (ONRR), we prepared a special compilation of all reports issued by ONRR contractors since January 1974. This recent compilation identified 114 documents and updated a previous compilation.

Another unusual activity relating to the work of the Center which occurred during the period was our participation through a manned display in the visit and tour of Oak Ridge facilities by the Tennessee State Legislature on February 5. We received numerous requests for NSIC reports and *Nuclear Safety* from the over 100 members of the Legislature and their staff who attended the presentation.

The Laboratory has not yet implemented the practice of "cost recovery" for information services rendered to non-ERDA and non-NRC personnel, pending resolution of several problems with the proposed mechanics. However, these were largely resolved at a meeting in March involving Headquarters, ORO, and Laboratory personnel, and we are now awaiting a clarifying directive.

2.3 ORNL-NSIC REPORTS

Work was continued or initiated on several reports as follows:

1. ORNL-NSIC-116, "Index to Nuclear Safety" [Volume 11(1) — Volume 15(6)] (in reproduction).
2. ORNL-NSIC-117, "Protection of Nuclear Power Plants Against External Disasters" (in reproduction).
3. ORNL-NSIC-119, "A Selected Bibliography on Pressure Vessels for Light-Water-Cooled Power Reactors" (in reproduction).
4. ORNL-NSIC-83, "Reliability Engineering Methods in Reactor Safety Technology" (being revised).
5. ORNL-NSIC-55, Volume IV, "Design Data and Safety Features of Commercial Nuclear Power Plants" (composition completed).
6. ORNL-NSIC-118, "Siting of Nuclear Facilities - Reviews from Nuclear Safety" (preparation initiated).
7. ORNL-NSIC-120, "Annotated Bibliography on Hydrogen Considerations in Light-Water-Power Reactors" (in preparation).
8. ORNL-NSIC-121, "Abnormal Reactor Operating Experiences 1972—1974" (in preparation).
9. ORNL-NSIC-122, "Annotated Bibliography of Safety-Related Occurrences in Nuclear Power Plants as Reported in 1974" (final draft completed).

2.4 SYSTEM DEVELOPMENTS

The NSIC master file of abstracts became operational on the ERDA RECON remote terminal system in August 1974. During the reporting period, the NSIC file was used by over 160 searches at other terminals in the network.

RECON is operated at the ORNL computer center, while NSIC's input continues to go to the CTC computer via the Center's own remote terminal system. Long-range plans call for consolidating these activities on one computer.

2.5 NUCLEAR SAFETY JOURNAL

The preparation and review of material for the technical progress review continue apace with the requirement of its bimonthly publication schedule. *Nuclear Safety* 15(6) was distributed early in January, 16(1) in February, and 16(2) by the end of March, thus making up over a month of prior schedule slippage. Final composition of *Nuclear Safety* 16(3) (by TIC) is nearing completion; all material (except Current Events) for *Nuclear Safety* 16(4) has been transmitted to TIC, and the material for *Nuclear Safety* 16(5) is in the process of review and editing.

We were advised in January that *Nuclear Safety* had won first place in the Technical Journal Category of the 1974 Technical Publications Competition sponsored by the East Tennessee Chapter of the Society for Technical Communication. As a local winner, *Nuclear Safety* has been entered in the Society's international competition to be held in conjunction with their 22nd International Technical Communication Conference in May.

3. FISSION PRODUCT BETA AND GAMMA ENERGY RELEASE

Neutron Physics Division
R. W. Peelle and J. K. Dickens

3.1 INTRODUCTION

The purpose of this experiment is to measure the total beta and gamma energy release rate from fission product decay following thermal neutron fission of fuel materials ^{235}U and then perhaps ^{239}Pu and other nuclides. The accuracy goal is ±3% on the overall energy release rate for ^{235}U and ±4% for ^{239}Pu, for times following fission of 2 to 2000 sec. The experimental methods were outlined in the first quarterly report.[1]

3.2 EXPERIMENTAL PROGRESS

The progress to date has involved the preparation of the experimental system and the initiation of the in situ determination of the response matrix for the gamma-ray detector. The major emphasis during this quarter was the final design, fabrication, installation, and testing of the electrical and electronic system for controlling and monitoring the rabbit movement in the pneumatic tube to and from the irradiation position at the reactor.

The data taking computer routine now includes commands for rabbit movements. Irradiation periods and counting-time limits are entered via teletype, and the computer controls the experiment from the time the rabbit is sent to the reactor until the last counting-time interval has expired. Initial tests of the whole system were performed by measuring the 1.6-MeV photon decay of ^{20}F made by the $^{19}F(n,\gamma)$ reaction. These tests indicate that the actual irradiation period is ~0.6 sec longer than the typed-in value because of the definition of the signals actually timed. In addition, the transit times for travel to and from the reactor were studied in a series of measurements to obtain these times and their variances. The travel time to the reactor is ~1.1 sec, and the time to return ~1.5 sec (reflecting the longer return distance), with the standard deviation of each time distribution being 0.05 sec.

Preparation for the *in situ* determination of the gamma-ray detector's response matrix was initiated during the quarter by assembling a series of calibrated photon-sources as well as preparation of non-fissile samples for irradiation. These include samples of several separated isotopes, *viz*, sample enriched in the isotopes ^{41}K and ^{36}S. The calibration was initiated at the end of the quarter.

REFERENCE

1. Quarterly Progress Report on Reactor Safety Programs Sponsored by the Division of Reactor Safety Research for April–June 1974, ORNL-TM-4655, Vol. I, pp. 33–41.

4. ZIRCONIUM METAL–WATER OXIDATION KINETICS

Metals and Ceramics Division
J. V. Cathcart

The basic purpose of this program continues to be to determine the isothermal oxidation characteristics of Zircaloy-4 in steam between 900 and 1500°C (1652–2732°F) with sufficient accuracy to allow the data to be used in the prediction of the transient temperature oxidation behavior of Zircaloy. To this end we shall determine isothermal oxidation rates, measure the diffusivity of oxygen in β-Zircaloy, prepare a computer code that relates the diffusivity and isothermal rate data to transient temperature oxidation, and, ultimately, measure oxygen consumption under transient temperature conditions to test experimentally the results of our computer code.

Considerable progress was made in all parts of the program during the last quarter. New diffusivity data for oxygen in β-Zircaloy were obtained, and the development of the computer code was completed. Testing of our reaction rate apparatuses and the gathering of preliminary oxidation rate data continued. In this work special emphasis was placed on the identification and elimination (or minimization) of potential sources of temperature measurement errors.

4.1 THERMOMETRY

R. K. Williams

A comparison calibration of the thermocouple wire used in this program has been run to 1500°C (2732°F). In this test, several thermocouples, including two NBS-calibrated Pt–10% Rh vs Pt thermocouples, have a common hot junction; and the emf values of the various pairs are compared with the standards. The data indicate that the reference grade 0.010- and 0.020-in.-diam (0.25- and 0.51-mm) Pt–10% Rh vs Pt Sigmund-Cohn wire behaves very much like the NBS-calibrated thermocouples. Data were also obtained for Pt–30% Rh vs Pt–6% Rh thermocouples that

are used in the diffusion experiments, and temperature-emf tables are now being prepared. A nickel melting-point experiment will be used to check these tables at a single high-temperature point, 1453°C (2647°F).

An automatically balancing optical pyrometer has been received. This instrument, which will be used in the diffusion experiments, has been submitted for calibration checks.

4.2 DIFFUSION OF OXYGEN IN β-ZIRCALOY

R. A. Perkins

The tracer and chemical diffusivity of oxygen in β-Zircaloy-4 was measured between 1000 and 1400°C (1832–2552°F) by the ^{18}O radioactivation technique. For the tracer diffusion experiments an oxide scale was formed thermally in ^{18}O, and for the chemical diffusion experiments half of a diffusion couple was enhanced with ^{18}O to a total oxygen content of about 0.6 wt %. After the diffusion anneal, the specimen was bombarded by a proton beam on a cross section parallel to the diffusion direction. The beam passes through a 1- x 7-mm slit and strikes the specimen, which is oscillated through the beam parallel to the diffusion direction. This procedure ensures that the bombardment is uniform in the diffusion direction. The beam current is about 1 μA, and the specimen is bombarded for ~20 min for tracer diffusion experiments and 10 min for chemical diffusion experiments. The actual oxygen profile is then determined by autoradiography. Four independent microphotometer traces are made across each autoradiograph, and the results are averaged to obtain values for percent transmission as a function of diffusion distance. The details of the method have been discussed more fully in previous quarterly reports.[1,2] A statistical method of analysis is being developed to allow better determination of the diffusion coefficients with appropriate confidence limits, but the preliminary data for the tracer specimens are shown on the Arrhenius plot in Fig. 4.1 along with the other data of other investigators.[3–5] Our results are about 50% lower than the data of Mallett et al., and a linear fit to the results yields a slightly larger slope than that obtained by Mallett.

The welding of chemical diffusion couples at 1000°C (1832°F) using a 1000-g load yielded very good welds after a 10-min anneal. Making use of this technique, chemical diffusion measurements were made at 1250 and 1300°C (2282–2372°F). Diffusivity values were obtained as a function of oxygen concentration across the couples by use of the Matano-Boltzmann analysis. No significant dependence of diffusivity on oxygen concentration was observed over the range 0.1 to 0.6 wt % O. The measured diffusion coefficients were $(1.9 \pm 0.3) \times 10^{-6}$ cm^2/sec at 1250°C (2282°F) and $(2.6 \pm 0.4) \times 10^{-6}$ cm^2/sec at 1300°C (2372°F). These values agree well with the corresponding tracer diffusivities (see Fig. 4.1).

Problems associated with the apparent macroscopic segregation of ^{18}O were encountered with the 1250°C (2282°F) sample. The effect of the segregation was averaged through the use of multiple microphotometer traces, and a reasonable diffusivity value was obtained. This effect was not observed at 1300°C (2372°F), nor is its cause at 1250°C (2282°F) understood. We are investigating the phenomenon further.

The equipment necessary to resume Auger electron spectroscopy (AES) measurements with the desired beam size (≈10 μm) has been received and tested. After the equipment is installed, AES measurements will commence to complement the radioactivation results.

4.3 REACTION RATE STUDIES

R. E. Pawel, G. J. Yurek, R. E. Druschel, J. J. Campbell,
E. T. Rose, and S. H. Jury

We are continuing preliminary experiments on the steam oxidation of Zircaloy tube specimens emphasizing the low-thermal-inertia (MiniZWOK) apparatus. Considerable attention was given to potential problems of temperature measurement and control. The high-thermal-inertia (MaxiZWOK) oxidation apparatus has undergone minor changes, and testing is continuing. The first version of the computer program SIMTRAN-I, which models heat and mass transport behavior in an oxidizing Zircaloy fuel tube, has been written.

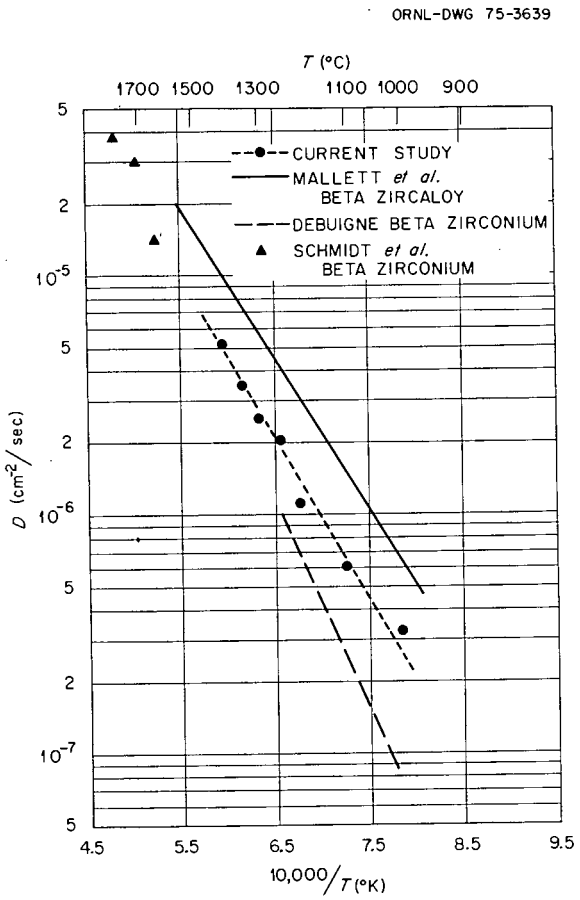

Fig. 4.1. Arrhenius plot of data for the diffusivity of oxygen in β-zirconium and β-Zircaloy. The Mallett[3] data were obtained with Zircaloy-2 and Zircaloy-3, while Debuigne[4] and Schmidt[5] worked with pure zirconium. The current study uses Zircaloy-4 samples.

4.3.1 Apparatus Development

We have continued to follow two parallel lines of development in the design of our reaction rate apparatuses. Two devices, one based on a low-thermal-inertia concept (MiniZWOK) and the other involving a high-thermal-inertia system (MaxiZWOK), have been constructed. During the past quarter our apparatus development efforts have centered on the testing and debugging of these devices, with special attention being given to problems of temperature measurement and control.

Low-thermal-inertia apparatus (MiniZWOK) - G. J. Yurek and R. E. Druschel

The MiniZWOK apparatus is employed to determine the isothermal oxidation kinetics of Zircaloy-4 PWR tubes in steam as a function of temperature and several other experimental variables.[1,2] This apparatus

will also be used to determine oxidation kinetics for several time-temperature transients. The major difficulty that we have encountered with the MiniZWOK apparatus is the accurate measurement of the specimen temperature during oxidation. The experimental requirements, including a rapid heatup to the temperature of oxidation followed by isothermal control, combine to make the problem of temperature measurement a difficult one. The MiniZWOK apparatus was modified during the last quarter to minimize potentially large temperature-measurement errors; and, for reasons outlined in Sects. 4.3.3 and 4.3.4, we believe that, with the possible exception of errors related to electrical shunting at very high temperatures, the error in our temperature measurements in MiniZWOK approaches that inherent in any well calibrated Pt—Rh vs Pt thermocouple.

The modified MiniZWOK apparatus is constructed to allow oxidation only on the outside of a Zircaloy tube specimen. A schematic representation of the one-sided oxidation apparatus is shown in Fig. 4.2. The Zircaloy tube specimen is supported between two quartz tubes. During an experiment steam flows past the outside surface of the specimen, and a positive pressure of helium is maintained inside the tube.

The methods of steam generation and heating of the specimen are identical with those presented previously for two-sided oxidation experiments.[1,2] Three thermocouples are welded to tantalum tabs on the inside surface of the Zircaloy specimen. One couple is used for the temperature controller, and two couples are employed to measure the specimen temperature. The method of temperature measurement is discussed in more detail in Sect. 4.3.3. The inlet and outlet steam temperatures are also monitored during an experiment.

The Zircaloy specimens are approximately 30 mm long by 10.7 mm OD by 9.3 mm ID. The ends of the specimens are machined flat and counterbored to provide good contact between the specimen and the quartz support tubes. Quartz gaskets are placed between the Zircaloy specimen and the quartz support tubes to minimize the leakage of helium to the outside of the tube and to minimize the flow rate of helium required to exclude steam from the inside of the tube. A light spring pressure is applied parallel to the tube axis to help seal the joints between the specimen and the quartz tubes.

ORNL-DWG 75-1465R

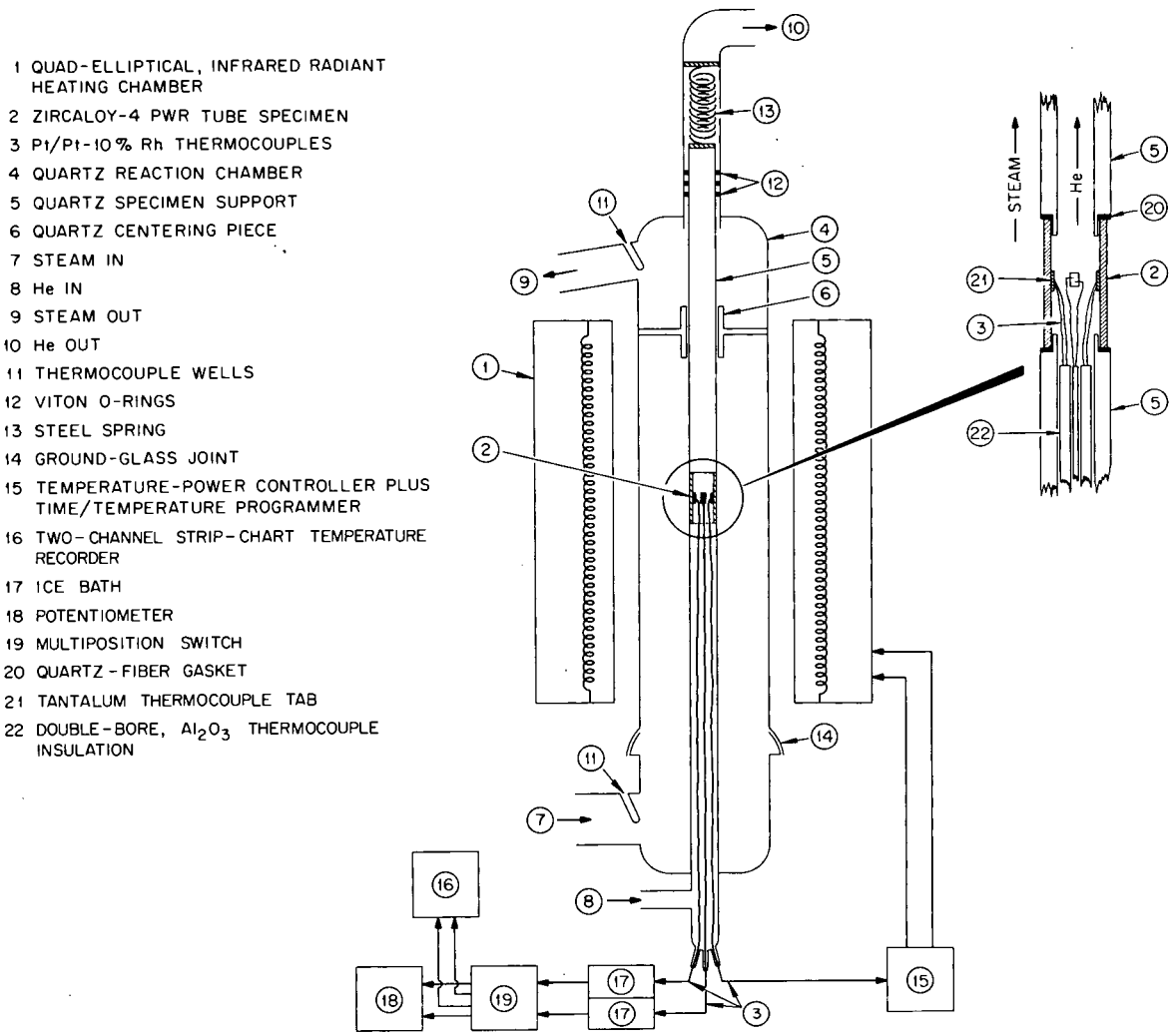

Fig. 4.2. Schematic drawing of the MiniZWOK one-sided oxidation apparatus.

The one-sided oxidation apparatus has several important advantages compared with the two-sided apparatus. Because the atmosphere inside the tube is inert, tantalum thermocouple tabs can be employed. The use of tantalum tabs eliminates the problem of melting at the tab-Zircaloy interface that was encountered when iridium tabs were employed.[1] We reported earlier[2] that the apparent temperature difference between two thermocouples that were attached to a Zircaloy specimen during two-sided oxidation depended on the flow rate of inert gas or steam past the thermocouple hot junctions. The one-sided oxidation apparatus is

designed to minimize the flow rate of helium past the thermocouple hot junctions, thereby minimizing this source of error in our temperature measurements. In addition, that portion of the electrical shunting between thermocouple wires that occurs by thermionic emission at elevated temperatures is reduced since less thermionic emission is expected to occur in helium than in steam.

The one-sided oxidation apparatus has been used to obtain preliminary oxidation data and to conduct experiments to determine the magnitude of temperature measurement errors. The results of these experiments are presented in Sects. 4.3.2 and 4.3.3.

High-thermal-inertia apparatus (MaxiZWOK) - S. H. Jury, J. J. Campbell, and R. E. Pawel

The MaxiZWOK steam oxidation apparatus, as described in previous quarterly reports,[1,2,6] is essentially completed and is undergoing testing to assess its capabilities in its present configuration. Some minor but time-consuming problems were encountered during preliminary tests; most of these have now been corrected, and we will proceed with the examinations during the next quarter.

Current experiments are designed to establish the characteristics of the steam supply and the steam superheater system. To date, the superheater has been operated at power levels up to about 8 kW at steam flow rates from 0.3 to 1.25 lb/min (2.3–9.4 g/sec). Maximum steam temperatures were about 500°C at a steam flow rate of 0.5 lb/min (3.8 g/sec). Tests are in progress to determine the optimum flow conditions and thus the maximum test temperatures available for our present power capability. Additional power is being brought to the MaxiZWOK location to permit us to operate the steam superheater at its maximum capability of 20 kW.

4.3.2 Preliminary Isothermal Oxidation Results

G. J. Yurek and R. E. Druschel

A series of isothermal oxidation experiments at 1040°C (1904°F) has been conducted in the one-sided oxidation apparatus (MiniZWOK). An analysis of the data (oxide and alpha phase thicknesses) has not been completed; however, the rate of thickening of the oxide phase apparently obeys a parabolic rate law. The alpha phase thicknesses were somewhat irregular, primarily because of difficulties in determining the position of the alpha-to-beta interface. We are experimenting with different techniques for making this measurement.

A photomicrograph of a cross section of a Zircaloy tube that was oxidized on the outside surface for 1170 sec at 1040°C (1904°F) is shown in Fig. 4.3. The thin layer of alpha at the inside surface of the tube was caused by absorption of either oxygen from steam that had leaked to the inside of the tube or impurities in the helium. The amount of oxygen absorption at the inner surface is small compared with the amount of oxidation at the outer surface. However, because oxygen penetration from the inside surface could affect the rate of oxidation at the outside surface at long times of oxidation, additional steps have been taken to eliminate oxygen from the inside of the tube.

The oxidation rates that are obtained from one-sided oxidation experiments can be used to calculate the rate of oxidation when both the inner and outer tube surfaces are exposed to steam. To confirm this statement, we shall compare calculated and experimental oxidation rates for one- and two-sided oxidation of Zircaloy.

4.3.3 Temperature Measurements during Oxidation

G. J. Yurek, R. E. Druschel, R. E. Pawel, and R. K. Williams

Problems that we have encountered in our attempts to measure the temperature of a Zircaloy specimen during oxidation and some of the steps that we have taken to eliminate these problems have been described in past quarterly reports.[1,2] Our new one-sided oxidation apparatus (see Sect. 4.3.1) was designed primarily to increase our ability to specify the correct temperature of a specimen during oxidation.

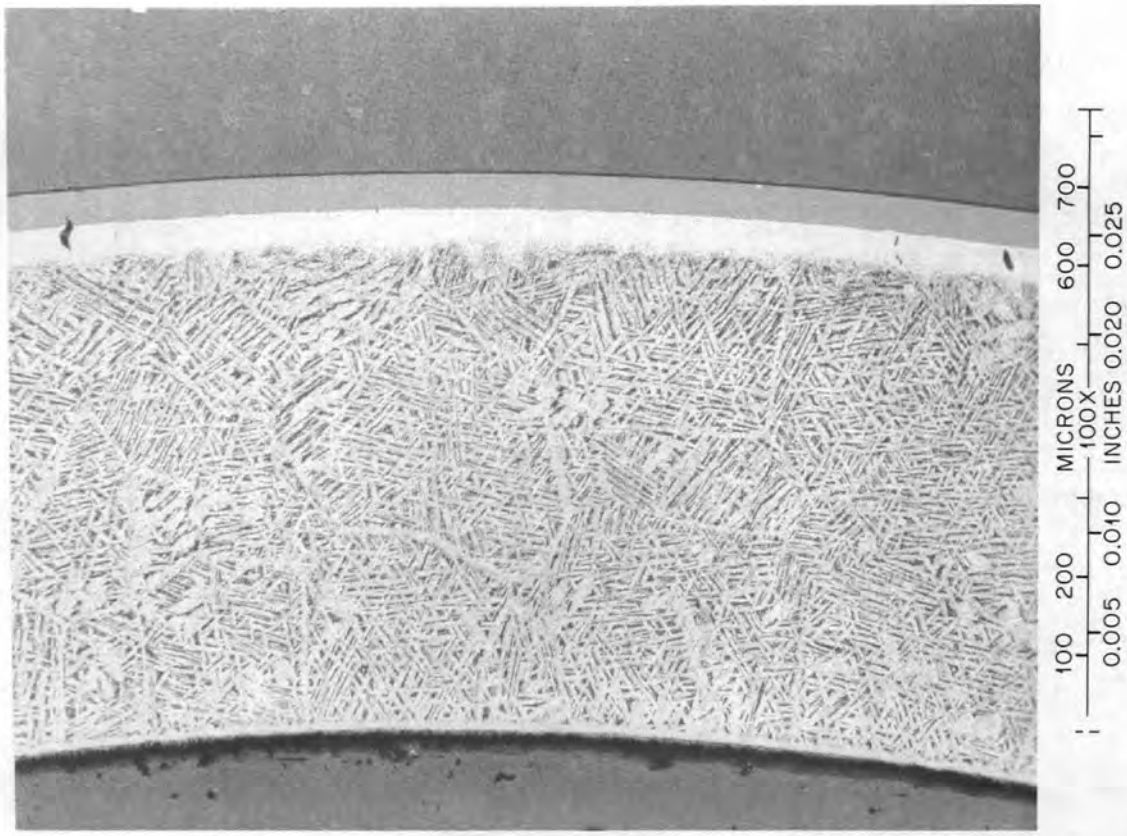

Fig. 4.3. Cross section of a Zircaloy tube that was oxidized for 1170 sec at 1040°C in steam. Etchant: Kroll's reagent. 100x.

A variety of experiments has been performed in this apparatus in order to identify temperature-measurement errors. The results of these experiments and our method of temperature measurement are described in the following paragraphs. In addition, a mathematical analysis of temperature measurement errors produced by the flow of gases past a thermocouple is presented in Sect. 4.3.4.

Method of temperature measurement

The arrangement that is employed to measure thermocouple emf's during an oxidation experiment is shown schematically in Fig. 4.2. Three Pt–10% Rh vs Pt thermocouples are welded to tantalum tabs (0.08 x 2 x 2 mm) on the inside of the Zircaloy specimen. The tabs

prevent contact between the thermocouple wires and the Zircaloy specimen, thereby eliminating melting at the hot junction for reaction temperatures above the zirconium-platinum eutectic temperature.

The thermocouple wires are spot-welded to the tabs, and this composite structure is then spot-welded to the inside surface of the Zircaloy specimen. Special efforts are made to ensure good contact between the tabs and the Zircaloy and to avoid contamination of the thermocouple wires.

The thermocouple wires are led away from the tab along the tube wall in a path perpendicular to the axis of the tube (supposedly an isothermal path) for about ten wire diameters to minimize conduction errors (see inset, Fig. 4.2). The separation between the thermocouple wires on the tab is about one wire diameter. The vertical sections of thermocouple wire between the tabs and the double-bore Al_2O_3 insulation (see inset, Fig. 4.2) are covered with single-bore Al_2O_3 insulation. We have broken the single-bore insulation into small pieces to minimize heat conduction to or away from the hot junctions. However, comparison with unbroken insulation revealed no difference in the temperature measurement. Therefore, unbroken single-bore insulation is employed because it is easier to handle.

One of the three thermocouples that are welded to a Zircaloy specimen is used to supply input voltage to the temperature controller. The other two thermocouples are employed to measure the temperature of the specimen. The cold junction of the measuring thermocouples is an ice bath. The thermocouple wires are connected to high-quality copper wire in a glass tube that is filled with mineral oil; the glass tubes are immersed in the ice bath.

The copper leads from the ice bath are connected with thermal-free solder to a multiposition switch, which is thermally insulated from the surroundings. The switch is connected to a two-channel strip-chart recorder and to a calibrated potentiometer.* The wiring between the

---

*Leeds and Northrup, 7553 type K-3 universal potentiometer.

potentiometer, standard cell, constant-voltage supply, and galvanometer is in accordance with the manufacturer's specifications. The standard cell is thermally insulated from the surroundings.

The output from both measuring thermocouples can be recorded simultaneously on the strip-chart recorder. In order to determine the emf of a particular thermocouple, the appropriate channel of the recorder is switched out of the circuit and the emf is read on the potentiometer. This procedure eliminates parasitic emf's that could result from the circuit of the recorder. The temperature of a specimen is obtained only from the potentiometer reading. The temperature during oxidation can be determined at two positions on a specimen with the present arrangement.

Effects of type and flow rate of inert gas on temperature measurement

We reported earlier[2] that the rate of flow of inert (argon) or reactive gases (steam, air) past a specimen in our two-sided oxidation apparatus affected both the measured temperature and the magnitude of the temperature difference between two thermocouples on the specimen. This result suggests that a major source of temperature error is associated with differential conduction of heat away from the thermocouple hot junctions to the cooler gas stream.

Two inert gases, helium and argon, were tested for use in our one-sided oxidation apparatus. The temperature difference between two thermocouples located at the same position along the axis of the Zircaloy tube and spaced approximately 120° apart on the circumference of the tube increased as the flow rate of either helium or argon past the thermocouple hot junctions was increased. However, the effect of flow rate was much less in helium than in argon. At a nominal temperature of 1000°C (1832°F), the temperature difference between the two thermocouples in a rapid flow of argon was about 20°C (36°F); the temperature difference in a comparable flow of helium was about 2°C (3.6°F). No temperature differences were observed in either stagnant helium or argon (circulation of the gases owing to a chimney effect not included). On

the basis of this result and the condition that a very slow flow of inert gas must exist inside the specimen to maintain a positive pressure of inert gas, we have decided to employ helium as the inert gas in our one-sided oxidation apparatus.

The effect of thermocouple wire diameter on temperature measurement

The diameter of the thermocouple wires is expected to be an important variable in the determination of temperature measurement errors (see Sect. 4.3.4). We have conducted experiments at approximately 1040°C (1904°F) with 5- and 10-mil (0.13- and 0.25-mm) thermocouple wire to determine the effect of wire diameter on the measured temperature.

In each experiment, one of the measuring thermocouples was welded to the same tantalum tab as the thermocouple that was used for the temperature controller. The temperature at the temperature-controller tab is the same in each experiment for the same controller set point. The results of two experiments are given in Table 4.1.

Table 4.1. The effect of wire diameter on measured temperature

Wire diameter		EMF	Mean temperature[a]
mils	mm	(mV)	(°C)
5	0.13	10.018–10.025	1039.5
10	0.25	10.013–10.021	1039

[a]Obtained from a standard emf-temperature conversion table.

The results presented in Table 4.1 show that wire diameter has essentially no effect on the measured emf at approximately 1040°C (1904°F). The reproducibility of the experiments has not been determined; however, to check this result we will compare the measured emf's from 5- and 10-mil-diam (0.13- and 0.25-mm) thermocouples that are welded to the same tab. We will also compare the same size wires at higher temperatures. If we find no difference between the wires, then we shall use the 10-mil-diam thermocouples because they are easier to handle.

Temperature gradients during oxidation

A series of experiments has been conducted at approximately 1040°C (1904°F) in which the two measuring thermocouples were separated along the axis of the Zircaloy tube. Both 5- and 10-mil-diam (0.13- and 0.25-mm) thermocouple wires were employed. In each experiment, the maximum temperature difference between the two hot junctions, separated by approximately 5 mm along the tube axis, was 2°C (3.6°F)

Control experiments were performed in which both measuring thermocouples were placed on the same tantalum tab. In each case, the measured emf's of the two thermocouples agreed to within 5 μV [~0.5°C (0.9°F)]. This indicates that the temperature measurement errors associated with thermocouple installation procedures are small and that the measured temperature differences along the axis of a Zircaloy tube specimen are real, albeit small.

Measurements of the oxide and alpha phase thicknesses on a longitudinal cross section of a specimen that had been oxidized at 1040°C (1904°F) show that the phase thicknesses are constant over at least a 20-mm length about the center of the tube. The thicknesses decrease slightly near the ends of the specimen. Given the exponential dependence of oxidation rate on temperature, this result also indicates that the temperature gradient at 1040°C (1904°F) is small.

We concluded from these results that the temperature gradients in our oxidizing specimens produce no significant error in our temperature measurements. It is true that, because of the Seebeck effect, the existence of a temperature gradient in a sample leads to the generation in a thermocouple of an additional emf (~5 μV/°C) that is proportional to the temperature difference between the two wires of the thermocouple at the hot junction. However, the measured temperature gradient at 1040°C (1904°F) is only 0.4°C/mm (0.7°F), and the separation of the thermocouple leads at the hot junction is ~0.25 mm. Thus the error associated with the gradient is on the order of 0.5 μV and totally negligible. We are conducting similar experiments at 1300°C (2372°F) to determine whether larger temperature gradients exist at higher reaction temperatures.

Because small temperature gradients along the tube axis of a specimen are unavoidable during oxidation, measurements of oxide and alpha phase thicknesses will be made only on cross sections taken from the center of a specimen at the position of the controller thermocouple and one measuring thermocouple. The second measuring thermocouple will be placed at a different position along the tube axis to determine the magnitude of the temperature gradient during oxidation.

4.3.4 "Perturbation" Errors in Temperature Measurements

R. E. Pawel and G. J. Yurek

The fact that circumferentially positioned thermocouples on specimens in the MiniZWOK apparatuses may under certain conditions indicate different temperatures was discussed in Sect. 4.3.3 and in the previous quarterly report.[2] The sensitivity of such differences to gas flow rate, temperature, and composition clearly indicates a perturbation in the temperature distribution of the system occasioned by heat flow from the specimen to the cooler gas stream via the thermocouples. Temperature measurement errors of this type are frequently referred to as "perturbation" errors and have been discussed by a number of investigators,[7] who have made suggestions for both minimizing the errors and for calculating their magnitude.

The analytical problem is essentially one of establishing an acceptable model for the heat transfer system, and then solving the heat flow equations so that the temperature at a given point in the absence of the sensor can be calculated. While such solutions have been obtained[8-10] for several cases relevant to the operation of thermocouples on specimens suspended in flowing gas streams, these solutions are generally based on oversimplified system geometries. Obviously, under these circumstances an experimental calibration of the system is desirable; but frequently it is impractical or even impossible, as in our case, to carry out such a direct calibration for a real system. For this reason we have taken the position that we should design our apparatuses in such a way as to minimize perturbation errors, while at the same time making use of existing computational procedures to

estimate the magnitude of the errors involved. Equations derived by Nusselt (reported by Jakob[8] and others) or Boelter[9] proved useful in the latter effort; and they have the added virtue that, because of the nature of the assumptions made in each derivation, the calculated perturbation error is believed to be greater than the actual error. Thus the results described below may be regarded as indicating the approximate maximum possible perturbation error in our experiments.

The equation reported by Jakob[8] is based on the following model: An infinitely extended, homogeneous body bounded by a plane surface is perfectly insulated against heat loss except for a small circular area. From this area, a cylinder or wire extends perpendicular to the plane surface into an environment having a temperature different from the uniform temperature of the body. The equation relates the temperature of the interface between the body and the wire to the temperatures of the body and its environment and to the several parameters that govern the flow of heat. The temperature perturbation created by a two-wire thermocouple is identical, at least for the ideal model, to that for a single wire. The heat flow from the junction into the wire is given by:[8]

$$q_0 = \pi(2k_w h r_0^3)^{1/2}(t_0 - t_e) \ , \qquad (1)^*$$

where k_w = thermal conductivity of the thermocouple leads,

h = heat transfer coefficient between thermocouple leads and environment,

r_0 = radius of thermocouple leads,

t_0 = temperature of the interface between body and environment (this is the temperature measured by the thermocouple),

t_e = environment (fluid) temperature.

The flow of heat out of the body into the area created by the junction of the thermocouple lead is

$$q_0 = 4r_0 k(t - t_0) \ , \qquad (2)$$

---

* A typographical omission exists in Jakob's[8] presentation of this equation.

where r_0 = the effective junction radius, assumed to be identical to the wire radius,

k = thermal conductivity of the body,

t = temperature of the body.

For steady-state conditions, the heat flows in Eqs. (1) and (2) are equal. Thus, combining the two expressions and rearranging:

$$t - t_0 = \frac{\frac{\pi}{k}\sqrt{\frac{k_w h r_0}{8}}}{1 + \frac{\pi}{k}\sqrt{\frac{k_w h r_0}{8}}}(t - t_e) . \qquad (3)$$

This expression affirms that the perturbation error $(t - t_0)$ in the temperature measurement depends upon the temperature difference between the body and its environment $(t - t_e)$, the thermal conductivities of the body and the thermocouple leads, and the heat transfer characteristics between the leads and the environment. Jakob also suggests an empirical expression for the heat transfer coefficient h which, when substituted into the above equation, results in a perturbation error that is independent of the thermocouple wire diameter. However, Otter[7] points out that in practice the wire size is generally a real variable.

Boelter et al.[9] analyzed the perturbation error for the temperature measurement of a thin plate with a cold fluid on one side and a hot fluid on the other. The thermocouple is mounted with its leads perpendicular to the surface of the plate in the hot fluid. Boelter's model is not directly applicable to the specimen geometry and heat-flow conditions in the MiniZWOK apparatus; however, within the limits set by the additional simplifying assumptions, the perturbation error should be similar for both cases. The analysis is based on a balance of heat-transfer rates on the plate concentric about the thermocouple wire attachment area. The solution is given in several forms. Utilizing

several approximations that are valid for small perturbation errors, Boelter derived the following equation:

$$\frac{t - t_0}{t - t_e} \cong \frac{r_0 \sqrt{2hk_w r_0}}{kb} \left[-\ln \left(\sqrt{\frac{\beta}{2}}\, r_0 \right) - 0.577 \right] , \qquad (4)$$

where b = thickness of the plate, $\beta = (h_0 + h_i)/bk$, where h_0 and h_i are the appropriate heat-transfer coefficients on the opposite sides of the plate, and the other symbols have the same meaning as in Eqs. (1) and (2).

This equation shows the relationship between the perturbation error $(t - t_0)$ and the parameters of the system in a manner generally consistent with Eq. (3). The thermocouple and plate dimensions appear as more important variables in Eq. (4). This obtains, at least in part, because of the different geometries and because of Boelter's assumption that no temperature gradient exists in the plate normal to its surface. For minimum error, it is seen that the thermocouple leads should have a low thermal conductivity and a small diameter; the plate should be thick and of high thermal conductivity. In addition, if the effective heat transfer coefficient, h, between the thermocouple and the flowing fluid can be decreased by insulation or by positioning, then the perturbation error will be reduced accordingly.

Equation (3) was used to estimate the maximum perturbation error anticipated in our one-sided MiniZWOK apparatus. A major uncertainty in the calculation lies in the assignment of the fluid (helium or argon) temperature and flow characteristics in the vicinity of the thermocouple installations. Not only does this temperature enter directly into the equation for the perturbation error, but the heat-transfer parameters are also involved. For example, the effective heat transfer coefficient, h, between the fluid and the thermocouple wire can be calculated on the basis of forced convection at low flow rates or on the basis of natural convection with assumed temperature differences in the system.[11] Both methods give

the same value of h within a factor of 2 for low-conductivity gases such as air. If we assume that a reasonable value for the heat transfer coefficient between the inert gas in MiniZWOK and the thermocouple wires is 10 Btu hr^{-1} ft^{-2} $°F^{-1}$ [57 W $m^{-2}°K^{-1}$], about an order of magnitude higher than the steam-specimen heat transfer coefficient, then we can calculate an approximate value for the perturbation error. The thermal conductivity of the thermocouple wire, k_w, is approximately 40 Btu hr^{-1} ft^{-2} $(°F/ft)^{-1}$ [70 W $m^{-1}°K^{-1}$]; the thermal conductivity of the specimen, k, is taken as 18 Btu hr^{-1} ft^{-2} $(°F/ft)^{-1}$ [31 W $m^{-1}°K^{-1}$]. Therefore, substituting directly into Eq. (3), we obtain:

$$Z = (t - t_0)/(t - t_e) = 0.025 . \qquad (5)$$

This result predicts that for bare-wire thermocouples extended at right angles into the inert gas stream the perturbation error will be 2.5% of the difference between the specimen and inert gas temperatures. The effective argon or helium gas temperature in the vicinity of the thermocouple installation is unknown. However, aside from circulation owing to convection, the flow rate on the inside of the tube should be very small, allowing the gas to be heated by contact with the components of the system that are heated directly by the radiant heating furnace. If, for example, the effective gas temperature in the cylindrical volume defined by the specimen is within 100°C of the specimen temperature, then a maximum perturbation error of 2.5°C would be anticipated. Of course, because our thermocouple installations are constructed to minimize this effect, the actual perturbation error should be less. As described elsewhere in this report, the experimental results are consistent with the prediction that the perturbation error is small for measurements of temperature in our one-sided MiniZWOK oxidation apparatus.

As emphasized earlier, the Boelter equation, Eq. (4), for plate specimens was derived with a different model and assumptions than those employed for the case of the insulated semi-infinite slab. While we

have no basis for ascertaining which of these treatments is best suited to describe our particular system, it is of interest to note that the Boelter expression leads to a similar value for the perturbation error when the same system parameters are used. For our case, the "plate" thickness is 0.686 mm (0.00225 ft); and we assume for purposes of calculation that the heat transfer coefficients on either side of the plate, h_0 and h_i, are each 1 Btu hr^{-1} ft^{-2} $°F^{-1}$ (5.7 W $m^{-2}{}^{\circ}K^{-1}$). The insertion of these values into Eq. (4) yields

$$Z = (t - t_0)/(t - t_e) = 0.0336. \qquad (6)$$

Thus, Eq. (4) predicts that the perturbation error will be 3.36% of the difference between the specimen and coolant temperatures, which is quite close to the error predicted by Eq. (3). In addition, the error is only moderately dependent upon the particular values chosen for the plate heat transfer coefficient, Z varying from about 4 to 2% as the coefficients change from 0.1 to 100 Btu hr^{-1} ft^{-2} $°F^{-1}$ (0.6 to 600 W $m^{-2}{}^{\circ}K^{-1}$).

The results of these calculations are recognized as being approximate. Their contribution, therefore, lies not so much in a precise prediction of error values but in the fact that they indicate the relationship between some of the important system parameters that affect temperature measurement errors, thereby suggesting means for reducing these errors to a minimum. Our thermocouple installations are constructed with these ideas in mind.

4.3.5 Computer-Simulated Oxidation Experiments

S. Malang* and R. E. Pawel

A computer program has been written to simulate the oxidation of Zircaloy fuel tubes over a wide range of conditions. Briefly, the code considers a one-dimensional solution, in cylindrical coordinates, of the

---

*On assignment to ORNL from Karlsruhe Nuclear Research Center, West Germany.

multiphase, moving boundary diffusion problem in a tube wall of finite thickness. Physical property data, as well as kinetic and thermodynamic parameters, serve as the basic input to the code, which, on the basis of an ideal model, can then examine both the heat and mass transport processes that occur during a given reaction. Both isothermal and transient-temperature oxidation can be studied as well as oxidation in a particular reaction environment where self-heating of the specimen might take place. A working preliminary version of the code is presently in hand, and comprehensive testing to provide code verification will begin shortly.

REFERENCES

1. Quarterly Progress Report on Reactor Safety Programs Sponsored by the Division of Reactor Safety Research for July–September 1974, I. Light-Water-Reactor Safety, ORNL-TM-4729, Vol. I, Chap. 4.
2. Quarterly Progress Report on Reactor Safety Programs Sponsored by the NRC Division of Reactor Safety Research for October–December 1974, I. Light-Water-Reactor Safety, ORNL-TM-4805, Vol. I, Chap. 4.
3. M. W. Mallett, W. M. Albrecht, and P. R. Wilson, "The Diffusion of Oxygen in Alpha and Beta Zircaloy-2 and Zircaloy-3 at High Temperatures," J. Electrochem. Soc. 106, 181–84 (1959).
4. Jean Debuigne, "Contribution to the Study of the Oxidation of Zirconium and of the Diffusion of Oxygen in the Oxide and in the Metal," Métaux, Corrosion, Industrie 501, 186–201 (1967).
5. F. A. Schmidt, O. N. Carlson, and C. E. Swanson, "Electrotransport of Carbon, Nitrogen, and Oxygen in Zirconium," Met. Trans. 1, 1371–74 (1970).
6. Quarterly Progress Report on Reactor Safety Programs Sponsored by the Division of Reactor Safety Research for April–June 1974. I. Light-Water-Reactor Safety, ORNL-TM-4655, Vol. I, Chap. 4.
7. Summaries of pertinent phenomena, approaches, and remedies are given in (a) A. J. Otter, Thermocouples and Surface Temperature Measurement, AECL-3062 (March 1968) or (b) Manual on the Use of Thermocouples in Temperature Measurement, American Society for Testing and Materials, Spec. Tech. Publ. 470A, Philadelphia, 1974, particularly Chapter 9.
8. M. Jakob, Heat Transfer, Vol. II., Wiley, N. Y., 1957, p. 147.
9. L. M. K. Boelter et al., An Investigation of Aircraft Heaters XXVIII – Equations for Steady-State Temperature Distribution Caused by Thermal Sources in Flat Plates Applied to Calculation of Thermocouple Errors, Heat-Meter Corrections, and Heat Transfer by Pin-Fin Plates, NACA-TN-1452 (1948).
10. L. M. K. Boelter and R. W. Lockhart, Thermocouple Conduction Error Observed in Measuring Surface Temperatures, NACA-TN-2427 (1951).
11. W. H. McAdams, Heat Transmission, McGraw-Hill, New York, 1942, pp. 219 and 237.

5. MULTIROD BURST TESTS

Reactor Division
R. H. Chapman

5.1 INTRODUCTION

The objectives of this program are to delineate the deformation behavior of unirradiated Zircaloy cladding under conditions postulated for a LOCA and to provide a data base to facilitate assessment of the magnitude and distribution of geometrical changes in the fuel-rod cladding and of the extent of flow channel blockage that might result. Consistent and reliable data will be obtained from a single-rod and multirod experiments that include possible effects of rod-to-rod interactions on ballooning and rupture behavior to (1) establish the magnitude and distribution of cladding deformation during temperature excursions representative of a hypothetical LOCA, (2) determine the cladding rupture temperature-pressure relationship, and (3) provide flow resistance information that can be related to the resultant coolant channel blockage.

Internally pressurized Zircaloy tubes containing tubular electric heaters (to simulate nuclear fuel pellet heating) will be tested to failure in a low-pressure, superheated-steam environment. These assemblies will be heated uniformly over a 3-ft length at a constant rate (50°F/sec) for differential pressures ranging from 100 to 2000 psi, corresponding to approximate rupture temperatures from 2200 down to 1300°F. Examination of the tested tubes will include comparison of pre- and posttest flow resistance (for the multirod arrays); sectioning; and measurement of deformation, rupture strain, and channel blockage.

Preliminary program plans and conceptual design descriptions were presented previously.[1] Effort this quarter concentrated on further definition of program plans and test schedules, detailed design of components and systems, development tests and evaluations, and procurement of long delivery items.

5.2 PROGRAM PLANS

5.2.1 Planning and Analysis

R. H. Chapman

A program plan, describing in detail the objectives, scope, and experimental concepts to be used in this research, was completed and submitted to RSR for review and comment. Plans and accomplishments to date were presented February 3 to the first of what probably will become regularly scheduled RSR Fuel Cladding Research Review meetings; these meetings are designed to provide informal exchange of results and ideas of mutual interest to the various programs. One result of this first meeting has a significant bearing on a performance criterion specified for the MRBT heaters; further discussion on this point will be deferred to Section 5.3.4.

Some exploratory calculations, using the SIMTRAN computer program under development in the ZWOK program, were performed to determine the influence of the exothermic oxidation reaction on cladding heating relative to that due to the internal electric heater. For essentially unoxidized cladding, these calculations indicate that the contribution to the cladding heating due to the reaction may become significant above about 1900°F. It should be emphasized that the calculations are preliminary and must be evaluated in view of experimental evidence. Such evidence will be obtained in the ZWOK program and in the single-rod scoping tests to be performed in this program.

New test schedules, consistent with delays encountered with heater procurement and budgetary guidelines, were formulated. Current plans are based on completing the first group (~15) of single-rod burst tests in the second quarter of FY 1976 and the first group (3) of 4 x 4 bundle tests in the second quarter of FY 1977. Examination, analysis, and reporting of the data will lag these milestones about six months.

5.2.2 Posttest Examination of Fuel Pin Simulators

R. H. Chapman

Detailed measurements of the single- and multirod test arrays are required to determine the magnitude and distribution of cladding deformation and derived parameters, e.g., rupture strain, flow channel blockage, rod displacement, etc. Examination of the single-rod test assemblies will consist of measuring the circumference of the deformed cladding at discrete locations along the length to establish axial profiles of swelling and strain. The measurements will be made by the "Scotch tape method," i.e., by carefully wrapping a length of tape around the tube, marking the circumferential length, removing the tape, and accurately measuring the developed length. This technique has been used by other investigators with good success to determine deformation. The method will not provide information related to the shape of the deformed section; details of this nature must be obtained from cross-sectional profiles. Since this test series employs circumferential symmetry, it is expected that the need for sectional profiles will be limited to the burst area. Detailed metallurgical and metallographic examination will be limited to the burst area of representative specimens. Examination of the 4 x 4 (and larger) bundles will be more tedious, since the Scotch tape method is not applicable. Instead, the bundles will be cast in epoxy and sectioned at appropriate intervals along the length for detailed measurement. The mounted and sectioned specimens must be polished sufficiently to remove the worked material before measurements are taken. Automated measuring techniques are under investigation.

One available method is based on the use of a Quantimet-720 Image Analyzing Computer. This system extracts quantitative data from images obtained from mounted specimens or photographs. A number of feature-function components are available to obtain such parameters as area, perimeter, density, etc. Basically, the image field is divided into 650,000 discrete picture points to form an x-y grid; each picture point is digitized and stored for subsequent use. Signals from the required features are isolated from the remainder of the image by a detection

process based on gray level criteria. For example, the two simplest criteria are: all areas lighter or darker than a preset threshold and that area whose gray level is between two selected levels. A computer module makes the desired measurement from the detected signals (interrupted light beams). Output data are displayed on the console and can be preserved on a punched tape. For MRBT applications, the system can provide quantitative measurements of total perimeter, tube wall area, coolant flow channel area, etc.; it does not appear capable of locating centroids. The average wall thickness is calculated from the tube wall area and total perimeter. By programming in pretest data, the system can calculate and provide output of such parameters as total strain, area reduction of wall and coolant channel, percent blockage, etc. Although this system appears to have tremendous capability, it may not provide all the needed geometrical data. For example, if the individual rods are displaced from their original position, it may not be possible to determine the net movement by this technique.

Another method available for use, essentially a computer-controlled electronic planimeter, is also attractive and can provide location of centroids. Basically, this system consists of a 17-in. x 17-in. platen with closely spaced (0.010-in.) embedded wires, forming an x-y coordinate system, and a movable stylus. When the stylus is energized at a point on the grid, the computer calculates the x-y coordinates of that point and stores the value for further processing. As the stylus is moved over the grid, signals are emitted either as single pulses on demand or in the continuous mode (approximately 100 pulses/sec). The stored point coordinates are processed by the computer according to programmed instructions to give areas, lengths, locations, etc. Output data are displayed on the console and can be printed out, plotted, or preserved on a punched tape. For MRBT applications, an enlarged photograph of the mounted specimen would be placed on the platen and an operator would trace out the boundaries of the tubes. The computer would process the data according to the programmed instructions. Much of the same information can be obtained from this method of analysis as from the Image Analyzing Computer; however, considerably more operator time is involved. This system works equally well on skewed channels and on uniform displacements.

Both of these methods have potential for automation of posttest examination of the MRBT test assemblies and probably will be used, since each complements the other and offers advantages for certain types of information. Further, the fact that measured and derived results can be output as paper tape records facilitates subsequent computer handling.

5.2.3 Temperature Profiles in No. 1 (4 x 4) Bundle

R. H. Chapman

Steady-state and transient temperature measurements are planned for the first 4 x 4 multirod bundle to:

1. Determine axial and radial temperature profiles.
2. Provide guidance for judicious location of tube inside thermocouples in subsequent test bundles.
3. Permit modeling of the temperature distribution so that local failure temperatures can be inferred from a limited number of temperature measurements in subsequent test bundles.
4. Correlate tube outside surface temperature with inside tube thermocouple measurements.
5. Determine the influence of steam flow rate on bundle temperature distribution.
6. Determine the effect of the steam environment by comparison with data obtained with an inert environment.

The maximum temperature in these tests will be limited to 1700 to 1800°F to permit the use of stainless-steel-sheathed thermocouples, while avoiding formation of a zirconium-nickel eutectic (≥1750°F). Most of the tests (with steam environment) will be limited to about 1500°F to avoid excessive oxidation of the cladding; higher temperatures may be used in the comparative inert environment tests. The fuel-pin simulator helium pressure will be limited to about 50 to 100 psi (differential) to preclude cladding deformation. In the final experiment (steam environment), the helium pressure will be increased to cause deformation and rupture at approximately 1800°F; this then becomes the first multirod burst test.

This test will also provide information on the performance of the inside thermocouples as affected by tube deformation; similar and more extensive information will be obtained from the single-rod tests.

Approximately 114 thermocouples, involving several types, are contemplated for the mapping experiments. An identification code, given in Table 5.1, was devised to facilitate assembly instructions, record keeping, data acquisition, and computer manipulations.

Figure 5.1 shows a plan view of the bundle and shroud and gives the angular position selected for each rod thermocouple; the elevation of each thermocouple, in sixteenths of an inch above or below the data section midpoint, is tabulated also. Grid and shroud thermocouples are included to complete specification of all the thermocouples. Table 5.2 specifies details, in the coded format of Table 5.1, of all the internal thermocouples; Table 5.3 gives similar information for the outside thermocouples.

In selecting the locations for the thermocouples (both inside and outside the tube), advantage was taken of radial and axial symmetry to obtain profiles in typical corner, midwall, and interior rod positions. In the rods with outside thermocouples, an inside thermocouple is matched to one of the outside group to provide a correlation between inside and outside temperature measurements. The shroud thermocouples are also located opposite rod thermocouples for the same reason. The bundle thermocouples are concentrated in the regions where the gradients are expected to be more pronounced. One thermocouple is attached to each of the grids that define the data section end points. A few thermocouples are located outside the grids to give reasonable definition of the profile in these regions. The bundle is designed and instrumented on the basis of downflow of steam; the upstream heated length, required as a thermal entrance region, precludes testing the effect of steam flow direction in this bundle. This type of information will be obtained in the single-rod tests.

As indicated in Fig. 5.1, tube outside thermocouples (total of 42) are provided only on "short" fuel pin simulators to facilitate thermocouple attachment as the bundle is built up by layers. It should be noted also that rods 01 and 16 are taken together to give a complete profile of

Table 5.1. Thermocouple alphanumeric identification

Thermocouple specification: $\underbrace{A\ B\ C\ D\ E\ F\ G\ H}_{1} - \underbrace{X\ X}_{2} - \underbrace{X\ X\ X}_{3} - \underbrace{X\ X\ X}_{4}$

1. Eight letter general identification:

   Letter 1 denotes general location as follows:

   I = inside of Zircaloy tube
   O = outside of Zircaloy tube
   G = attached to grid
   S = attached to outside of bundle shroud

   Letters 2 and 3; i.e., TC, shorthand for thermocouple

   Letters 4 and 5 denote sheathed or unsheathed and sheath material as follows:

   BW = bare wire (unsheathed)
   SS = stainless steel sheath
   TS = tantalum sheath

   Letters 6 and 7 denote thermoelement material (ISA type) as follows:

   TK = Chromel P vs Alumel
   TS = Pt vs Pt + 10% Rh

   Letter 8 denotes location of thermocouple junction relative to midpoint of data section as follows:

   A = above midpoint of span
   B = below midpoint of span
   Ø = on midpoint of span

2. Two digit number identifies rod position in bundle (see Fig. 5.1).

3. Three digit number gives angular orientation of thermocouple junction in degrees clockwise from north looking down on top of bundle.

4. Three digit number gives elevation (in 1/16 of an inch) relative to midpoint of data section. Eighth letter in prefix will tell if above, below, or on midpoint.

   Example: ITCTSTKB 01 090 152 denotes an inside, tantalum-sheathed, type K thermocouple in rod position number 1 and located 90 degrees clockwise from north (when viewed from above) and 152/16 (= 9.5) in. below the midpoint of the data section of the bundle.

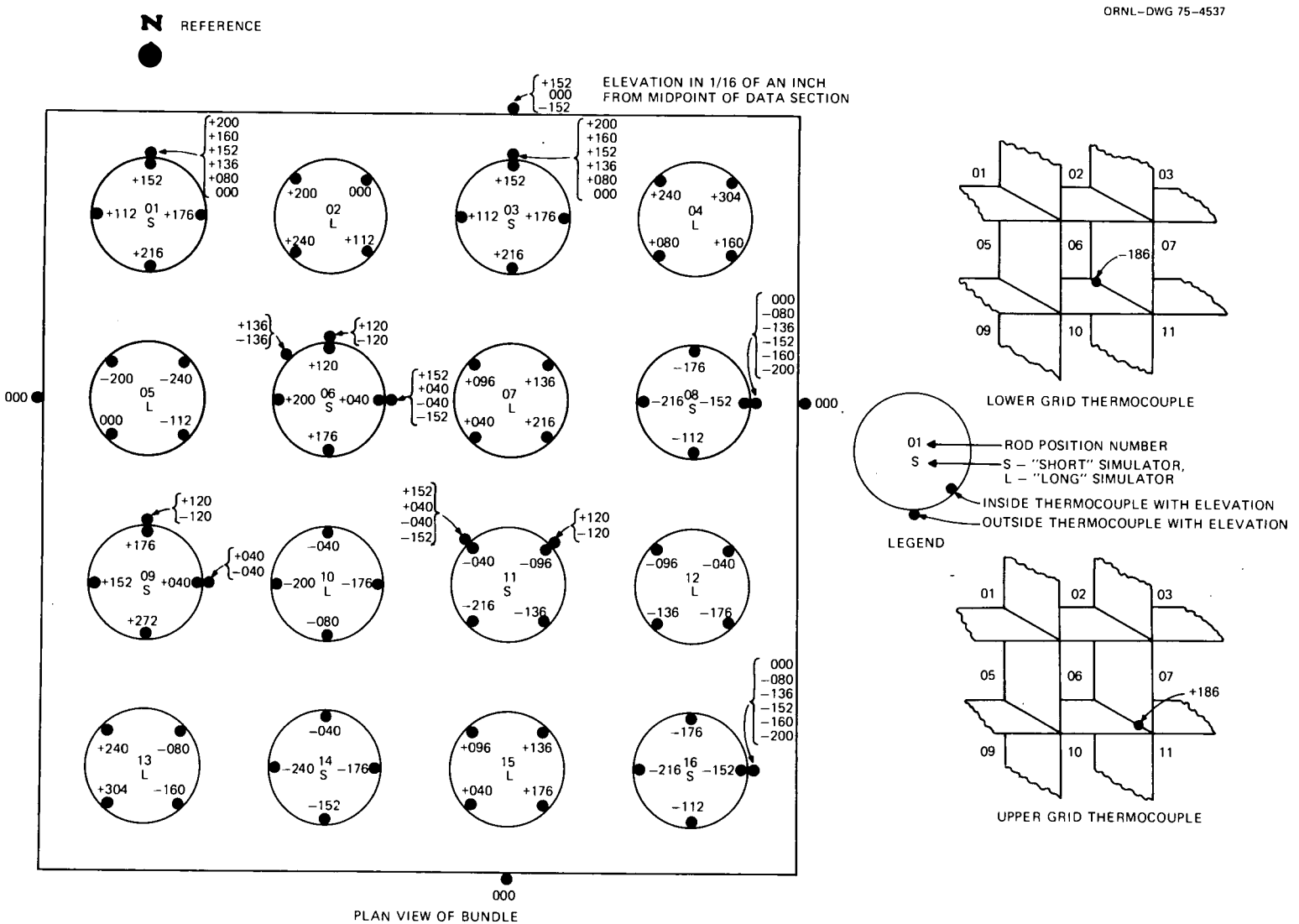

Fig. 5.1. Orientation and elevation of bundle, grid, and shroud thermocouples for determining temperature distribution.

Table 5.2. Listing of inside tube thermocouples
(57 stainless steel and 7 tantalum sheathed, type K)

T/C No.	General ident.	Rod position	Orient. (deg)	Distance (1/16 in.)	T/C No.	General ident.	Rod position	Orient. (deg)	Distance (1/16 in.)
1	ITCSSTKA	01	180	+216	33	ITCSSTKA	07	135	+216
2	ITCSSTKA	01	090	+176	34	ITCSSTKA	07	045	+136
3	ITCTSTKA	01	000	+152[a]	35	ITCSSTKA	07	315	+096
4	ITCSSTKA	01	270	+112	36	ITCTSTKA	07	225	+040
5	ITCSSTKB	16	180	-112	37	ITCTSTKB	11	315	-040[a]
6	ITCSSTKB	16	090	-152[a]	38	ITCSSTKB	11	045	-096
7	ITCSSTKB	16	000	-176	39	ITCSSTKB	11	135	-136
8	ITCSSTKB	16	270	-216	40	ITCSSTKB	11	225	-216
9	ITCSSTKA	03	180	+216	41	ITCSSTKA	09	180	+272
10	ITCSSTKA	03	090	+176	42	ITCSSTKA	09	000	+176
11	ITCTSTKA	03	000	+152[a]	43	ITCSSTKA	09	270	+152
12	ITCSSTKA	03	270	+112	44	ITCSSTKA	09	090	+040[a]
13	ITCSSTKB	08	180	-112	45	ITCSSTKB	14	000	-040
14	ITCSSTKB	08	090	-152[a]	46	ITCSSTKB	14	180	-152
15	ITCSSTKB	08	000	-176	47	ITCSSTKB	14	090	-176
16	ITCSSTKB	08	270	-216	48	ITCSSTKB	14	270	-240
17	ITCSSTKA	02	225	+240	49	ITCSSTKA	15	135	+176
18	ITCSSTKA	02	315	+200	50	ITCSSTKA	15	045	+136
19	ITCSSTKA	02	135	+112	51	ITCSSTKA	15	315	+096
20	ITCTSTKØ	02	045	000	52	ITCSSTKA	15	225	+040
21	ITCSSTKØ	05	225	000	53	ITCSSTKB	12	045	-040
22	ITCSSTKB	05	135	-112	54	ITCSSTKB	12	315	-096
23	ITCSSTKB	05	315	-200	55	ITCSSTKB	12	225	-136
24	ITCSSTKB	05	045	-240	56	ITCSSTKB	12	135	-176
25	ITCSSTKA	06	270	+200	57	ITCSSTKA	04	045	+304
26	ITCSSTKA	06	180	+176	58	ITCSSTKA	04	315	+240
27	ITCSSTKA	06	000	+120[a]	59	ITCSSTKA	04	135	+160
28	ITCTSTKA	06	090	+040[a]	60	ITCSSTKA	04	225	+080
29	ITCTSTKB	10	000	-040	61	ITCSSTKB	13	045	-080
30	ITCSSTKB	10	180	-080	62	ITCSSTKB	13	135	-160
31	ITCSSTKB	10	090	-176	63	ITCSSTKA	13	315	+240
32	ITCSSTKB	10	270	-200	64	ITCSSTKA	13	225	+304

[a]Outside tube T/C matched with inside tube T/C at these positions.

Table 5.3. Listing of outside tube, shroud, and grid thermocouples (44 bare wire, type S; and 6 SS-sheathed, type K)

T/C No.	General ident.	Rod position	Orient. (deg)	Distance (1/16 in.)
1	ØTCBWTSA	01	000	+200
2	ØTCBWTSA	01	000	+160
3	ØTCBWTSA	01	000	+152[a]
4	ØTCBWTSA	01	000	+136
5	ØTCBWTSA	01	000	+080
6	ØTCBTWSØ	01	000	000
7	ØTCBWTSØ	16	090	000
8	ØTCBWTSB	16	090	-080
9	ØTCBWTSB	16	090	-136
10	ØTCBWTSB	16	090	-152[a]
11	ØTCBWTSB	16	090	-160
12	ØTCBWTSB	16	090	-200
13	ØTCBWTSA	06	090	+152
14	ØTCBWTSA	06	315	+136
15	ØTCBWTSA	06	000	+120[a]
16	ØTCBWTSA	06	090	+040[a]
17	ØTCBWTSB	06	090	-040
18	ØTCBWTSB	06	000	-120
19	ØTCBWTSB	06	315	-136
20	ØTCBWTSB	06	090	-152
21	ØTCBWTSA	09	000	+120
22	ØTCBWTSA	09	090	+040[a]
23	ØTCBWTSB	09	090	-040
24	ØTCBWTSB	09	000	-120
25	ØTCBWTSA	03	000	+200
26	ØTCBWTSA	03	000	+160
27	ØTCBWTSA	03	000	+152[a]
28	ØTCBWTSA	03	000	+136
29	ØTCBWTSA	03	000	+080
30	ØTCBWTSØ	03	000	000
31	ØTCBWTSØ	08	090	000
32	ØTCBWTSB	08	090	-080
33	ØTCBWTSB	08	090	-136
34	ØTCBWTSB	08	090	-152[a]
35	ØTCBWTSB	08	090	-160
36	ØTCBWTSB	08	090	-200
37	ØTCBWTSA	11	315	+152
38	ØTCBWTSA	11	045	+120
39	ØTCBWTSA	11	315	+040
40	ØTCBWTSB	11	315	-040[a]
41	ØTCBWTSB	11	045	-120
42	ØTCBWTSB	11	315	-152
		Shroud thermocouples		
43	STCSSTKA	Outside	North	+152
44	STCSSTKØ	Outside	North	000
45	STCSSTKB	Outside	North	-152
46	STCSSTKØ	Outside	East	000
47	STCSSTKØ	Outside	South	000
48	STCSSTKØ	Outside	West	000
		Grid thermocouples		
49	GTCBWTSA	06	SE	+186
50	GTCBWTSB	06	SE	-186

[a]Outside T/C matched with inside T/C at this position.

a corner position; rod positions 03 and 08 are required to obtain a complete profile for a central rod. Tube 09 supplements position 03 by providing exterior thermocouples that "look at" adjacent interior and exterior rods. The tube interior thermocouples are oriented to give broad coverage of all directions and to fill in the basic profiles obtained from the outside surface measurements.

5.3 DESIGN, DEVELOPMENT, AND PROCUREMENT

5.3.1 Zircaloy Tubing Procurement

R. H. Chapman

Procurement of approximately 8500 ft of reactor grade Zircaloy tubing, for use in all the RSR-sponsored fuel cladding studies, is approximately on schedule. An inspector from ORNL visited the supplier's production facilities to witness a number of the required inspections and tests. Shipment of the tubing is anticipated during the week of April 21, about two weeks later than originally scheduled. Special requirements and characteristics of the tubing were reported previously.[2]

5.3.2 Grids

R. H. Chapman

A standard fuel assembly grid having the proper rod pitch-to-diameter ratio was obtained from one of the reactor vendors and was cut into unit cells to produce prototype "single-rod grids" for use in the single-rod burst tests. Since a grid represents a heat sink in addition to imposing some localized restraint on the cladding, use of a grid unit cell introduces another element of reality in the single-rod experiments.

Grids for the multirod test arrays are being fabricated by the reactor vendor. Those necessary for the 4 x 4 bundle tests are scheduled for shipment in May; grids for the larger bundles are scheduled for delivery in mid-1976.

5.3.3 Component Development

J. L. Crowley

To avoid axial restraint of the multirod test arrays, the lower end of the fuel pin simulators terminate within the test vessel. Thus, the lower end seals between the internal electric heater and the cladding must seal against 2000 psi helium pressure at a temperature of 650°F (ambient steam) while providing electrical insulation against 300 V dc. Current design concepts for the mechanical seal are based on modifications to commercial glands. Testing of a gland recommended by the manufacturer for this application proved the Teflon sealant to be unsatisfactory (as expected) above about 550°F. Tests with other sealants thus far indicate crushed lava may be satisfactory, if the electrical isolation problems can be resolved. High-temperature epoxy coatings, alone and with combinations of various insulating sleeve materials, were tested without success in meeting all requirements. Testing of improved concepts now under development are expected to resolve the remaining problems with this seal.

The upper seal, which is external to the multirod test vessel, appears to be satisfactory using the Teflon sealant in combination with a heat shrink Teflon sleeve on the conductor. Both the helium retention and electrical insulation requirements were satisfied simultaneously in tests to 300°F and above. In addition to the copper conductor, this gland also must seal four sheathed thermocouples and two pressure tubes, all within a maximum diameter of 0.675 in.

A steam heater was designed, fabricated, and tested successfully. Current plans are for this heater to supply 650°F steam for the single-rod tests and 900°F steam for preoxidization of the Zircaloy tubes. Tests thus far have shown that the heater can supply 5 lb/hr of superheated steam at 900°F. An autoclave was fabricated for use in an existing furnace to permit simultaneous pretreatment (both interior and exterior surfaces) of seven Zircaloy tubes; test specimens will be metallurgically evaluated to qualify the procedure.

A fixture for precisely locating and spot welding the sheathed thermocouples to the inside surface of the cladding was designed and fabricated.

The device can accommodate up to four (90° intervals) thermocouples at any desired axial position within the Zircaloy tubing. Procedures and welding parameters are currently under development. Promising results have been obtained with an energy pulse of 4 to 8 W-sec with 4 lb applied force.

5.3.4 Heater Development and Procurement

D. L. Clark and R. W. McCulloch

Test and evaluation of a number of development heaters were performed; Table 5.4 summarizes the results. Although these heaters were procured on a best-effort basis so that test and evaluation could proceed as quickly as possible, previously discussed[2] fabrication difficulties delayed delivery. As indicated in the table, nondestructive examination and operational tests revealed the effects of the fabrication problems. In general, uniformity of surface heat flux was not acceptable as indicated by the infrared scanning results. Radiographs revealed density variations in the crushed magnesium oxide cores on which the heating element is wound. Evaluation of the test results indicates that each manufacturer must improve appreciably his fabrication techniques and procedures in order to produce an acceptable heater.

Information presented at the February 3, 1974, Fuel Cladding Review Meeting (see Sect. 5.2.1) is important to a performance criterion specified for the heaters. Strain at failure in a stressed Zircaloy specimen depends on strain rate. To remove this extraneous parameter from consideration in the burst tests, the strain rate in the pressurized fuel pin simulators prior to and at the time of failure should be approximately the same in all the tests. In a constant pressure process, i.e., a constant loading condition, the strain rate will be proportional to the rate of temperature increase. This situation is reasonably approximated during a portion of the MRBT temperature transient. Originally one of the MRBT heater design criteria specified a temperature increase of 50°F/sec ± 10% for the cladding in the region of 1000 to 1600°F. To maintain approximately the same strain rate at failure in all the tests, this criterion has been modified to require the temperature increase to be 50°F/sec (±10%) over the 500°F test range preceding failure. Figure 5.2 shows

Table 5.4. Test and evaluation of development heaters

Heater supplier	Heater serial No.	Sheath material	Temperature transient[a]			Results	
			Power (kW)	Maximum temperature (°F)	Cycles	Infrared[b] scan	Transient tests
Watlow	3	Inconel	6.4–9.5	~1600	4	Very poor	Survived
			8.5	~2200	10		Survived
Watlow	4	Zircaloy	7.5	~1600	5	Satisfactory	Survived
			7.7	~2200	2		Element burnout; hole melted in sheath; sheath swelling over entire heated length
Watlow	5	Titanium	7.8	~2100	1	Very poor	Element burnout; sheath swelling over entire heated length
Watlow	2	Tantalum coated on carbon steel	8.3	~1700	1	Poor	Survived
			8.4	~2200	9		Survived; white oxide formed over heated length
Watlow	6	Tantalum	6.5	~1400	1	Very poor	Survived
			5.6	~1700	1		Survived
			7.0	~2100	4		Survived
			7.7	~2200	6		Survived
RAMA	1	Inconel	6.9	~1700	2	Poor	Survived
			8.0	~2200	12		Survived
			10.0	~2200	1		Survived
Watlow	7	Zircaloy	8.6	~1800	1	Poor	Sheath split in ballooned region;[c] swelling over entire heated length
SEMCO	1	Inconel	6.9	~1700	2	Fair	Survived[d]
			8.6	~2200	11		Survived[d]
RAMA	2	Zircaloy	3.8	~1600	2	Very poor	Cracks in sheath initially; sheath swelling over heater length; heater element burned out in last cycle and shorted to sheath
			9.0	~2200	2		
			11.0	~2200	8		
			13.0	~2000	2		

Table 5.4. (Cont'd)

Heater supplier	Heater serial No.	Sheath material	Temperature transient[a]			Results	
			Power (kW)	Maximum temperature (°F)	Cycles	Infrared[b] scan	Transient tests
RAMA	3	Tantalum coated on carbon steel	6.3&11 14.2 14.2	~1700 ~2200 ~2000	2 9 1	Fair	Survived Survived Severe bowing; terminated test; severe oxidation; coating removed
Watlow	9	Zircaloy	7.9	~1600	1	Poor	Failed by split in locally[c] ballooned area
RAMA	4	Molybdenum coated on carbon steel	9.2 11.4 12.0 13.8	~1700 ~1700 ~2200 ~2200		Poor	Coating oxidized (evolution of white smoke); on last cycle coating began to spall; particles wedged in expansion joint, heater buckled
SEMCO	2	Inconel				Fair	Holding for future evaluation[e]

[a]Temperature transients started at about 500°F; rate of increase in range 40 to 60°F/sec; tests conducted in an argon atmosphere, using a dc motor-generator power supply.

[b]All heaters x-rayed and tested with an infrared scanning technique to determine element concentricity in sheath and uniformity of surface heat flux. The heater element eccentricity exceeded 0.006 in. in all heaters except the SEMCO heater, which was less than this value. The qualitative evaluation in the table relates to the surface heat flux uniformity.

[c]The sheath exhibited significant localized ballooning in two or three nodes, one of which resulted in splitting the sheath. Failure appears to be a result of internal pressure increase during heatup cycle.

[d]This heater was rejected initially on the basis of metallic inclusions in the boron nitride insulation between the heater element and the sheath. These inclusions caused a short in the infrared scanning tests, which melted two small holes in the sheath without damaging the element. The heater survived the transient tests without difficulty.

[e]This heater is a replacement for rejected heater (see note d above). Operational testing is being postponed for time being; may be used in development tests of plasma spray coating.

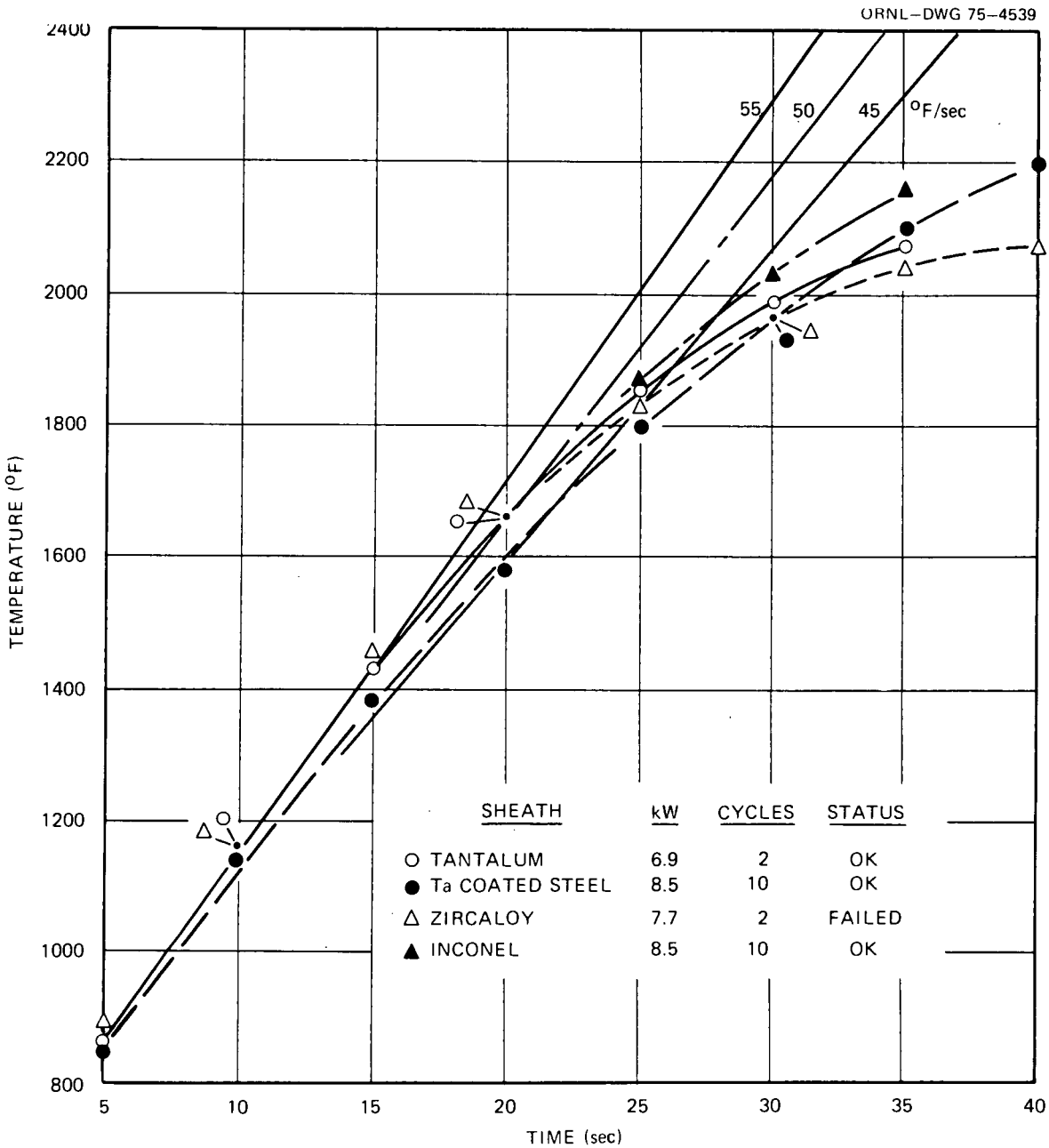

Fig. 5.2. Typical heating cycle results for MRBT development heaters.

typical performance data on four of the development heaters for constant applied voltage. Based on evaluation of all the test data, this new criterion implies a higher heatup rate in the lower temperature range or an adjustment in applied voltage in the higher range; a choice between the alternatives has not been made.

Zircaloy is desired as the heater sheath material for compatibility reasons; however, as indicated in Table 5.4, the initial performance of the Zircaloy-sheathed heaters was not encouraging, and for the immediate future, further consideration will not be given to this material. However, since Zircaloy-sheathed heaters have been fabricated successfully and used in a number of test programs, we will continue to investigate this material for use later in the program. For the near term, we will focus on stainless steel sheaths with a protective plasma spray coating of refractory metal or oxide.

Development and evaluation of plasma spray coatings are under way in the Y-12 Plant, using existing equipment and some of the development heaters that survived the evaluation tests. Candidate coatings of current interest are tantalum, tungsten, calcium-stabilized zirconium oxide, and depleted uranium dioxide. The evaluation will include adherence quality (to stainless steel and Inconel), chemical and metallurgical capability with Zircaloy-4, and effective emittance.

Based on the test and evaluation results gained from the development heaters and on revised design criteria, the prototype heater has been redesigned. Stainless steel, type 316, is specified as the sheath material. A suitable protective plasma spray coating will be applied to preclude formation of zirconium-based eutectics. Application of the protective coating will be in-house to maintain quality control and to assure timely availability of acceptable heaters.

Purchase of 20 of the redesigned heaters has been initiated from each of two manufacturers, i.e., the two most favorable responses to bid requests sent to the three manufacturers who supplied heaters for evaluation; no information will be available on delivery until the bids are opened in mid-April. Based on performance evaluation of the two lots of heaters, an option to purchase additional heaters will be exercised. This strategy will enhance the probability that suitable heaters can be obtained on a

timely basis for further evaluation and for use in the initial single-rod tests. To expedite fabrication of the heaters, an order was placed earlier for a quantity of stainless steel sheath tubing that will be supplied to the selected manufacturers. Delivery of the tubing, expected in late April, should not delay fabrication of the heaters. Kanthal ribbon material (heating element) and high-purity boron nitride powder also will be supplied to the manufacturers; these materials will be withdrawn from our existing supply.

The lack of manufacturers qualified to produce acceptable heaters is a problem for this and other test programs. We plan to procure additional development heaters from other prospective suppliers for test and evaluation in an effort to improve the situation. Although this effort is not expected to alleviate the situation with respect to heaters for the initial single-rod and 4 x 4 burst tests, it is anticipated that some relief will be obtained by the time significant quantities of heaters are required for the 8 x 8 multirod test bundles.

5.3.5 Instrumentation and Data Acquisition

K. R. Carr* and T. G. Kollie*

Pressure

The helium pressure (100 to 2000 psi) in each fuel pin simulator will be measured with a fast ($\tau \approx 1$ msec) strain-gage-type pressure transducer and the signals recorded by a computer controlled data acquisition system (CCDAS). Important system design considerations include:

1. A 2-in. length of 0.015-in.-ID tubing is required in the upper seal gland on the simulators (see Sect. 5.3.3) to interconnect the simulator gas volume to the external measuring system.

2. The pressure transducer must be located at a sufficient distance from the test bundle to avoid high-temperature calibration drift (≥350°F at the simulator end seal).

---

*Instrumentation and Controls Division.

3. The transducer and connecting tubing volume must be sufficiently small so that the total internal volume of each simulator system is no greater than 2 in.^{3} for proper fuel pin simulation.

4. The connecting tubing must have a sufficiently large ID so that the tubing will cause insignificant time delay or distortion of the pressure signal.

A model of the fuel-pin simulator pressure-measuring system, shown in Fig. 5.3, was assembled and tested to determine the approximate time response of three tubing configurations as given in the figure. The tests were conducted as follows:

1. The system was pressurized with helium to 500 psig and isolated from the gas supply by valve HV-1.

2. Rupture of the fuel-pin simulator was simulated by opening valve HV-2 to vent the system.

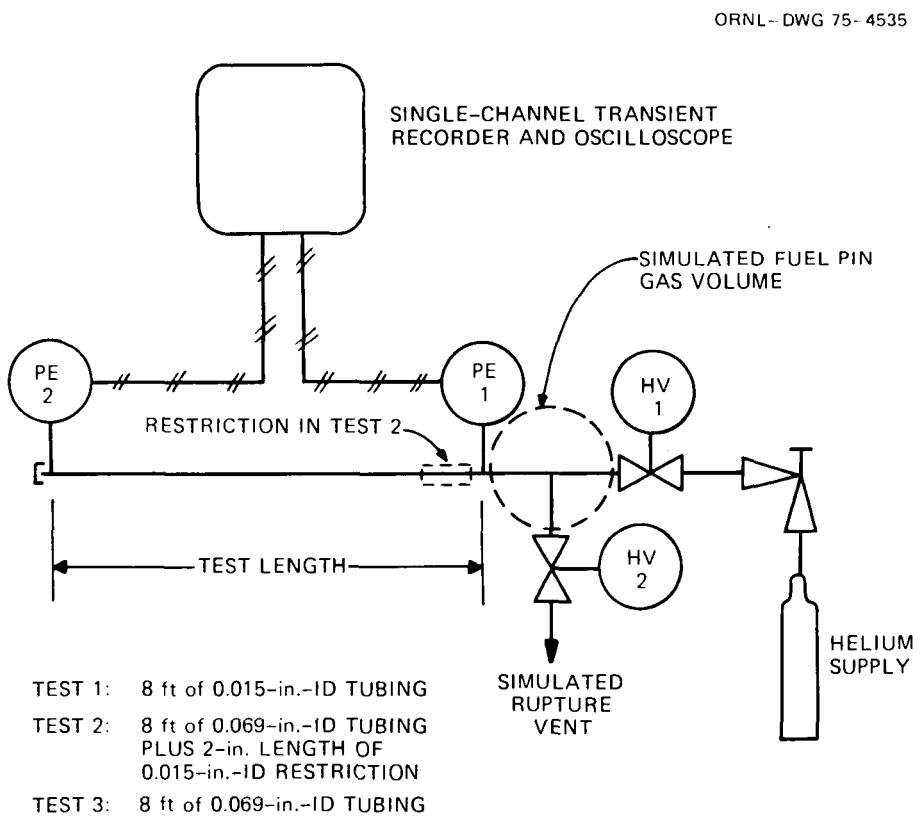

Fig. 5.3. Model of fuel pin simulator pressurization system for determining pressure transient response.

3. A single-channel transient recorder (Biomation model 802) was used to record the transducer signal from either PE-1 or PE-2. The data were output from the transient recorder to an oscilloscope, and a photograph was made of the display for subsequent analysis.

4. Approximate pressure transient time constants (63% response) and time intervals required to reach 0 psig were determined from the photographic records.

Typical data records are shown in Fig. 5.4; the trace for PE-1 shows the response expected for a transducer closely coupled to the simulator gas volume and should be essentially independent of the external tubing configuration. The trace shown in the figure for PE-2 shows the effect of locating the transducer remote (8 ft of 0.015-in.-ID tube) from the simulated volume. Results for the three tubing configurations are given in Table 5.5. These data do not include the time delay ("dead time") before the pressure transient first arrives at PE-2; calculations indicate this delay to be a few msec (3 to 5 at most).

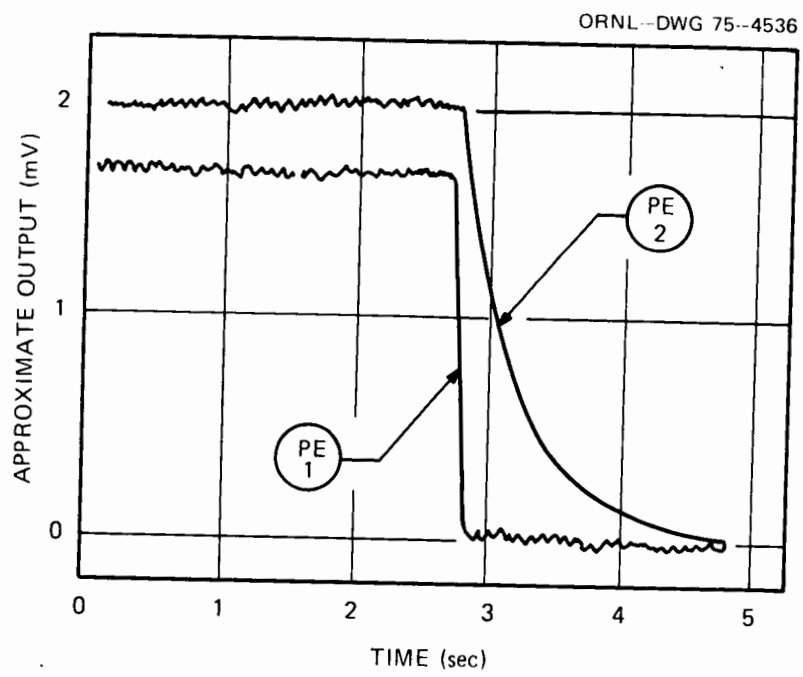

Fig. 5.4. Superimposed data records for system simulation shown in Fig. 5.3. Test conditions: 500 to 0 psig.

Table 5.5. Summary of transient test results for pressure-measuring systems shown in Fig. 5.3

Transducer	Time constant (63% response) (sec)	Time to reach 0 psig indication (sec)
Test No. 1: 8 ft of 0.015-in.-ID connecting tubing		
PE-1	0.04	0.09–0.13
PE-2	0.5	2.5
Test No. 2: 8 ft of 0.069-in.-ID tubing plus 2 in. of 0.015-in.-ID restriction		
PE-1	0.06	0.2
PE-2	0.3	1.2
Test No. 3: 8 ft of 0.069-in.-ID connecting tubing		
PE-1	0.04	0.12
PE-2	0.05	0.19

Note: These data do not include time delay ("dead time") for pressure transient to arrive at transducer.

The effect of locating the transducer remote from the fuel-pin simulator is obtained for each of the tested configurations by taking the difference in the time constant for the two transducers. These preliminary results indicate the design goals can be achieved without significant degradation of the pressure data. Further tests are planned to obtain better definition of the response and to evaluate alternative configurations.

Thermometry

Calibrations of the bare-wire, type S thermocouple material were completed. The calibration deviations from ASTM E-230 (i.e., NBS Monograph 125) are within the ±1/4% specification for type S wire with nominal (usually about 9.91 wt %) 10% rhodium content of the platinum/10% rhodium

thermoelement. (The exact, i.e., 10 ± 0.05 wt % rhodium, composition wire was ordered but the manufacturer supplied the nominal 10% composition wire. With the proper attention that is being given to calibrations, the nominal 10% rhodium wire is acceptable for use.) The calibration deviations are a smooth, negative, monotonic function of increasing temperature with maximum deviation of less than −5°C (−9°F) at 1500°C (2732°F). Tables and functions based on the IPTS-68 temperature scale are now being prepared for use in converting the thermal emfs of these thermocouples to temperature. The principal use of this bare-wire, type S material will be for measurements of the outside surface temperature of the Zircaloy tubing in the single-rod tests and for use as a secondary working standard to facilitate calibration of sheathed thermocouples purchased in the future.

A variety of thermocouples are on order for evaluation and use in the initial tests; Table 5.6 summarizes the procurement status. Design and procurement of the components necessary for evaluation of the 0.030-in.-OD tantalum-sheathed thermocouples are complete. Evaluation of these thermocouples will include comparative calibration to working standard type S thermocouples over the range 20 to 1315°C (68 to 2400°F) and measurement of the high-temperature sheath-to-wire resistance if the measured temperature deviates appreciably from that indicated by the standard.

As discussed in Section 5.2.3, bare-wire, type S thermocouples will be attached to the outside surface of a number of fuel pin simulators in the first 4 x 4 bundle to obtain temperature profiles. To alleviate assembly problems and to provide support for the fragile wire, 0.063-in.-OD stainless-steel-sheathed thermocouples were selected. The sheath will be stripped back a few inches from the sensing end to expose the thermoelements for welding to the cladding. This requires a high-temperature hermetic end seal to prevent moisture entry into the sheathed portion; several end seal materials are under consideration. Procurement was initiated for 60 of these thermocouples.

Table 5.6. Thermocouple procurement status in the MRBT program

Thermocouple type	Sheath	Insulator	Sheath OD (in.)	Length (ft)	Quantity	Scheduled shipping date	Vendor
K	Ta	Al_2O_3	0.030	10	45	4/4/75[a]	SEMCO
K	Ta	Al_2O_3	0.030	10	25	6/1/75[b]	ARI
S	Ta	Al_2O_3	0.030	10	10	4/4/75[c]	SEMCO
K	310 SS	MgO	0.030	10	100	4/25/75[d]	Gordon
S	310 SS[e]	Al_2O_3	0.063	7	60	Out for bids	
S	Bare	Al_2O_3	0.010	250		Received	Bishop

[a]Partial shipment of about 15. Remainder to be shipped May 9, 1975.

[b]Partial shipment of 5. Remainder to be shipped July 18, 1975.

[c]Partial shipment of 2. Remainder to be shipped May 9, 1975.

[d]Partial shipment of 50. Remainder to be shipped July 15, 1975.

[e]Bare-wire sensing junction.

5.3.6 Design

J. L. Crowley, H. R. Payne,* and R. D. Stulting*

Single-rod tests

Design of a versatile, bench-type test stand was completed; this test stand will be used to develop, test, and evaluate design concepts and components, to establish test procedures, to determine temperature distributions in individual fuel pin simulators, to investigate parametric effects, and to perform single-rod burst tests. The test stand can be supplied with up to 10 lb/hr of 650°F (~1 psig) superheated steam; a dc motor-generator set supplies power for electrically heating the fuel pin simulator. Test data, i.e., temperature, pressure, etc., will be recorded with a computer-controlled data acquisition system (CCDAS). The design permits the use of up to 24 bare-wire, type S thermocouples on the outside surface of the cladding; four sheathed thermocouples can be attached to the cladding inside surface. Although the present design incorporates an unheated shroud around the fuel-pin simulator, modifications will permit the use of a heated shroud.

Multirod test facility

Significant progress was made on facility design; mechanical design of the facility and 4 x 4 bundle test components is approximately 70% complete, electrical design of the dc power supply modifications is about 50% complete, and design of the instrumentation and control system is about 30% complete.

The facility includes a 12-in.-ID test vessel for housing preassembled test bundles. Plant steam (250 psig, saturated), reduced in pressure to 100 psig and superheated to 650°F, is supplied to the test vessel; 30 psig steam is supplied for fast cooling of the test assembly. Helium will be supplied to a manifold from high-pressure helium cylinders. Each test rod will be connected to the manifold, and the connecting line pressure will be monitored by a pressure transducer. Electrical power is

---

*Engineering Division.

supplied from a large dc motor-generator set. A computer-controlled data acquisition system (CCDAS) will record multivolt signals from the process instrumentation system. The CCDAS will provide alarm and test termination signals according to preprogrammed instructions.

Figure 5.5 shows the conceptual design of the test vessel with a 4 x 4 bundle installed. The bundle is enclosed by a ohmic-heated shroud, fabricated from thin Inconel sheet stock. This heater will be electrically connected in series with the bundle heaters (all in parallel) to utilize the same power supply. A variable resistor paralleled with the heated shroud permits minor current adjustment (rate of heating) to match approximately the temperature rate of increase with that of the fuel pin simulators. Power for the bundle and heated shroud will be supplied from the existing dc power supply installed for the THTF facility. The existing feeder will be rerouted to disconnect switches to permit operation of either experiment. Each fuel pin heater will be provided with current-limiting fuse protection. Studies have been made to determine the cable and equipment requirements for the intermittent type load. The disconnect switches are on hand and other components for the system are being determined.

5.4 FABRICATION AND CONSTRUCTION

J. L. Crowley and J. D. White

The single-rod test stand is in the final stages of fabrication. Site preparations are complete and most of the equipment is in place.

A steam heater has been fabricated using existing electrical equipment. A 30-ft-long coil of 1/2-in.-diam stainless steel tube will be direct resistance heated with current supplied by a step-down transformer and controlled by a manually operated auto-transformer. The heater will supply up to 10 lb/hr of superheated steam at 650°F.

Power will be supplied to the fuel pin simulator by a small dc motor-generator set that has been reconditioned and installed in the test area. The M-G set is presently supplying power for test and evaluation of development heaters.

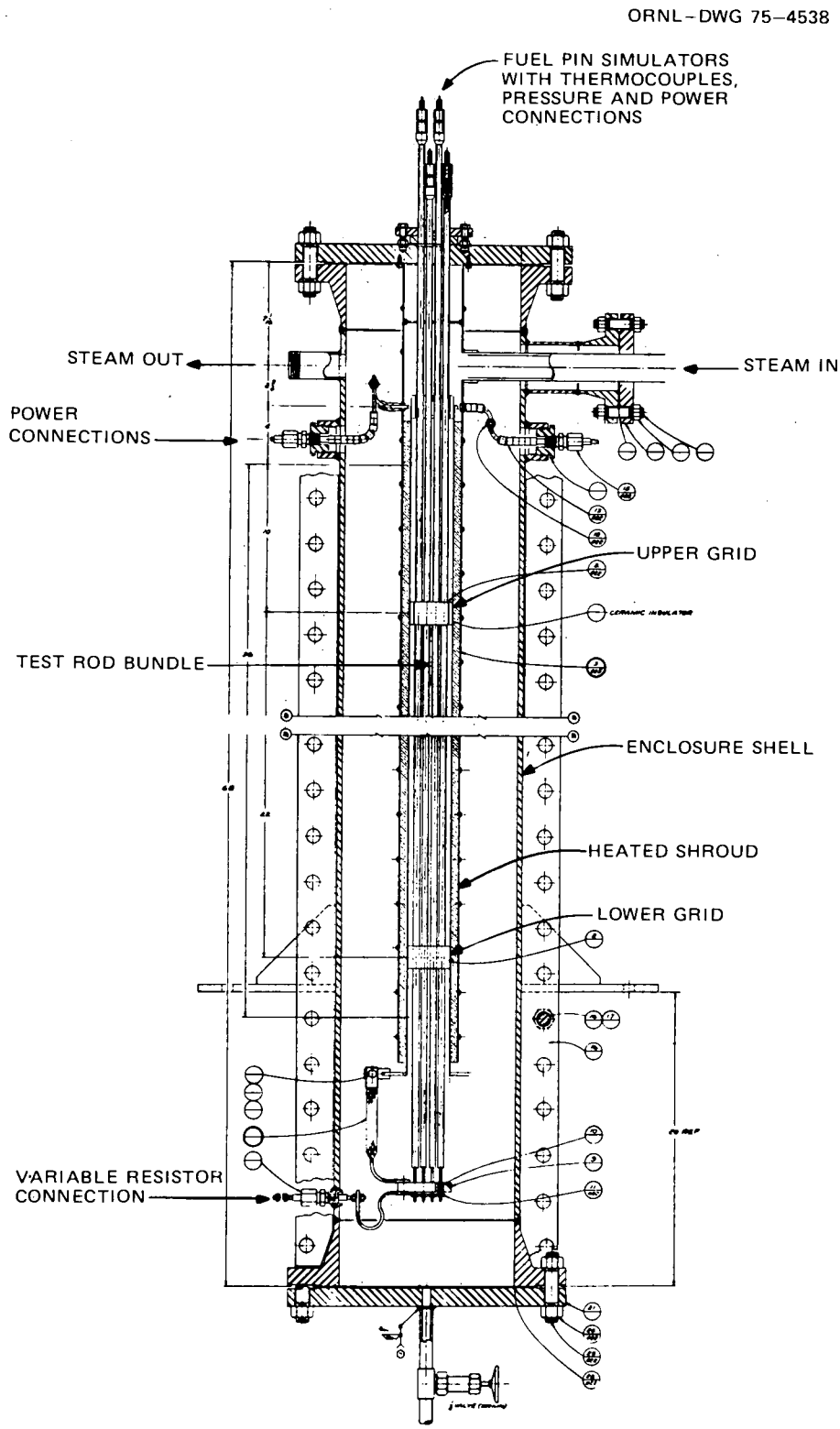

Fig. 5.5. Conceptual design of 4 x 4 test bundle.

Parts for the single-rod test container have been machined, and assembly is now in progress. The versatile test chamber is designed to accommodate the low-pressure (atmospheric) steam, allowing some leakage at various penetrations. A 1 1/2-in.-diam (unheated) shroud tube surrounding the fuel pin simulator is split into three sectors to allow assembly after the external thermocouples are attached to the simulator. Superheated steam, supplied by the steam heater, will enter the annulus formed by the shroud and the fuel pin simulator via an upper plenum.

Construction of the multirod facility site and additions to the dc power supply are scheduled to commence next quarter.

REFERENCES

1. Quarterly Progress Report on Reactor Safety Programs Sponsored by the Division of Reactor Safety Research for July–September 1974, ORNL-TM-4729, Vol. I, pp. 70–72.

2. Quarterly Progress Report on Reactor Safety Programs Sponsored by the NRC Division of Reactor Safety Research for October–December 1974, ORNL-TM-4805, Vol. I, pp. 102–110.

6. FISSION PRODUCT RELEASE FROM LWR FUEL

Chemical Technology Division

A. P. Malinauskas
R. A. Lorenz
M. F. Osborne

During this period the program work plan was revised to incorporate comments which were made in the course of review of the preliminary draft and to emphasize specific NRC data needs which were identified during the review. The revised work plan was transmitted to ONRR-NRC on March 7, 1975.

A contaminated hot cell has been cleaned. Installation of our experimental apparatus in this cell is progressing according to schedule; electrical wiring is being installed, and the components of the gas flow system are being connected and tested. Appropriate quality assurance approvals have been obtained for the apparatus design.

Irradiated fuel specimens which are currently available for use in the present experiments are limited in utility because of low burnup (~1000 MWd/metric ton) or low linear thermal power during irradiation (<160 W/cm). Thus, to maintain prototypical conditions as closely as is possible, it is desirable to obtain specimens of modern, high-burnup LWR fuel for testing. Accordingly, we have requested two fuel rods from the bundle of H. B. Robinson 2 (PWR rods) which are being acquired by ONRR-NRC. Detailed specifications have been developed for the examination and sectioning of the two fuel rods and for the preparation of specimens to be used in the experimental program. The specifications were submitted to three different hot-cell facilities for cost estimates; one of the estimates has been received, and the remaining two are expected shortly.

Representative rods from the H. B. Robinson 2 PWR bundle will be thoroughly examined for such characteristics as fission-gas release, fission product distribution within the pellets, burnup profiles, and dimensional changes; since these characteristics have pertinence to other NRC-funded activities as well as the Fission Product Release from LWR Fuel Program. We have specifically requested fission gas release and burnup profile determinations for the two rods to be

employed in our investigations. Subsequently, these rods will be cut into 1- and 2-ft lengths; and the sections will be sealed immediately. By selecting appropriate segments of the fuel rods for experimentation, as guided by the axial burnup distributions, we can span a range of burnups from 10,000 to 30,000 MWd/metric ton in the experiments.

Apparatus modifications which are required for studies of cesium release from UO_2-cesium mixtures using a Knudsen cell—mass spectrometer technique are proceeding somewhat more slowly than anticipated. This is due primarily to unexpected difficulties with both the vacuum system and the electronics associated with the apparatus.

7. CREEPDOWN AND COLLAPSE OF ZIRCALOY FUEL CLADDING

D. O. Hobson
Metals and Ceramics Division

Progress has continued this past quarter on both the theoretical and the experimental aspects of Zircaloy cladding collapse behavior. The theoretical portion has been concerned with a review of the subjects of tubing collapse in general, and the creep behavior of Zircaloy and the effects of anisotropy on the mechanical behavior of Zircaloy, specifically. The experimental aspects of the program have centered on the design, procurement, and installation of test equipment for the collapse studies, together with the necessary safety reviews for the use of high-pressure autoclaves.

All of the capital equipment necessary for the collapse testing is now on order — including a furnace, controller, and power supply; a gas-booster pump; and the most recently designed eddy-current strain gage coils. Installation of services to the autoclave pit area has started, and the high-pressure review committee has approved the installation and use of the high-pressure equipment. This equipment will be installed upon receipt.

Difficulty was experienced with the insulation on the first eddy-current coils when they were subjected to elevated temperatures during calibration. These were fabricated from flattened platinum wire and were wound into flat coils with insulation provided by a room-temperature-hardening "glass" solution. This design failed at approximately 200 to 300°F due to breakdown of the insulation. A new design was chosen that used aluminum foil that had been anodized to produce an approximately 3000 to 3500 Å oxide film on the surfaces. Coils wound from this material proved to be well insulated at room temperature. Elevated-temperature testing is now being done. Electronic stability problems have apparently been overcome — drifts amounting to only several tens of microinches liftoff have been found over periods of three to four days at room temperature. A five-unit block of coils has been fabricated as a prototype unit of the design to be used for the collapse and creepdown

tests. Proof of the efficacy of the design must await installation of the test equipment.

Review of previous work by others concerning tubing collapse, creep in Zircaloy, and the effects of anisotropy on the mechanical properties of Zircaloy has been completed, and the report will be issued as ORNL-TM-4913. One of the major findings of the study was that without exception, the anisotropic behavior of Zircaloy, in which the tensile and compressive strengths can differ widely from each other, has not been taken into account. Several of the previous studies, including those referenced in the document that described the BUCKLE code[1], do not acknowledge the extreme variations of mechanical properties with stress direction and stress ratio that Zircaloy can possess. Nor do those studies quantitatively take into account the effects of crystallographic texture (preferred orientation), effects that can radically change the way Zircaloy responds to a given stress distribution. It has become obvious that the experimental work to be done in the present study must address these items in a way that will produce quantitative correlations among stress state, texture, deformation behavior, and strain rate. This information is in addition to the correlations of the above with temperature, stress magnitude, and tubing – pellet geometries that obviously must be obtained.

REFERENCE

1. P. J. Pankaskie, BUCKLE, An Analytical Computer Code for Calculating Creep Buckling of an Initially Oval Tube, BNWL-1784 (May 1974).

ORNL-TM-4914
Vol. I
UC-78, -78a, -78c

Internal Distribution

1. A. H. Anderson
2. W. E. Baucom
3. M. Bender
4. R. F. Bennett
5. C. J. Borkowski
6. C. Brashear
7. J. R. Buchanan
8. J. J. Campbell
9. K. R. Carr
10. J. V. Cathcart
11. R. H. Chapman
12. C. J. Claffey
13. N. E. Clapp
14. D. L. Clark
15. W. B. Cottrell
16. J. L. Crowley
17. F. L. Culler
18. J. W. Cunningham
19. D. G. Davis
20. J. K. Dickens
21. R. E. Druschel
22. B. G. Eads
23. G. G. Fee
24. D. E. Ferguson
25. M. H. Fontana
26. J. H. Freels
27. M. J. Goglia
28. J. A. Hawk
29. T. L. Hebble
30. R. A. Hedrick
31. R. E. Helms
32. M. R. Hill
33. D. O. Hobson
34-43. H. W. Hoffman
44. S. H. Jury
45. L. D. Koffman (UT)
46. T. G. Kollie
47. J. W. Krewson
48. B. C. Leslie
49. R. A. Lorenz
50. T. S. Lundy
51. R. N. Lyon
52. R. E. MacPherson
53. F. C. Maienschein
54. S. Malang
55. A. P. Malinauskas
56. W. J. McCarthy
57. R. W. McCulloch
58. D. L. McElroy
59. C. J. McHargue
60. C. A. Mills
61. R. L. Moore
62. F. H. Neill
63. M. F. Osborne
64. R. E. Pawel
65. H. R. Payne
66. R. W. Peelle
67. R. A. Perkins
68. H. Postma
69. W. Ragan
70. J. L. Redford
71. E. T. Rose
72-73. M. R. Sheldon
74. J. D. Sheppard
75. R. L. Shipp
76. A. M. Smith
77. I. Spiewak
78. R. D. Stulting
79. J. J. Taylor
80-84. D. G. Thomas
85. D. B. Trauger
86. J. R. Weir
87. J. D. White
88. G. D. Whitman
89. W. J. Wilcox
90. R. K. Williams
91. Y. M. Yoo
92. G. J. Yurek
93. Patent Office
94-95. Central Research Library
96. Document Reference Section
97-101. Laboratory Records Department
102. Laboratory Records (RC)
103. Nuclear Safety Information Center

External Distribution

104-105. Director, Division of Reactor Safety Research, NRC, Washington, D.C. 20555
106. Director, Reactor Division, ERDA-ORO
107. Director, Research and Technical Support Division, ERDA-ORO
108-117. Special Distribution
118-364. Given distribution as shown in TID-4500 under categories UC-78, -78a, -78c (25 copies — NTIS)

☆U. S. GOVERNMENT PRINTING OFFICE: 1975-748-189/2